RESEARCH AND DEVELOPMENT OF AIRCRAFT CONTROL ACTUATION SYSTEMS. THE DEVELOPMENT OF A FLIGHT CONTROL SYSTEM SIMULATOR, RESEARCH ON A CONTROL SURFACE FLUTTER SUPPRESSION TECHNIQUE AND HIGH TEMPERATURE TESTING OF MIL-H-83282

Gavin D. Jenney

Dynamic Controls, Incorporated

Prepared for:

Air Force Flight Dynamics Laboratory

January 1975

AFFDL-TR-75-29

RESEARCH AND DEVELOPMENT OF AIRCRAFT CONTROL ACTUATION SYSTEMS

The Development of a Flight Control System Simulator, Research on a Control Surface Flutter Suppression Technique and High Temperature Testing of Mil-H-83282

DYNAMIC CONTROLS, INC.
DAYTON, OHIO 45404

TECHNICAL REPORT AFFDL–TR–75–29

MARCH 1975

FINAL REPORT FOR PERIOD JANUARY 1974 – FEBRUARY 1975

AIR FORCE FLIGHT DYNAMICS LABORATORY
AIR FORCE SYSTEMS COMMAND
WRIGHT–PATTERSON AIR FORCE BASE, OHIO 45433

NOTICE

When Government drawings, specifications, or other data are used for any purpose other than in connection with a definitely related Government procurement operation, the United States Government thereby incurs no responsibility nor any obligation whatsoever; and the fact that the government may have formulated, furnished, or in any way supplied the said drawings, specifications, or other data, is not to be regarded by implication or otherwise as in any manner licensing the holder or any other person or corporation, or conveying any rights or permission to manufacture, use, or sell any patented invention that may in any way be related thereto.

This report has been reviewed and cleared for open publication and/or public release by the appropriate Office of Information (OI) in accordance with AFR 190-17 and DODD 5203.9. There is no objection to unlimited distribution of this report to the public at large or by DDC to the National Technical Information Service (NTIS).

This technical report has been reviewed and is approved for publication.

Bruce H. Earley
Project Engineer

FOR THE COMMANDER

Paul E. Blatt
Mr. Paul E. Blatt, Chief
Control Systems Development Branch
Flight Control Division
Air Force Flight Dynamics Laboratory

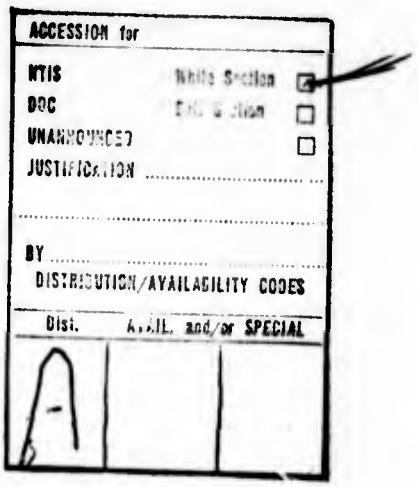

Copies of this report should not be returned unless return is required by security considerations, contractual obligations, or notice on a specific document.

AIR FORCE/56780/4 August 1975 — 100

UNCLASSIFIED

SECURITY CLASSIFICATION OF THIS PAGE (When Data Entered)

REPORT DOCUMENTATION PAGE		READ INSTRUCTIONS BEFORE COMPLETING FORM
1 REPORT NUMBER AFFDL-TR-75-29	2. GOVT ACCESSION NO. NA	3 RECIPIENT'S CATALOG NUMBER NA
4 TITLE (and Subtitle) RESEARCH AND DEVELOPMENT OF AIRCRAFT CONTROL ACTUATION SYSTEMS - The Development of a Flight Control System Simulator, Research on a Control Surface Flutter Suppression Technique and High Temperature Testing of Mil-H-83282		5 TYPE OF REPORT & PERIOD COVERED FINAL Jan 1974 - Feb. 1975 6 PERFORMING ORG. REPORT NUMBER NA
7 AUTHOR(s) Gavin D. Jenney		8 CONTRACT OR GRANT NUMBER(s) F33615-74-C-3020
9 PERFORMING ORGANIZATION NAME AND ADDRESS Dynamic Controls, Inc. P.O. Box 281, North Dayton Station Dayton, Ohio 45404		10 PROGRAM ELEMENT, PROJECT, TASK AREA & WORK UNIT NUMBERS Project 1987 Task 01
11 CONTROLLING OFFICE NAME AND ADDRESS Air Force Flight Dynamics Laboratory AFFDL/FGL Wright-Patterson Air Force Base, Ohio 45433		12 REPORT DATE January 1975 13 NUMBER OF PAGES 202
14 MONITORING AGENCY NAME & ADDRESS (if different from Controlling Office) Same		15 SECURITY CLASS. (of this report) Unclassified 15a DECLASSIFICATION/DOWNGRADING SCHEDULE NA

16. DISTRIBUTION STATEMENT (of this Report)

Approved for public release; distribution unlimited.

17. DISTRIBUTION STATEMENT (of the abstract entered in Block 20, if different from Report)

Same

18. SUPPLEMENTARY NOTES

None

19. KEY WORDS (Continue on reverse side if necessary and identify by block number)

Flight Control Systems
Flutter
Flutter Suppression
Redundant Systems
High Temperature Hydraulic Fluid
Flight Control Simulator

20. ABSTRACT (Continue on reverse side if necessary and identify by block number)

This report presents the results of the following three research and development activities:

1. The design, fabricationand test of a multi-channel flight control system hybrid simulator.

DD FORM 1 JAN 73 1473 EDITION OF 1 NOV 65 IS OBSOLETE

UNCLASSIFIED

SECURITY CLASSIFICATION OF THIS PAGE (When Data Entered)

2. The analysis and application of a flutter damping technique for hydraulically actuated slab type control surfaces.

3. The experimental testing of Mil-H-83282 hydraulic fluid in a pumping system at elevated temperatures.

In addition to documenting the design and performance aspects of the hybrid simulator, the report supports the following conclusions:

1. Hydromechanical damping of the torsional mode of a slab type surface is practical and will allow a reduction in the size and power requirements of the associated surface actuator.

2. Mil-H-83282 shows little physical deterioration from operation at temperatures to 450° F in a closed hydraulic pumping system for the length of time tested.

FOREWORD

The effort described in this document was performed by the Dynamic Controls, Inc., of Dayton, Ohio under Air Force Contract F33615-74-C-3020. The contract was performed under Project Number 1987, Task Number 01, entitled "Research and Development of Aircraft Control Actuation Systems". Work under the contract was carried out at Wright-Patterson Air Force Base utilizing United States Air Force facilities. The work was administered by Bruce H. Earley, (AFFDL/FG), Project Engineer, of the Flight Control Division.

The author wishes to express his acknowledgement and thanks to Col. E. Henry for his contributions in the computer simulation associated with the contracted effort. The author also wishes to express his appreciation to the Dynamic Controls, Inc. personnel Mr. Harry W. Schreadley, Heinrich J. Wieg, Carl N. Allbright, and William G. Talley for their contributions in the areas of analysis, design, fabrication and testing associated with the effort.

This report covers work performed between 23 January 1974 and 31 January 1975. The technical report was submitted by the author in January 1975.

This report contains no classified information extracted from other classified documents.

TABLE OF CONTENTS

TABLE OF CONTENTS (Cont'd.)

TABLE OF CONTENTS (Cont'd.)

TABLE OF CONTENTS (Cont'd.)

TABLE OF CONTENTS (Cont'd.)

LIST OF ILLUSTRATIONS

LIST OF ILLUSTRATIONS (Cont'd.)

LIST OF ILLUSTRATIONS (Cont'd.)

LIST OF ILLUSTRATIONS (Cont'd.)

LIST OF ILLUSTRATIONS (Cont'd.)

LIST OF ILLUSTRATIONS (Cont'd.)

LIST OF TABLES

LIST OF ABBREVIATIONS AND SYMBOLS

ABBREVIATIONS

A.	Absolute
cis	Cubic inches per second
db	Decibel
FM	Flowmeter
GPM	Gallons Per minute
HP	Horsepower
Hz	Hertz
IAP	Integrated actuator package
in.	Inch
LVDT	Linear variable differential transformer
N.	Nominal
P	Pressure
PSI	Pounds per square inch
PMS	Primary Motion Section
rad.	Radian
Ref.	Reference
sec., secs.	Second, seconds
SMS	Secondary Motion Section

SYMBOLS

A	Area
A_1	Isolation piston drive area
A_2	Damping spool drive area
A_p	Open area of orifice
a	Peak acceleration
B_1	Damping of body to structure motion
B_2	Damping of control actuator piston to surface motion
B_3	Damping of surface motion to structure
B_4	Damping of actuator piston to actuator body
C_1, C_3	$\frac{V}{4\beta}$
C_1'	Coefficient of lift
C_4	Leakage coefficient
C_5	Flow gain coefficient
C_6	Load sensitivity coefficient
E	Input voltage
e	2.7183
E_c	Load command signal voltage
F	Peak driving force
f	Frequency in Hz

SYMBOLS

f_d	The driving force
f_n	Resonant frequency
F_m	Peak force to drive mass
F_{sp}	Peak force to drive spring
H	The instantaneous deflection
H_o	Reference height
K	A proportional gain constant
K'	Spring rate
K_1	Isolation piston spring rate
K_2	Damping spool spring rate
K_f	Pressure feedback gain
k_{sp}	Spring rate of centering springs
K_w	Washout circuit gain
k_1	Actuator piston to structure spring rate
k_2	Actuator piston to surface spring rate
k_3	Load actuator spring rate
L	Lift vector
L_o	Reference lift
M,m	Mass
M_1	Mass of actuator body

SYMBOLS

M_2	Mass of surface member
M_3	Mass of load elements
m_{sp}	Mass of spool
n	Number of increments by which spool stroke is divided
ΔP	Differential pressure
ΔP_1	Pressure drop across damping spool
ΔP_2	Pressure drop across damping spool
ΔP_n	Flutter caused differential pressure across piston which opens damping spool to nth position
P_b	Static bias pressure
P_r	Return pressure
P_s	Supply pressure
Q	Flow through the damping orifice
Q_1	Flow generated by the isolation piston
Q_3	Flow used by damping spool
Q_i	Output flow from valve
$Q_{\Delta P}$	The flow due to the load pressure feedback
Q_b	Flow absorbed by fluid compliance
Q_p	Flow generated by moving piston

SYMBOLS

R_2	Washout orifice resistance
r	Distance between L and rotational centerline
r'	The ratio of the absolute value of the instantaneous lift to the steady lift
S	Laplace Operator
T	Temperature
T'	Valve time constant
T_d	Time delay constant
t	Time
U	Airstream Velocity
V	Total Volume of oil in actuator
V'	Valve
x_{ip}	Position of isolation piston
x_s	Surface Motion
x_{sp}	Damping spool position
x_t	Total actuator stroke
x_v	Peak spool stroke
X_t	Total stroke of spool
$\hat{x}$	Peak stroke

SYMBOLS

$\hat{\dot{x}}$	Peak velocity
x_1	Actuator body motion relative to structure
x_2	Actuator piston motion relative to structure
x_3	Surface member motion
π	3.1416
ζ	Damping ratio
#	Pounds
ω	Frequency in radians/second
Δ	Change
β	Bulk modulus
α	Angle of attack
$\sum$	Summation
γ	Time constant
ϕ	Phase angle by which instantaneous lift leads steady value
^{o}F	Degrees Farenheit
ρ	Density
β'	The phase angle by which the instantaneous lift leads the steady value at the frequency
Ω	Ohms

SECTION I

INTRODUCTION

This report describes the technical effort conducted by Dynamic Controls, Inc. for the Air Force Flight Dynamics Laboratory from January 1974 to January 1975 under Air Force Contract F33615-74-C-3020. The work was conducted at Wright-Patterson Air Force Base using government furnished facilities. The technical effort was divided into the following three activities:

1. The analysis, redesign, fabrication, assembly and test of a multi-channel flight control hybrid simulator.

2. The analysis of a hydro-mechanical damping technique for slab type control surface flutter suppression.

3. The testing of Mil-H-83282 hydraulic fluid in a pumping system at elevated temperatures.

The objective of the activity associated with the hybrid flight control simulator was to produce a simulator with which a wide range of flight control systems could be mechanized in hardware form.

The objective of the investigation conducted on flutter suppression was to show the particular design equations for the technique investigated and apply them to a current aircraft control surface configuration.

The objective of the Mil-H-83282 testing was to

evaluate the operating characteristics of Mil-H-83282 when used in an aircraft type pumping system at elevated fluid operating temperatures.

This report describes the preceding activities in the three separate sections. SECTION II of the report describes the simulator activity. SECTION III describes the flutter suppression analysis. SECTION IV describes the fluid test program.

SECTION II

DEVELOPMENT OF A HYBRID FLIGHT CONTROL SIMULATOR

1.0 TECHNICAL APPROACH

1.1 General

The simulator developed by Dynamic Controls, Inc. is based on the concept of using electro-hydraulic and mechanical components in combination with dedicated analog computer type electronics. The combination of the analog computer electronics with the electrohydraulic and mechanical elements allows maximum flexibility in mechanizing different flight control system configurations.

The general configuration for the simulator was provided to Dynamic Controls, Inc. by the Air Force Flight Dynamics Laboratory for analysis, modification and fabrication. Inital work on the general configuration was carried out by present Dynamic Controls, Inc. personnel while working for Lear Siegler, Inc. on Air Force contract F33615-73-C-3024.

1.2 Design Description

1.2.1 General

The hybrid simulator incorporates two motion sections, a Primary Motion Section (PMS) and a Secondary Motion Section (SMS). The ouput of the Secondary Motion Section is measured electrically and can be used to command the Primary Motion Section.

FIGURE 1 shows a pictorial of the complete hybrid simulator. Both the PMS and SMS incorporate loading actuators to allow static and dynamic loading of the control

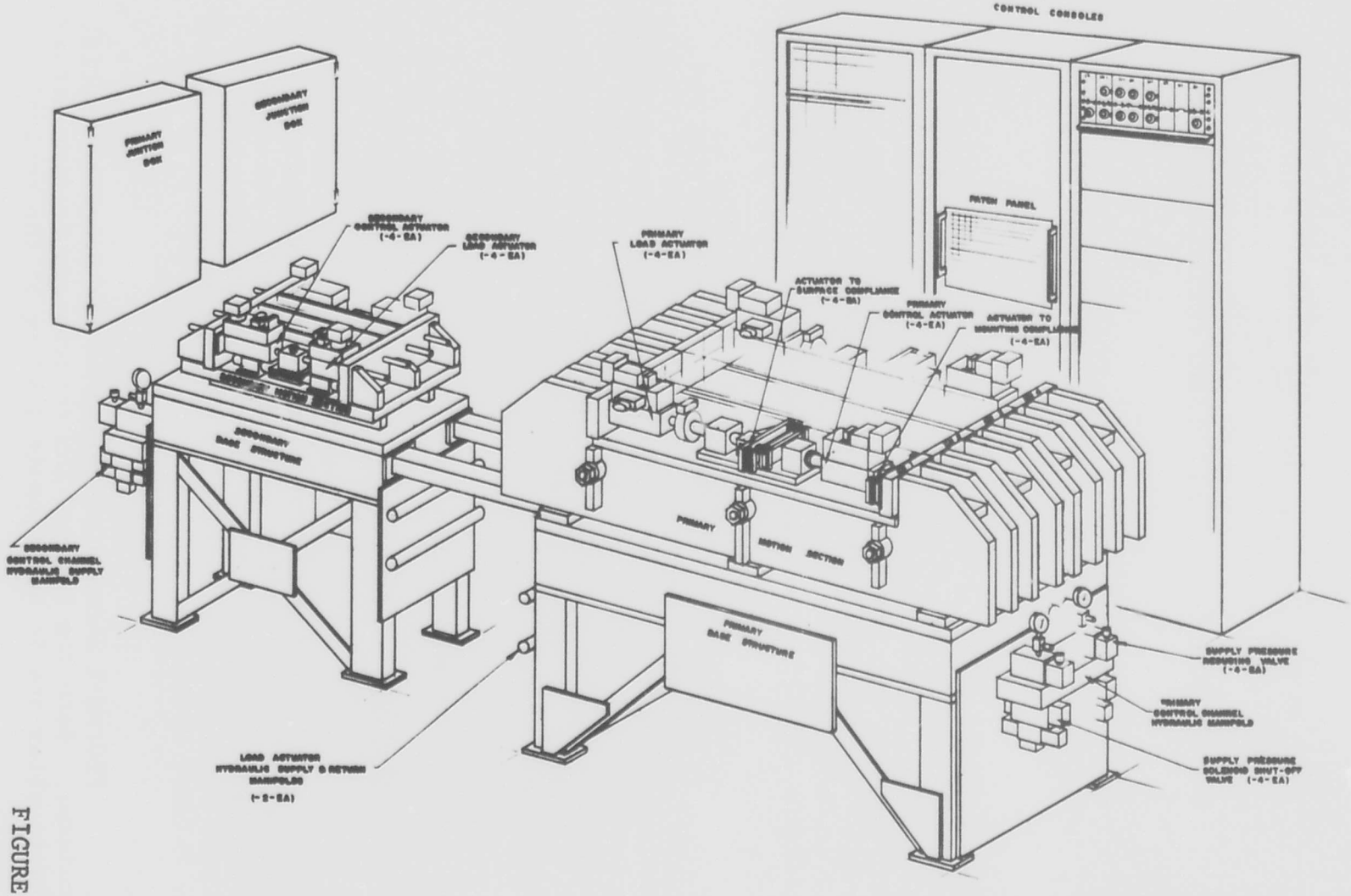

FIGURE 4

HYBRID SIMULATOR

PICTORIAL SCHEMATIC

channel actuators as required for the particular configuration and flight condition being simulated. Since the electro-hydraulic and mechanical elements of the simulator are relatively inflexible, the PMS and SMS are used as motion transducers, generating a mechanical motion in response to an electrical input signal. The frequency response and non-linear effects are inserted and varied using the analog computer elements installed in the control consoles.

The PMS and SMS each incorporate four control and loading actuators. All actuators are controlled by electrohydraulic servovalves. The simulator allows operating from 1 to 4 channels at a time with the output of the channels mechanically decoupled or coupled to each other. The coupling provisions allow configuring both active-standby and force-sharing flight control redundancy configurations.

Since electrohydraulic actuators are used on both the PMS and SMS units, the performance characteristics of the control channels are easily varied utilizing the analog electronic modules inserted into the control loops. Loads applied to the control channel actuators by the load actuators are also varied as required using electrical commands to control the force output of the load actuators.

The PMS incorporates mechanical compliance members in the control actuator mountings. Compliance members are used between the control actuator bodies and the mounting structure. Compliance members are also used between the control actuator piston rods and the PMS members representing the control surfaces. Variation of the compliances is accomplished by simple mechanical adjustment.

To allow evaluating redundancy mechanizations, the hybrid simulator electronics include a unit for channel performance comparison and failure detection. The unit allows monitoring of an selected voltage (represent-

ing a particular performance parameter) of either the PMS or SMS and the detection of failures. Both the PMS and SMS incorporate solenoid operated shutoff and bypass valves on the control and load actuators. These allow an actuator associated with a failed control channel to be decoupled by the failure monitor unit from the remaining control channel actuators.

Instrumentation is incorporated on the SMS and PMS to provide continuous measurement of all observable motions. This includes the following:

a. Measurement of the actuator piston position and velocity relative to the actuator body for all SMS load and control actuators.

b. Measurement of the PMS control actuator body position relative to the mounting structure.

c. Measurement of the PMS control actuator piston position relative to the mounting structure and output member. (surface member)

d. Measurement of the PMS output member (surface member) acceleration, velocity and position relative to the mounting structure.

In addition, instrumentation is incorporated on all the load and control actuators to measure the differential pressure across the actuator drive areas. The PMS also incorporates force transducers in the load

actuator connections in order to augment the pressure differential measurements of the PMS load actuator force outputs.

The control consoles contain the control and instrumentation electronics for the PMS and SMS. This includes the following:

a. Signal conditioners for the instrumentation

b. Failure logic unit

c. Control channel electronics

d. Load channel electronics

e. Interface patch panel

The control channel electronics are constructed to allow convenient gain changing, insertion of electronic filters, summers and non-linear modules as required. These modules are plug-in units which insert into the control channel electronic racks. Variation of the characteristics of the linear and non-linear characteristics of each module is made with direct reading digital dial pot knobs which read numerically the actual value of the parameter being changed. Included in the control consoles is the patch panel. This panel contains the outputs of all the instrumentation modules, system inputs and is used to close the feedback loops for the PMS and SMS. The patch panel also provides patching into the trunk lines used for interfacing with the AFFDL Simulation Facility.

The hybrid simulator is designed with variable performance capability. The electronics for the simulator are designed to operate at a $\pm$ 10 volt maximum output level. Input impedance for interface signal inputs is 100,000 ohms. Output impedance for the interface signals is a maximum of 10 ohms. The hydraulic system components are designed for

a maximum operating pressure of 3000 PSI. All load and control channel electronics except the servo driver operate at unity gain. The nominal electrohydraulic actuator characteristics are varied from their fixed values using the electronic modules.

1.2.2 SMS Mechanical Description

The portion of the SMS is constructed with 8 idential actuators. To minimize the flow required to drive the actuators to high frequencies, small drive areas were used in the actuators. To minimize the threshold for the actuators, hydrostatic bearings were used in both ends of each actuator and the piston was designed as a non-contact close fit with the actuator bore. No seals are used on the piston. Low friction Bal seals with the spring replaced with an "o" ring is used in each actuator end cap of each actuator.

The design values of the SMS electrohydraulic actuators are as follows:

1.	Actuator drive area	.188 $in.^2$
2.	Maximum servovalve flow @ 3000 PSI	15 $in.^3/sec.$
3.	Maximum actuator rate	80 in./sec.
4.	Minimum actuator frequency response	$\pm$ 1 db to 60 Hz
5.	Minimum full stroke frequency	20 Hz
6.	Actuator stroke	$\pm$ .25 in.

As shown in FIGURE 2, the load and control actuators for the SMS are solidly coupled together on axis through the coupling block. The block contains a bushing and pin arrangement to allow coupling and decoupling each of the four actuator sections to a bearing supported coupling bar. Stiffness of the supporting framework at the actuator mounting points was designed to be greater than 2×10^6 #/in. The high stiffness is required to prevent load forces from bending the frame to a degree which would misalign and bind the control-load actuator combination. FIGURE 3 shows the framework (without the actuators installed between the ends) and the bearing mounted coupling bar.

To ensure adequate frequency response from the secondary actuators, Model 31 Moog valves have a 90° phase shift at approximately 240 Hz were used. These valves are a two stage servovalve having an amplitude response which is flat within 2 db to 200 Hz.

The hydrostatic bearings were incorporated to eliminate both the cylinder port to low pressure seals in the ends of the actuator and any piston rod friction. The leakage flow from each bearing at 100° F oil temperature was designed to be a maximum of .125 in^3/sec. FIGURE 4 shows the actuator bodies, end caps and hydrostatic bearing housings after machining and prior to assembly.

The SMS incorporates both pressure reducing valves and solenoid shutoff valves for the hydraulic supplies to each of the control channels. FIGURE 5 shows the manifold and valves as installed at the end of the SMS supporting structure. The pressure reducing valves incorporated into the simulator to allow evaluating the effect of varying the hydraulic supply pressure on the performance of a configuration. Note that individual control channel pressure gauges are incorporated into the manifold assembly.

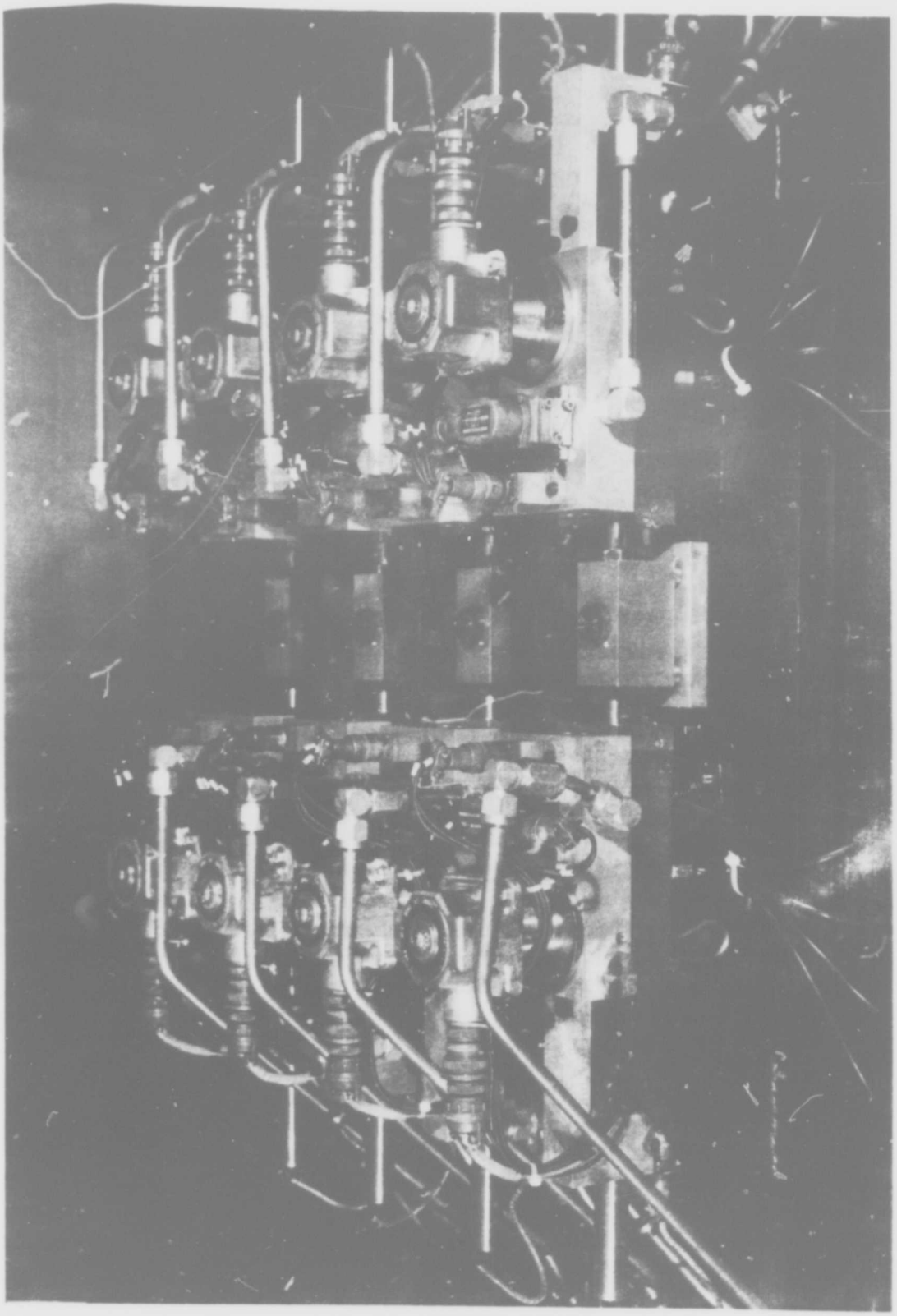

FIGURE 2 SMS Control and Load Actuators

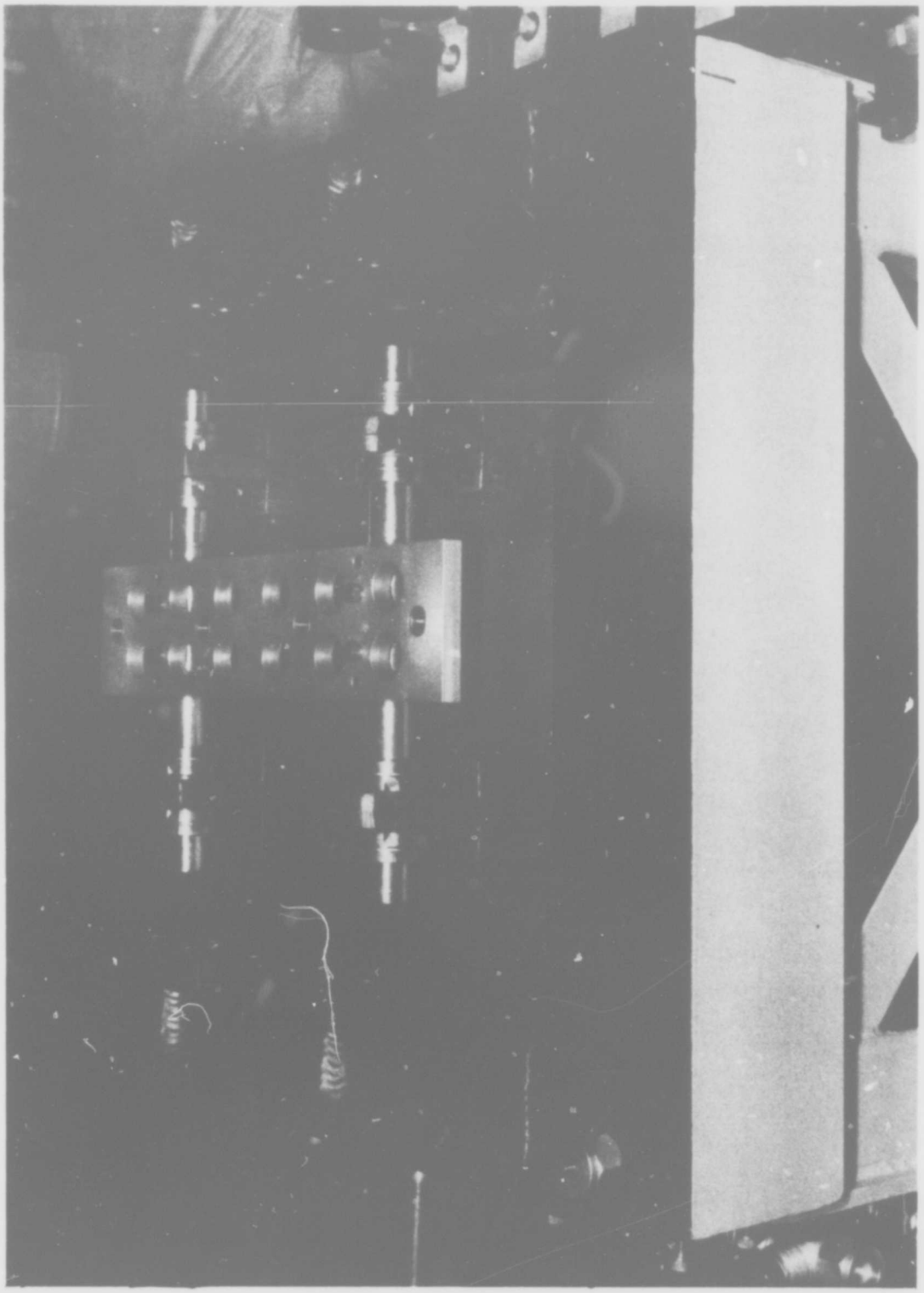

FIGURE 3 SMS Frame and Coupling Bar

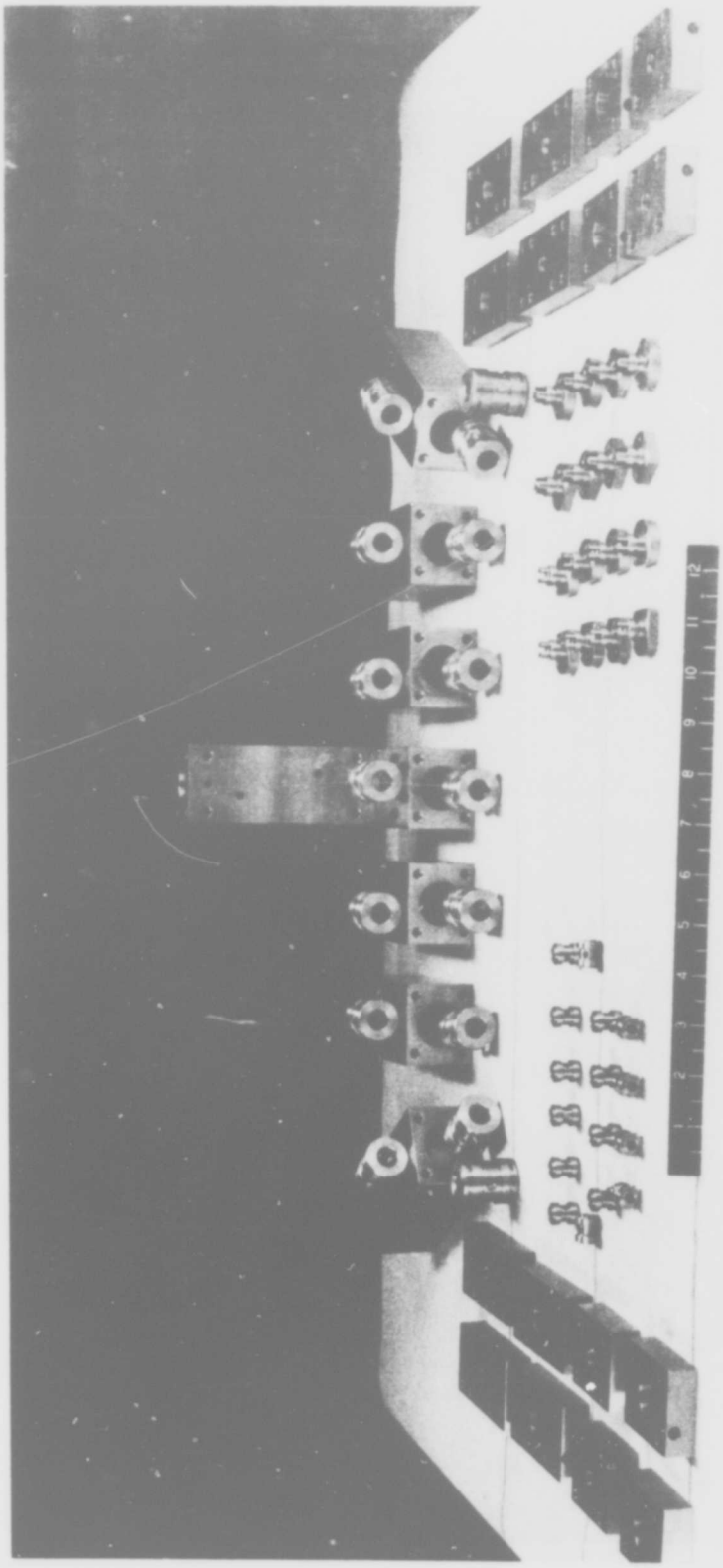

FIGURE 4 SMS Actuator Components

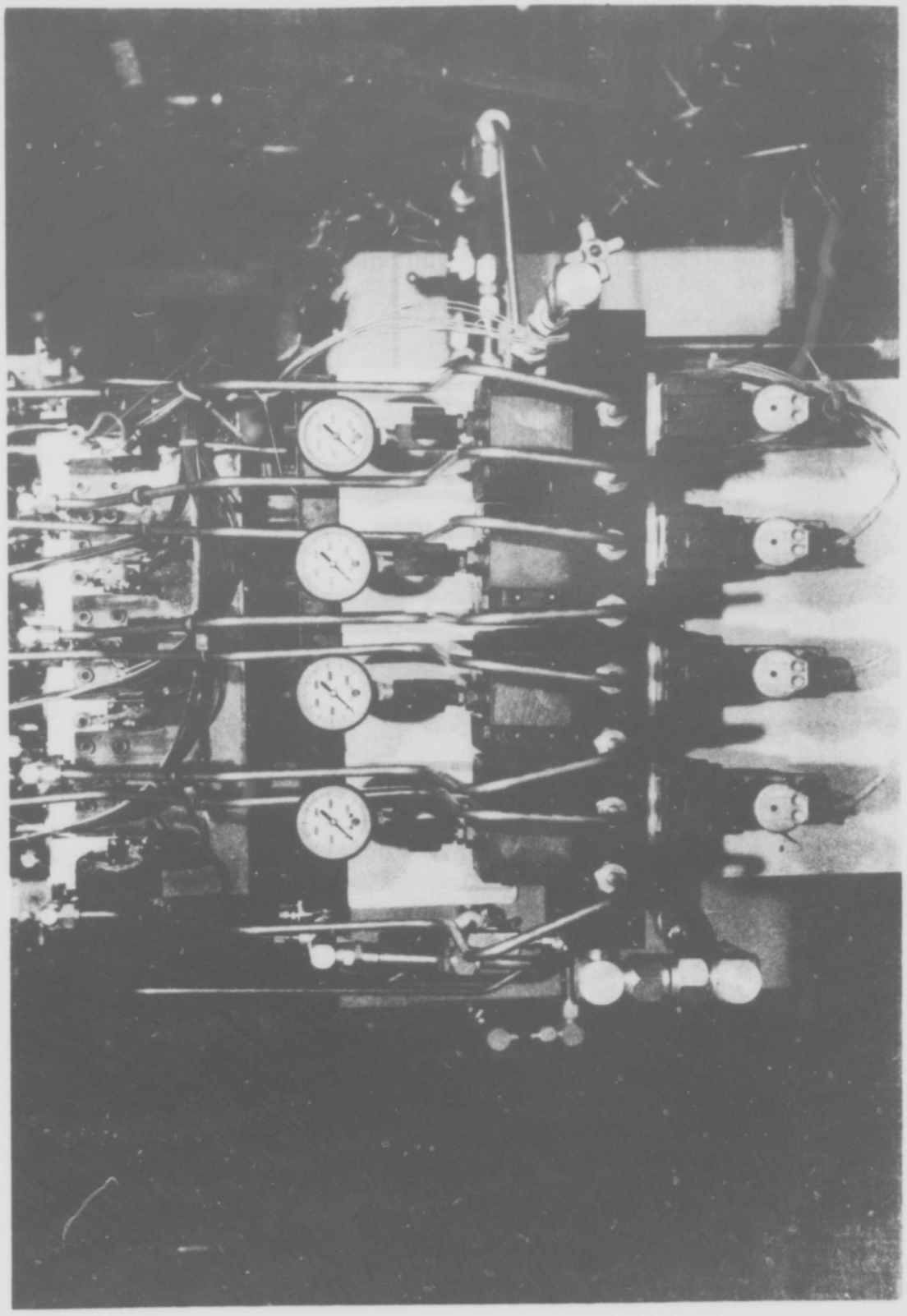

FIGURE 5 SMS Supply Control Manifold

Skinner solenoid valves are installed in the manifolds of each control and load actuator. The solenoid valves allow bypassing the actuator drive areas of the load and control actuators. The load solenoid valves are connected to toggle switches mounted in a hydraulic control panel. This panel, as shown in FIGURE 6, is mounted in the auxiliary control console below the patch panel. The control actuator bypass solenoids are connected to the failure logic unit. By using the failure logic unit test switches, manual bypassing of the SMS control actuators is available.

Since with multiple actuators pinned together it is possible to over-pressure a single actuator, cylinder port pressure relief provisions were designed into each SMS actuator. This was done by using pressure backed check valves. One side of each check valve is connected to an actuator cylinder port. The other side of the check valve is connected to supply pressure. The check valves are designed with 200 PSI cracking pressure so that cylinder port pressure would have to increase 200 PSI above supply pressure before the check valve opens, limiting the cylinder port maximum pressure.

Both the load and control actuators of the SMS have differential pressure transducers mounted on the actuator manifolds. These are connected to cylinder port pressure. For the load actuators, these transducers allow reducing the pressure gain of the control valves by using negative pressure feedback. This allows simulating low pressure gain valves with the high pressure gain two stage control valves.

FIGURE 7 shows an assembled SMS actuator with the solenoid operated bypass valve, servovalve and pressure transducer. The pressure relief check valves are mounted under the round cap at the right end of the manifold.

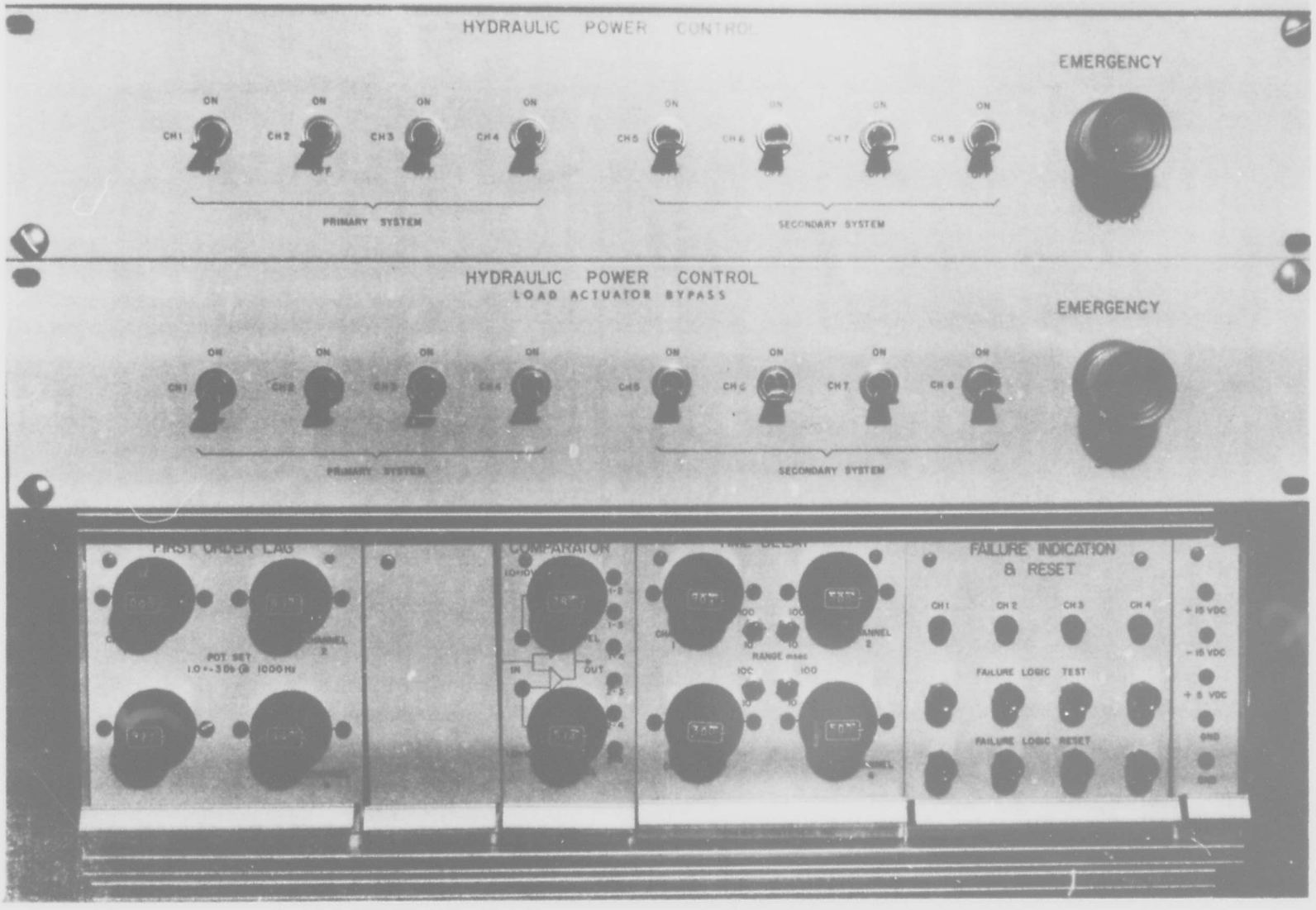

FIGURE 6 Hydraulic Power Control Panels

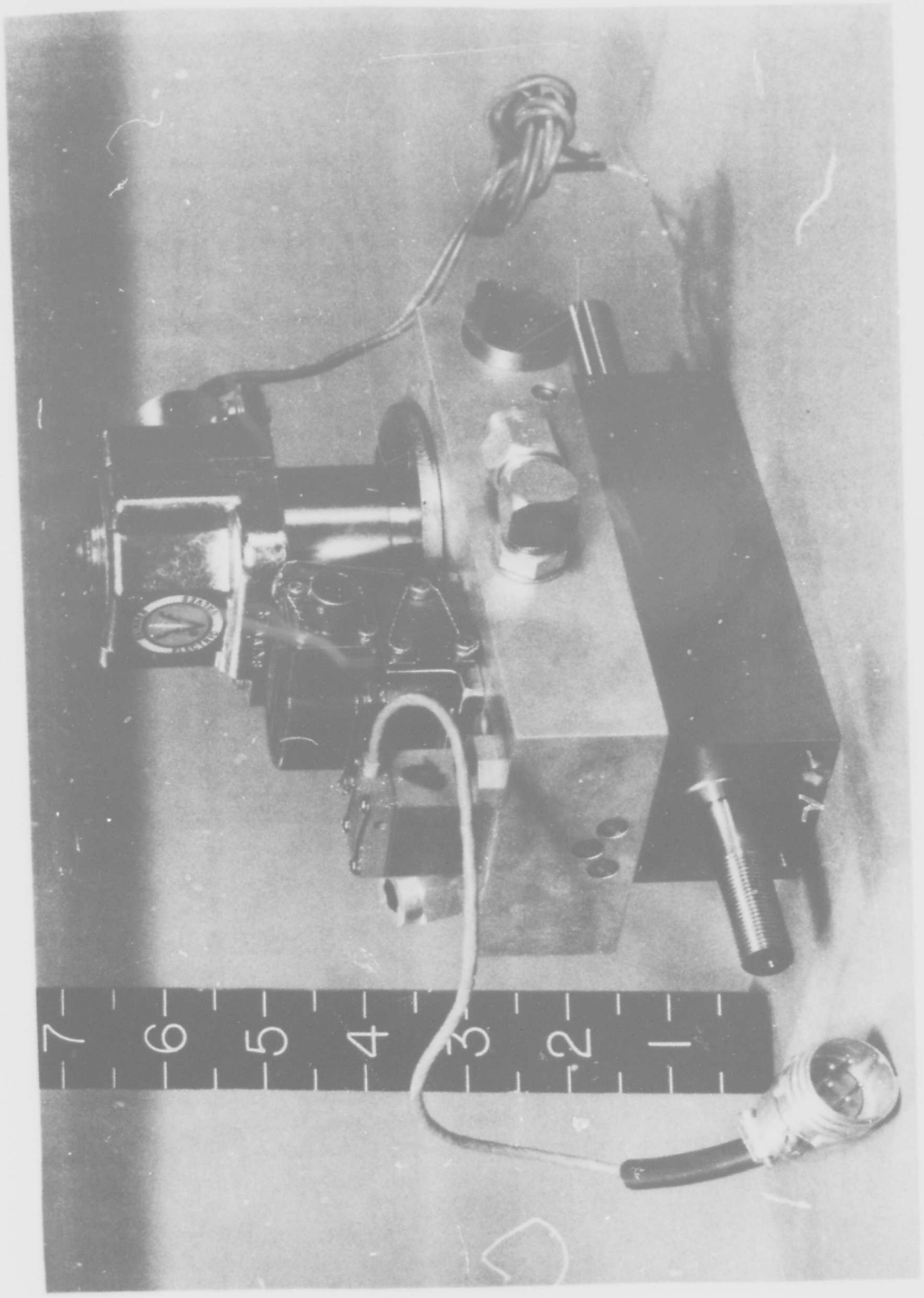

FIGURE 7 Assembled SMS Actuator

1.2.3 PMS Mechanical Description

The general design of the mechanical portion of the PMS is similar to the SMS design. The PMS also uses 8 identical actuators, four for control and four for load. The actuators are fabricated from commercial Sheffer actuator barrels, end caps and piston rods. To minimize actuator threshold, the end seals are replaced with close fitting bronze bushings which act both as rod supporting bearings and laminar path seals. The piston rod seals provided with the piston consist of a split teflon seal and a bronze filled teflon split sleeve. These were retained from the PMS actuators. To accommodate the leakage from the laminar path rod seals, end caps with a drain provision and a seal groove for a low friction Bal seals were fabricated for the end caps. The design values for the PMS electrohydraulic actuators are as follows:

1.	Actuator drive area	.982 $in.^2$
2.	Maximum servovalve flow @ 3000 PSI	31 $in.^3$/sec.
3.	Maximum actuator slow rate	31.6 in./sec.
4.	Minimum small signal frequency response	$\pm$ 1 db to 30 Hz
5.	Minimum full stroke frequency response	5 Hz
6.	Actuator stroke	$\pm$ 1.00 in.

To allow high frequency operation of the PMS actuators, Moog Type 32 valves were used to control the PMS actuators. These valves have a 90^o shift at approximately 175 Hz and an amplitude response which is flat within 2 db to 130 Hz.

As shown in FIGURE 8, the load and control actuators are coupled together through a compliance assembly. The compliance of the assembly is adjustable by changing the coupling spacing on a spring bar used in the compliance assembly. This is accomplished by positioning the two clamping blocks for the spring bar to the position desired for a particular compliance value. The spring bar is supported at the ends by flex supports. These allow the spring to act as a simple end supported beam without any support friction. A similar spring bar, support and clamp arrangement is used at the left end of the control actuators to provide a variable compliance mounting of the control actuator bodies to the mounting structure.

As with the SMS, the PMS load and control actuators are aligned axially in order to eliminate using coupling elements which could produce mechanical free play. The compliance assembly is supported by linear ball bearing bushings which are not required to transmit any force produced by the load or control actuators. The load actuators are connected directly to the center members. (Reference FIGURE 8) Each center member represents the control surface of a flight control system. As shown in FIGURE 8, the four channels of the system are uncoupled from each other. To provide for tying the center members together, mounting holes for coupling bars have been incorporated into each backup bar of the center assembly. Note that "surface" position, rate and acceleration transducers are installed as instrumentation for the motion of the "surface". This allows using the "surface" motion and it's time deriviatives as inputs to the load actuator. This allows to simulating aerodynamic loads and damping as well as surface inertia.

The PMS is constructed in four channels, each containing a control actuator and a load actuator. These modules are mounted on a welded steel framework. To damp structural resonance, the mounting structure is

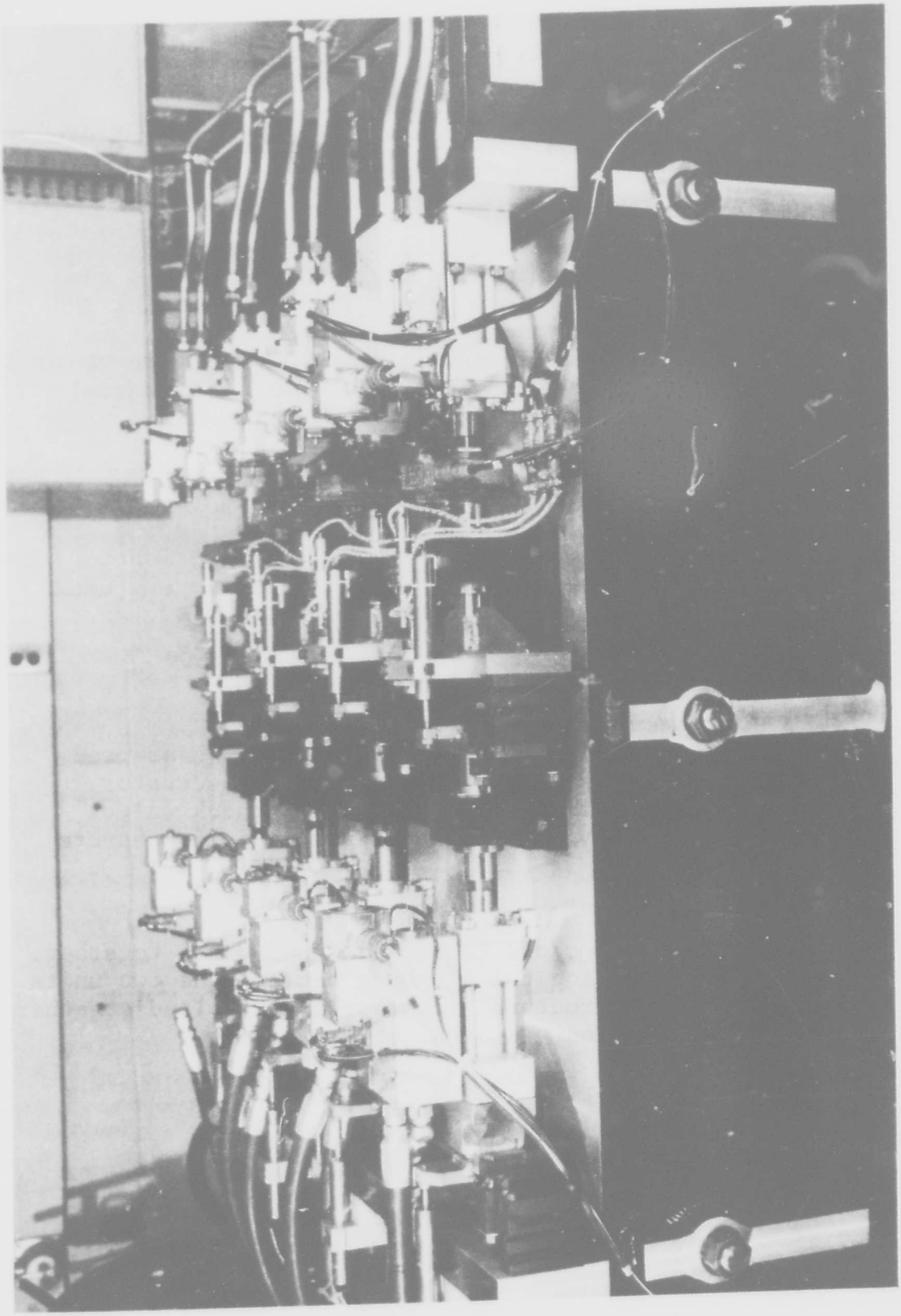

FIGURE 8 The PMS

constructed as a sand box (similar to the SMS structure). FIGURE 9 shows the mounting structure prior to installation of the sand top plate and actuator modules. The PMS structure contains approximately 800 pounds of dry white sand as a damping medium.

To allow evaluating the effects of hydraulic supply pressure variation on the performance of a configuration, the PMS incorporates pressure reducing and solenoid shutoff valves for the supply pressure lines to each control actuator. As with the SMS, pressure gauges for the hydraulic supply pressure to each PMS control actuator are mounted on the solenoid and reducing valve manifold.

The PMS load and control actuators contain a solenoid operated spool bypass valve in each actuator manifold. The spool valve is operated by a Skinner solenoid pilot valve and serves to simultaneously bypass the actuator drive area and block the servovalve flow. The spool is pressure operated and uses no bias springs.

As with the SMS actuators, over-pressure relief check valves are incorporated in each actuator manifold. These are similar to the SMS check valves and use the same type of cylinder port-supply pressure connections.

FIGURE 10 shows the PMS and SMS units together. To prevent distorting the plumbing between the two units, the PMS and SMS structural frameworks are bolted together with two box section tie bars.

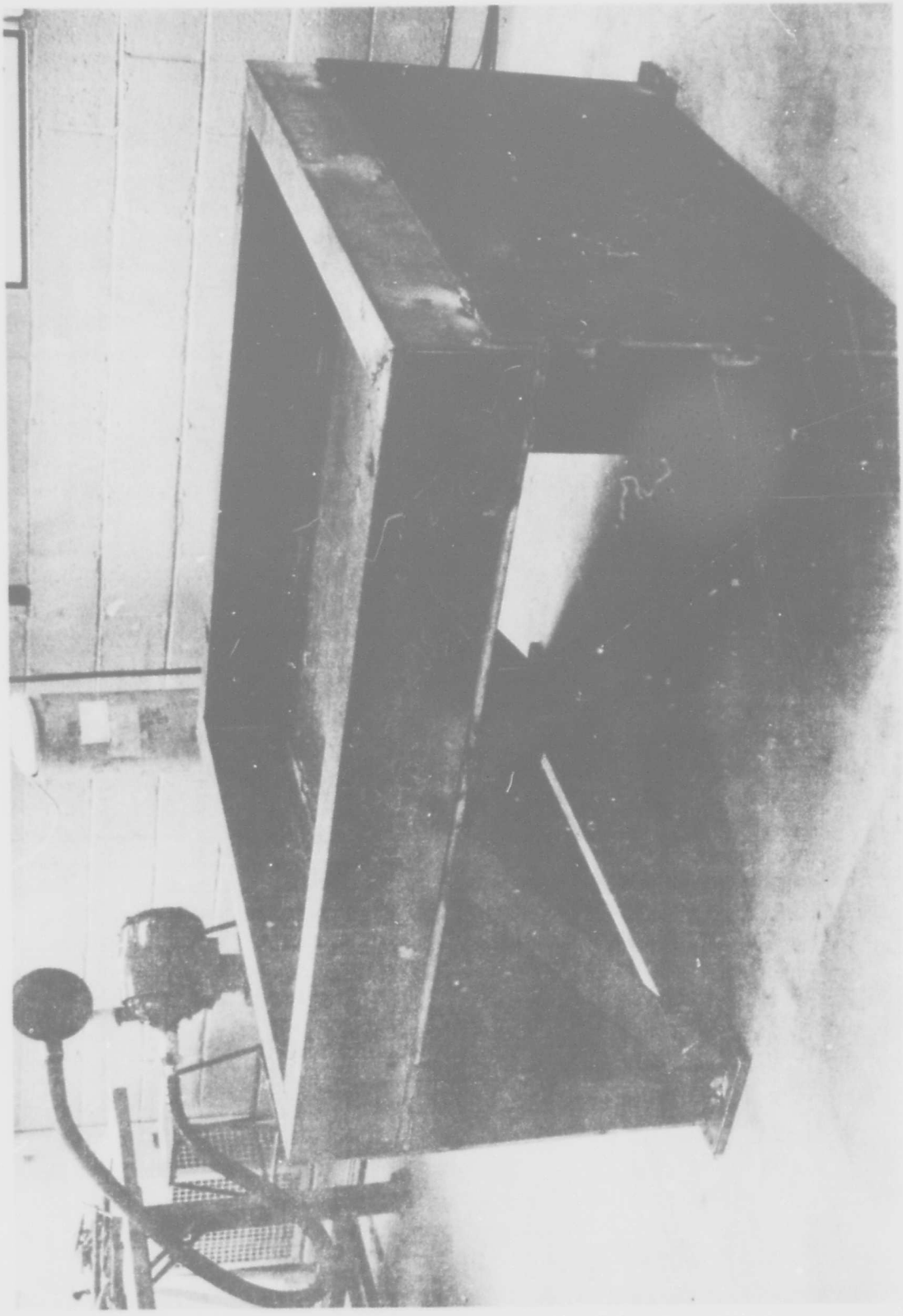

FIGURE 9 PMS Structural Mounting

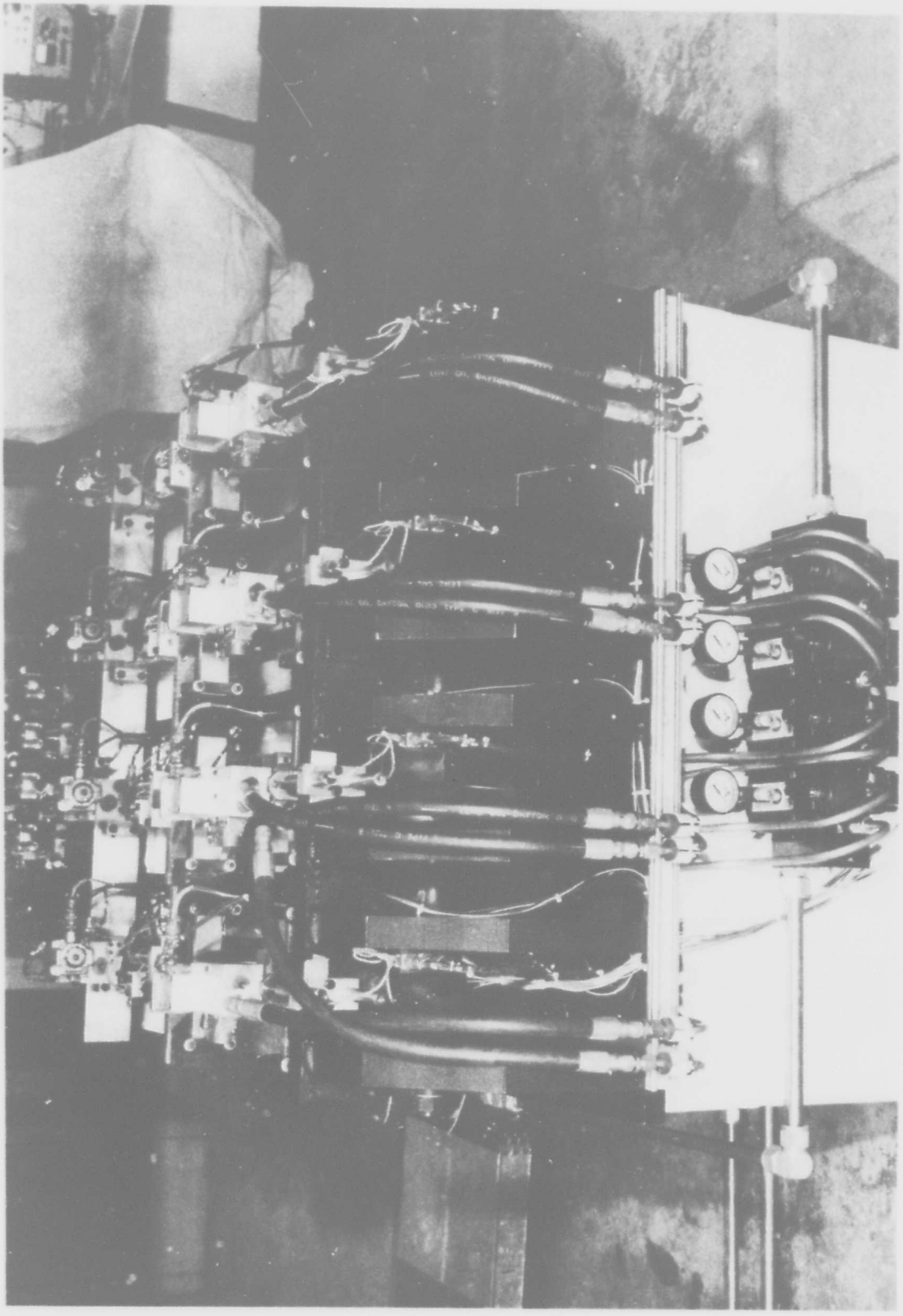

FIGURE 10 PMS End View

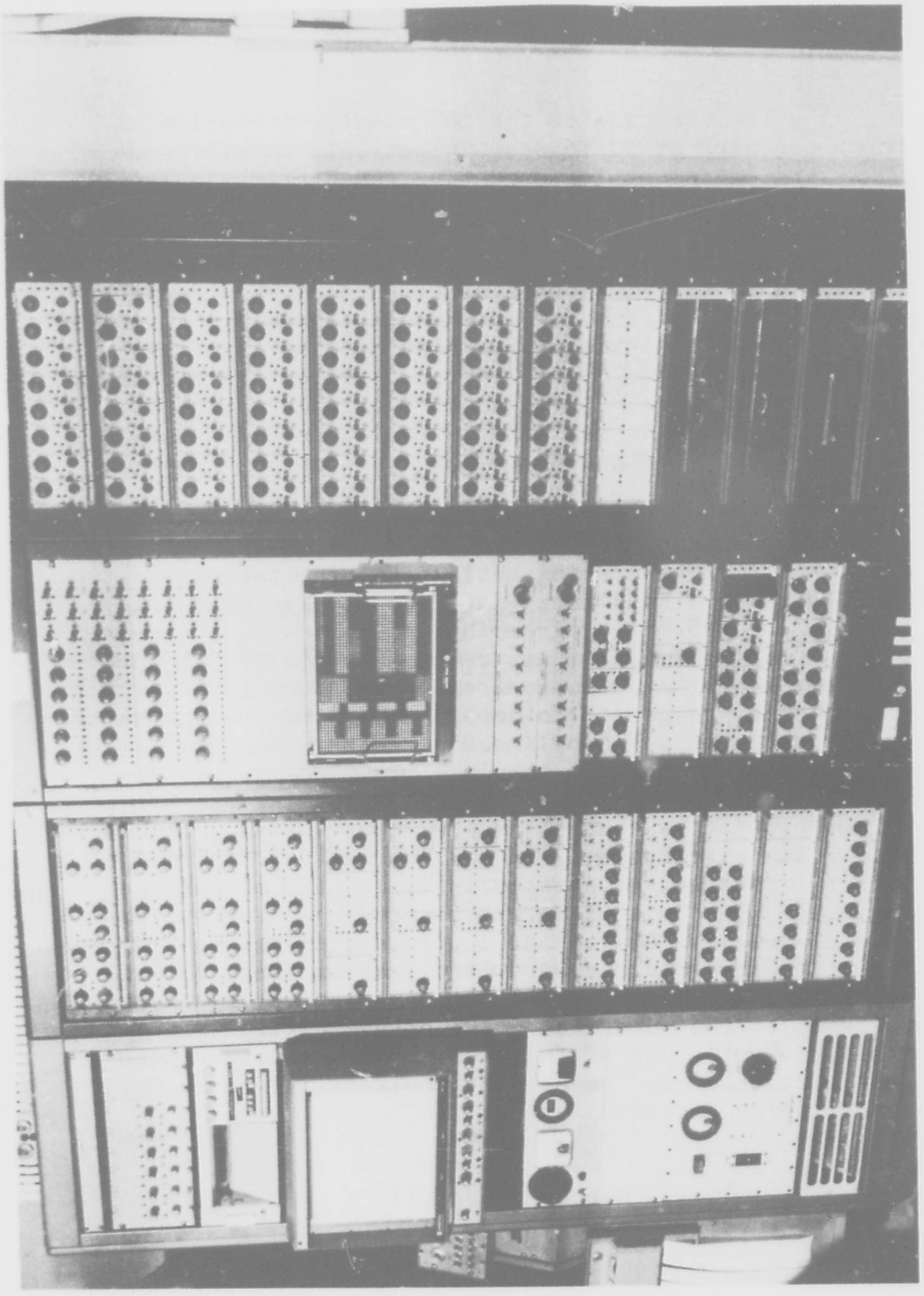

FIGURE 11 Hybrid Simulator Control Consoles

1.2.4 Electronics Design Description

The electronics for the simulator consist of three consoles of solid state electronic modules and auxiliary equipment for operating the hybrid simulator. These consoles are connected by trunk lines through two junction boxes to the SMS and PMS. FIGURE 11 shows the control consoles. The left console (control console) in FIGURE 11 contains the control channel and load channel electronics. The center console (auxiliary console) contains power supplies, hydraulic control panels, a patch panel and two general purpose switch and potentiometer panels. The right console (instrumentation console) contains D.C. and bridge amplifiers and demodulators. The three consoles together use over 400 operational amplifiers in the electronic modules.

In incorporating analog computer techniques into the hybrid simulator (in order to provide flexibility), the normal programming complexity of a general purpose analog computer was reduced by design. Rather than patching the potentiometers, resistors and operational amplifiers together to obtain a desired characteristic, selected linear and non-linear circuits were hard wired into individual plug-in modules. Each module was designed to have unity gain, allowing plugging any particular module into a control loop without changing the loop gain. The circuits used in each module are designed so that the particular characteristics of the circuit can be varied with potentiometers mounted on the front panel of each module. Digital dial drives are used for the potentiometers and the circuit values of the module are established so that the parameter variation value corresponds to the numerical value on the digital dial. Six different types of function modules were designed and fabricated for the hybrid simulator.
The six provided are:

1. Second order filter

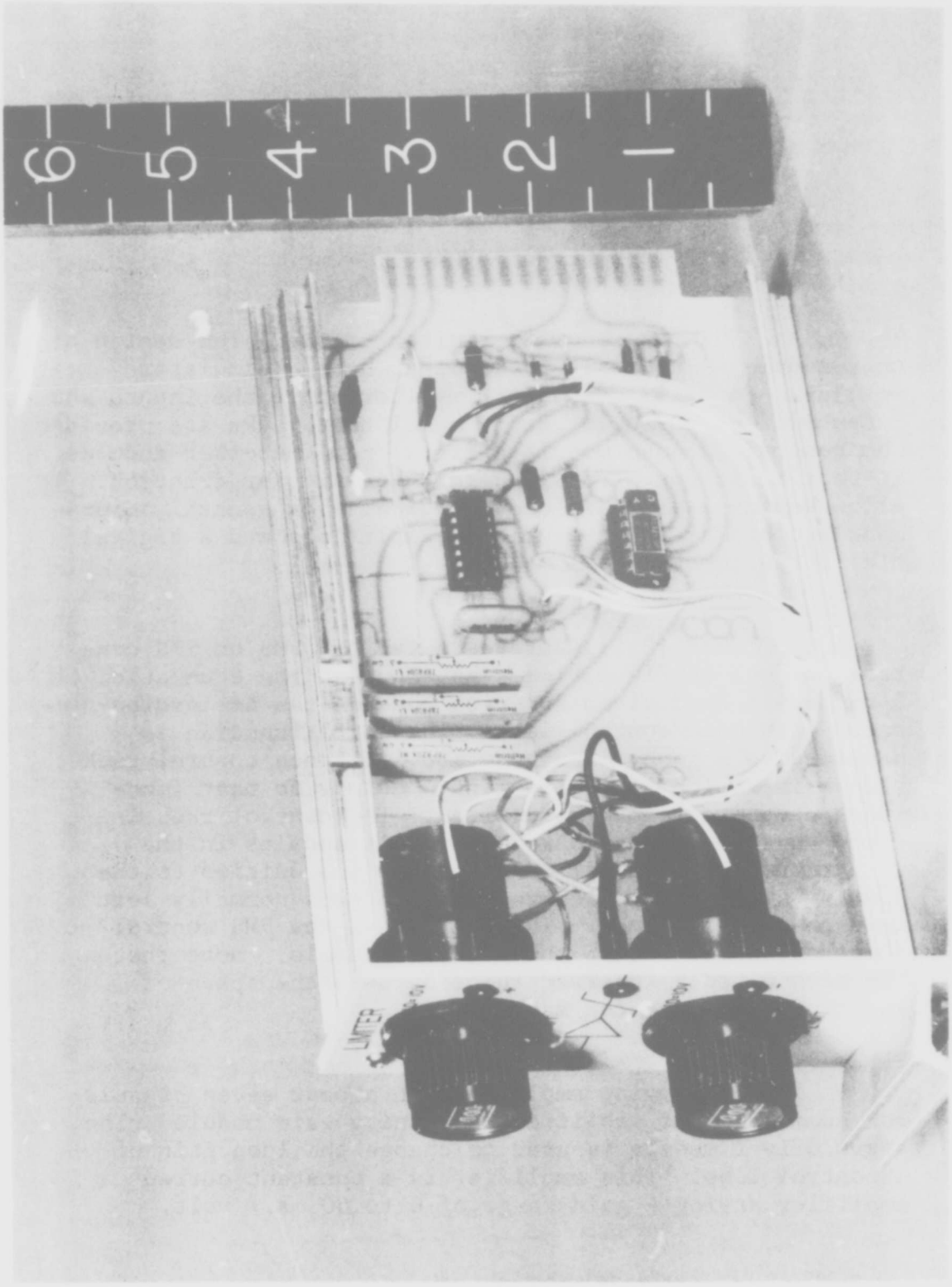

FIGURE 12 Limiter Module

2. Inverter

3. Jumper

4. Dead band

5. Saturation

6. General purpose

FIGURE 12 shows a limiter module. The design of this module is typical of the other hybrid simulator modules. To allow convenient monitoring of the inputs and outputs of each module, front panel test jacks are provided. The general purpose module differs from the other modules in that it is not hard wired for a particular function. To allow wiring a user defined function, each general purpose module contains two operational amplifiers and a digital dial potentiometer.

FIGURE 13 illustrates a typical PMS or SMS control channel configuration. As shown on the schematic, 5 different hard wired function modules can be incorporated into each control loop. The sixth function is provided as a general purpose module. Each control rack allows insertion of 6 different modules, so that functions can be cascaded as desired. The control rack is wired to allow insertion of up to six modules in the forward path. These six modules are in addition to the summing amplifier and servodriver modules normally left in each control rack. FIGURE 14 shows the PMS control electronics section in the control console. Note that the second order inserted function uses the space of any two other inserted modules.

Each summing amplifier can accept seven signals for summing. The amplifier is a unity gain module. The servo driver module is used to change the loop gain of a control loop. This amplifier is a constant current amplifier having a gain range of 0 to 50 ma./ volt.

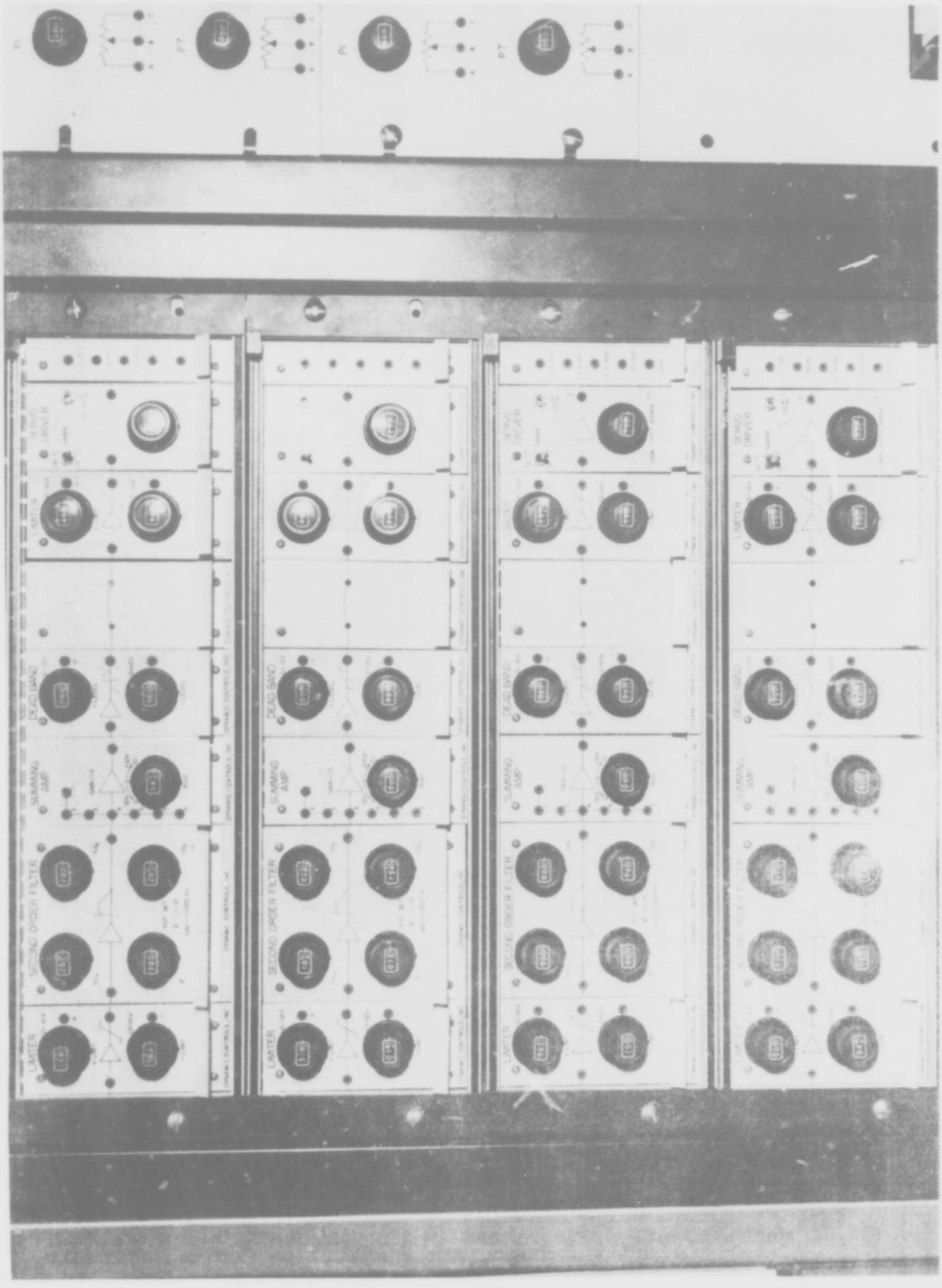

FIGURE 14 PMS Control Electronics

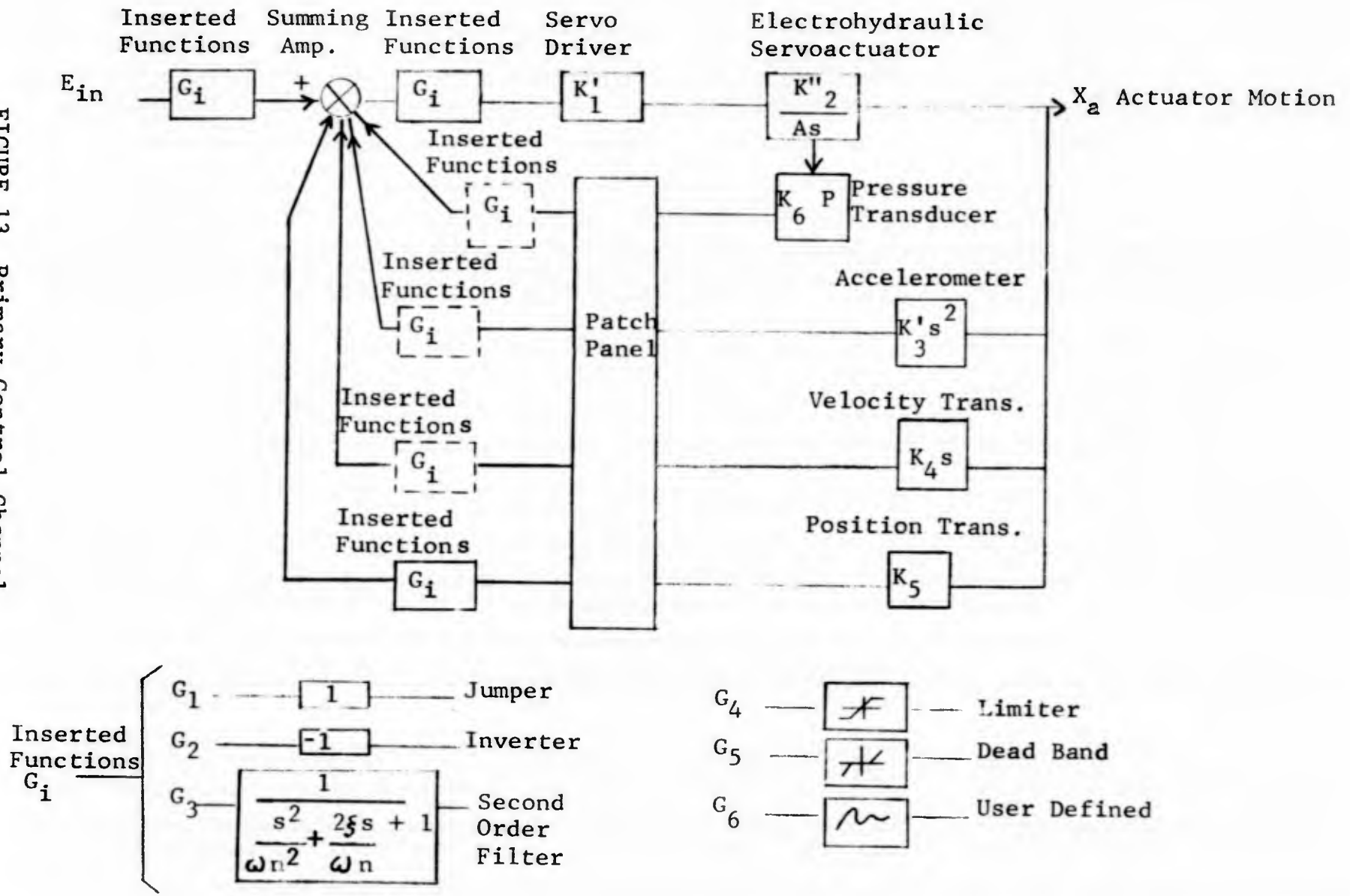

FIGURE 13 Primary Control Channel

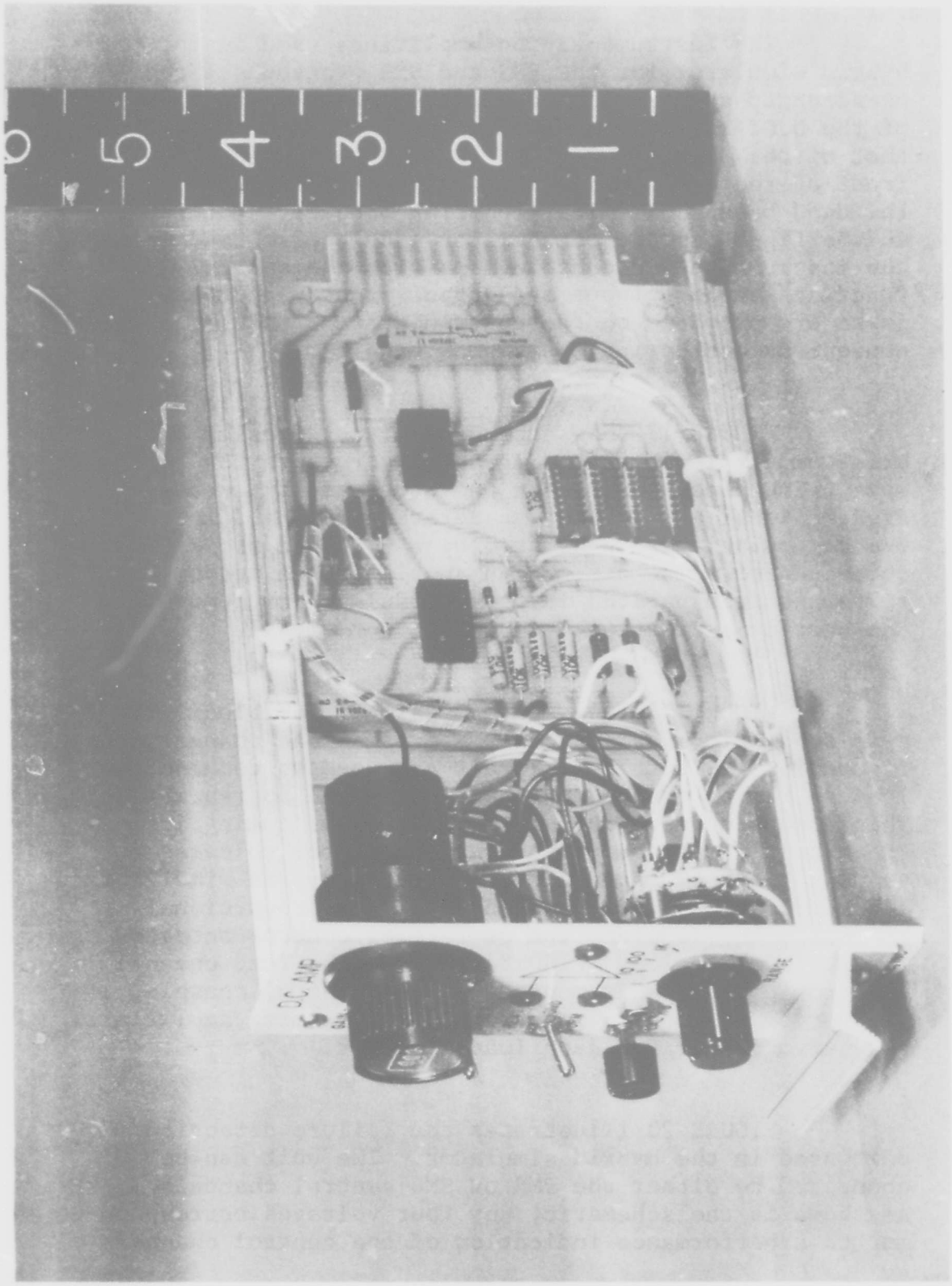

FIGURE 15 D.C. Amplifier

The instrumentation amplifiers used in the hybrid simulator for the PMS and SMS transducers are constructed as plug-in modules. As shown in FIGURE 15 of the D.C. amplifier, the construction is similar to that of the control modules. FIGURE 16 shows the front of the bridge and D.C. amplifiers along with the dead band and limiter function modules. Not shown in the figure is the demodulator module also used in the instrumentation console. As with the control function modules, input and output front panel test jacks are provided on the instrumentation modules for convenient monitoring and signal tracing.

FIGURE 17 shows the demodulator modules and bridge amplifiers mounted in the instrumentation console. The demodulators are based on a multiple design. Signal excitation and reference signals into the demodulator are generated by a 5,000 Hz oscillator connected to a low distortion amplifier. A notch filter is incorporated in the demodulator to remove the carrier excitation from the output signal.

FIGURE 18 illustrates a simplified block diagram schematic of a typical PMS or SMS load channel configuration. Electrical signals are used to command the load system by connecting the patch panel appropriately. This allows using either external signals coming into the hybrid simulator or internal simulator voltages to command the load system. The internal hybrid simulator instrumentation allows commanding loads proportional to postition, acceleration or rate of control actuator (or surface) motion. FIGURE 19 shows the load channel electronic modules as mounted in the control console. The bottom two module racks contain a summing amplifier and servo driver for each load actuator.

FIGURE 20 illustrates the failure detection unit used in the hybrid simulator. The unit can be connected to either the PMS or SMS control channels. As shown in the schematic, any four voltages corresponding to a performance indication of the control channels

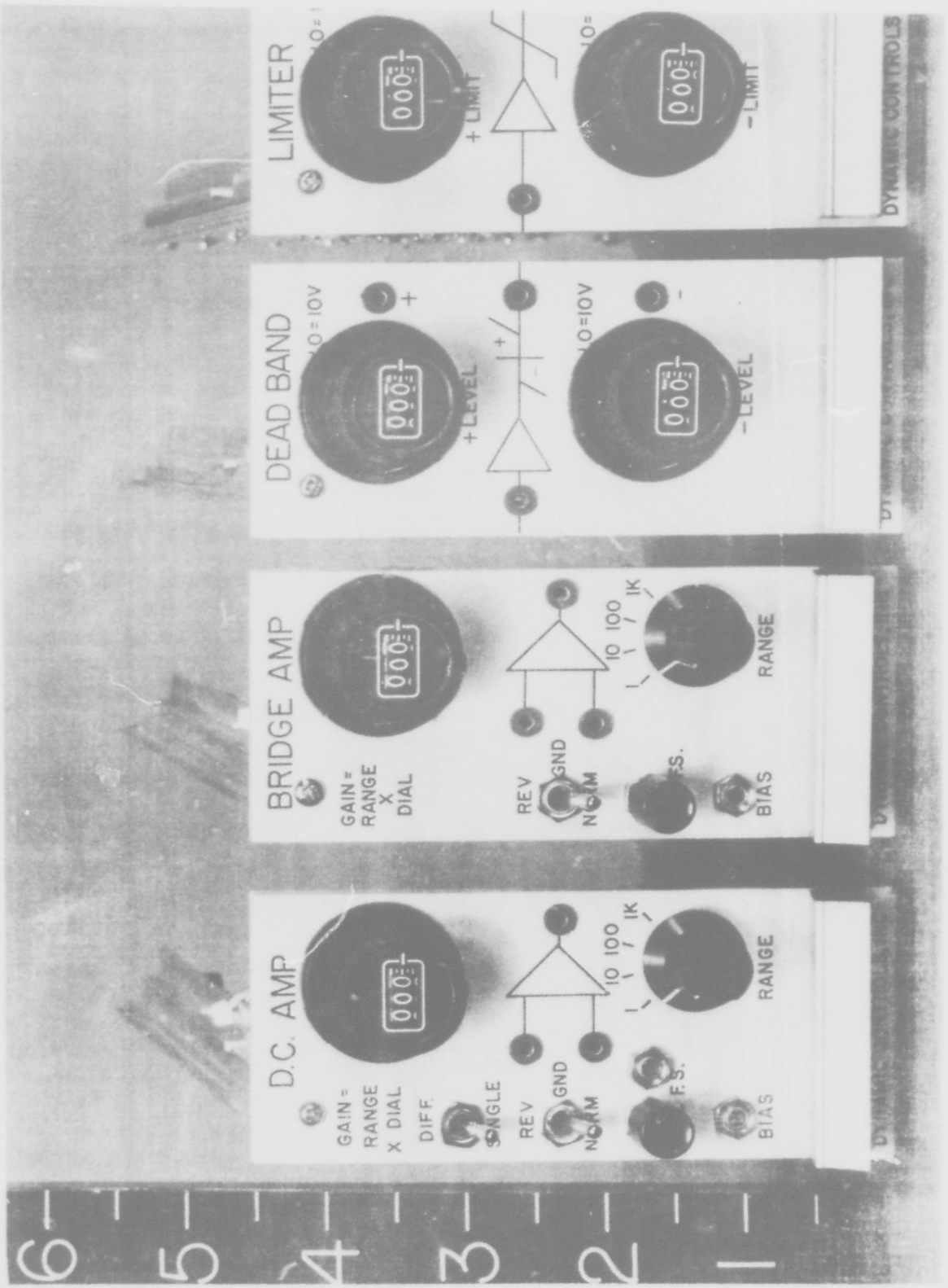

FIGURE 16 Instrumentation and Function Modules

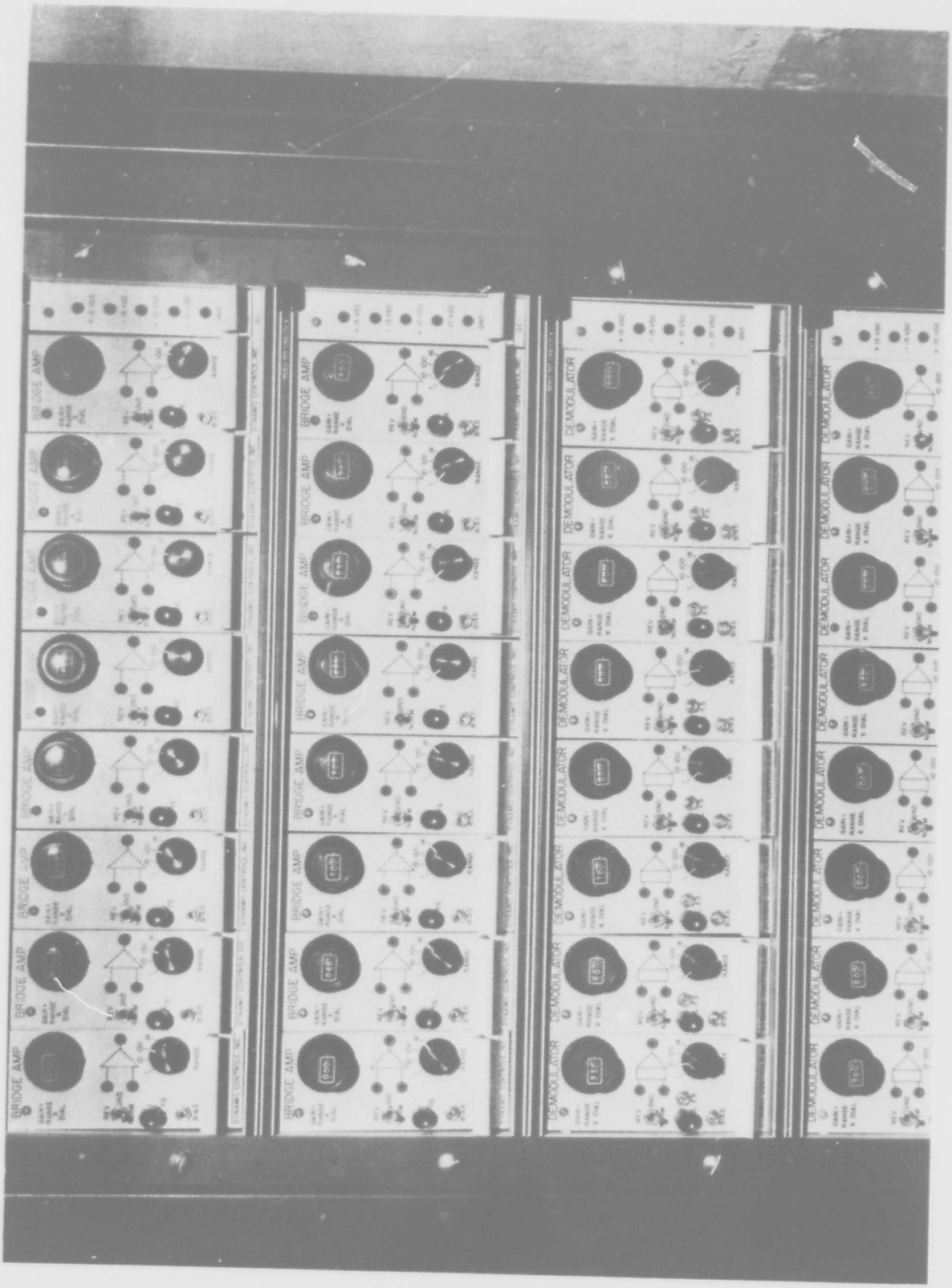

FIGURE 17 Instrumentation Modules in Instrumentation Console

Load Channel Configuration
(Typical PMS and SMS)

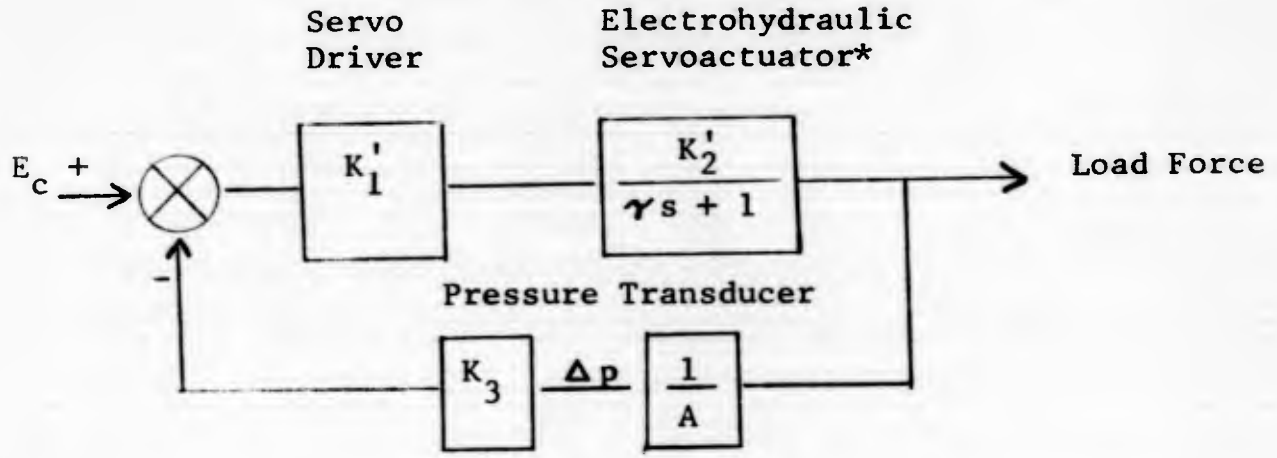

FIGURE 18

K_2' = Open loop force gain of actuator

E_c = Load command signal voltage

K_1' = Servo Driver variable gain

K_3 = Pressure transducer conditioned output gain (variable)

γ = Time constant

A_1 = Load actuator area

*Approximate transfer function for small actuator motions.

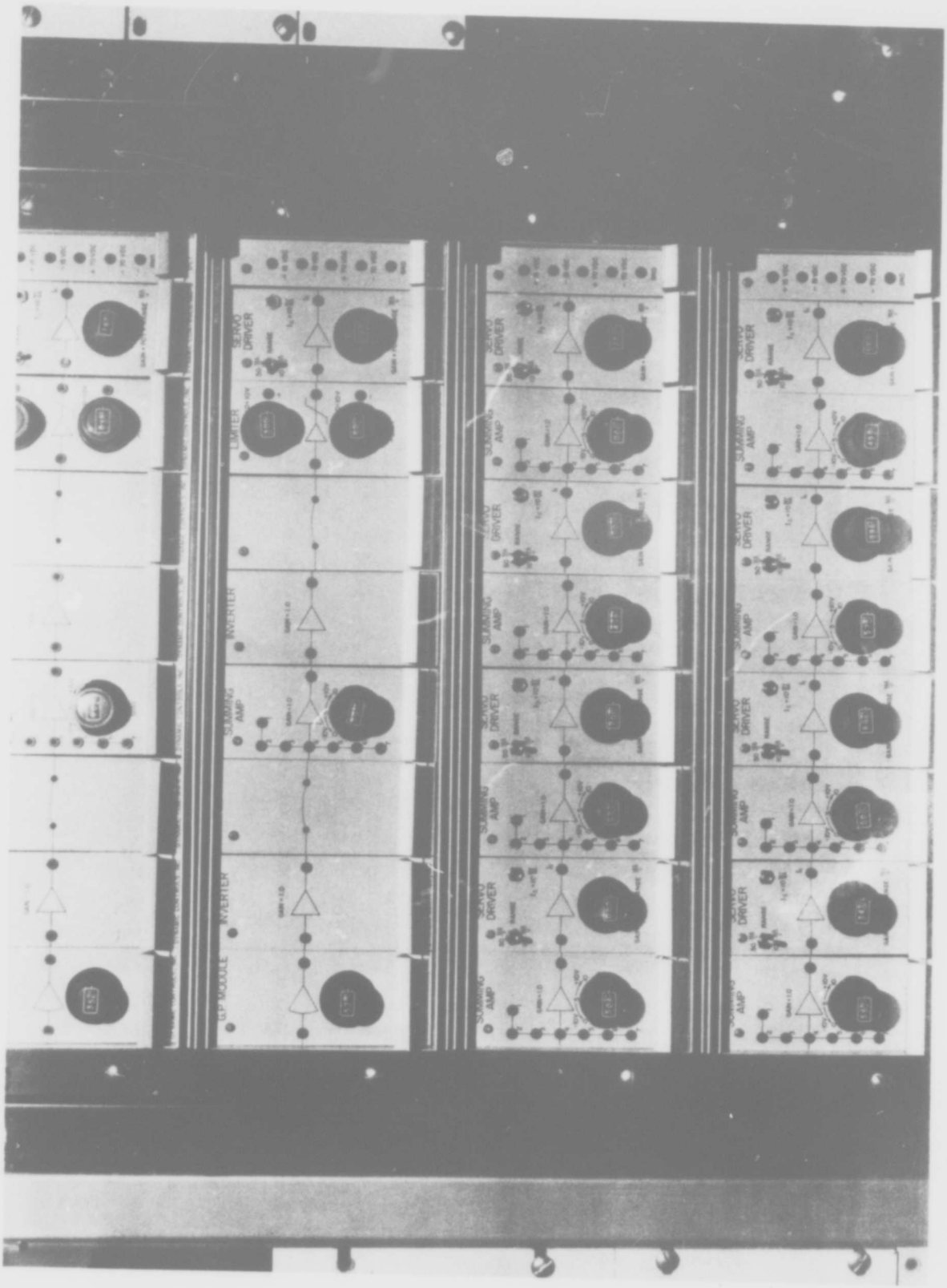

FIGURE 19 Load Control Electronic Modules

FAILURE DETECTION UNIT SCHEMATIC

* τ variable
** Detection threshold variable
*** T_d variable

FIGURE 20

can be connected to the failure detection unit. The unit then compares the "performance voltages" and votes on the agreement between the voltages. A failed channel causes the unit to disconnect that channel using the solenoid valves incorporated in the PMS and SMS electrohydraulic actuators. Upon a channel failure and transfer, the failure indication light is illuminated for the channel having the failure. This light remains on until the failure is removed and the logic reset. To provide a short transfer time for the solenoid switching, the solenoid drivers are constructed with current feedback and a 70 volt driving voltage. This provides a shorter solenoid transfer time than the normal 28 volt solenoid driver. The unit contains first order lag filters with a variable break frequency, comparators with a variable amplitude threshold and a variable time delay between the output of the logic and the solenoid transfer switch. The filtering and time delay allow setting the unit to ignore low amplitude level, high frequency content and/or short duration disagreement between the monitored performance voltages. The failure unit is mounted below the patch panel and the hydraulic control panel in the auxiliary console (Reference FIGURE 6). Status of the control system failures and operational test of the logic is provided by the failure indication and reset section of the failure unit.

Mounted in the auxiliary console is the patch panel used to interface instrumentation with the control and load channels and connect the hybrid simulator with external input and output lines. The panel is connected to trunk lines allowing plug-in connection to two Systron Donner 40/80 analog computers. This allows local simulation of simple aircraft dynamics and the evaluation of the effect of flight control system configuration on the aircraft motion. The patch panel also contains patching provisions for external instrumentation including connections to a servo-analyzer and 8 channel brush recorder. To allow interfacing with external inputs, two general purpose switch and potentiometer panels are provided above the patch panel with the switch and potentiometer

terminals connected to the patch panel. As shown in FIGURE 21 , these general purpose panels incorporate front panel test jacks for signal monitoring.

Besides providing the external interface patching provisions for the hybrid simulator, the patch panel is used for internal patching. The outputs from the instrumentation console modules are connected by the patch panel to the control channel and load channel modules for control feedback and command signals. The patch panel also allows patching the failure logic unit to the desired monitoring voltages for failure detection and transfer. Each section of the patch panel (corresponding to a particular set of input, output or instrumentation lines) is color coded for easy location and identification. All patching pins are arranged in matrix (row-column) for easy location and identification.

The trunk lines between the consoles and the PMS and SMS pass through two junction boxes. FIGURE 22 shows the junction boxes with the PMS junction box open. As shown in the picture, terminal strips are used for each wire junction connection. For each wire, the center and the shield are connected separately to the terminal strip. The terminal strip connections are grouped by function. The terminal strip construction was selected to allow convenient signal tracing of the voltages to and from the PMS and SMS.

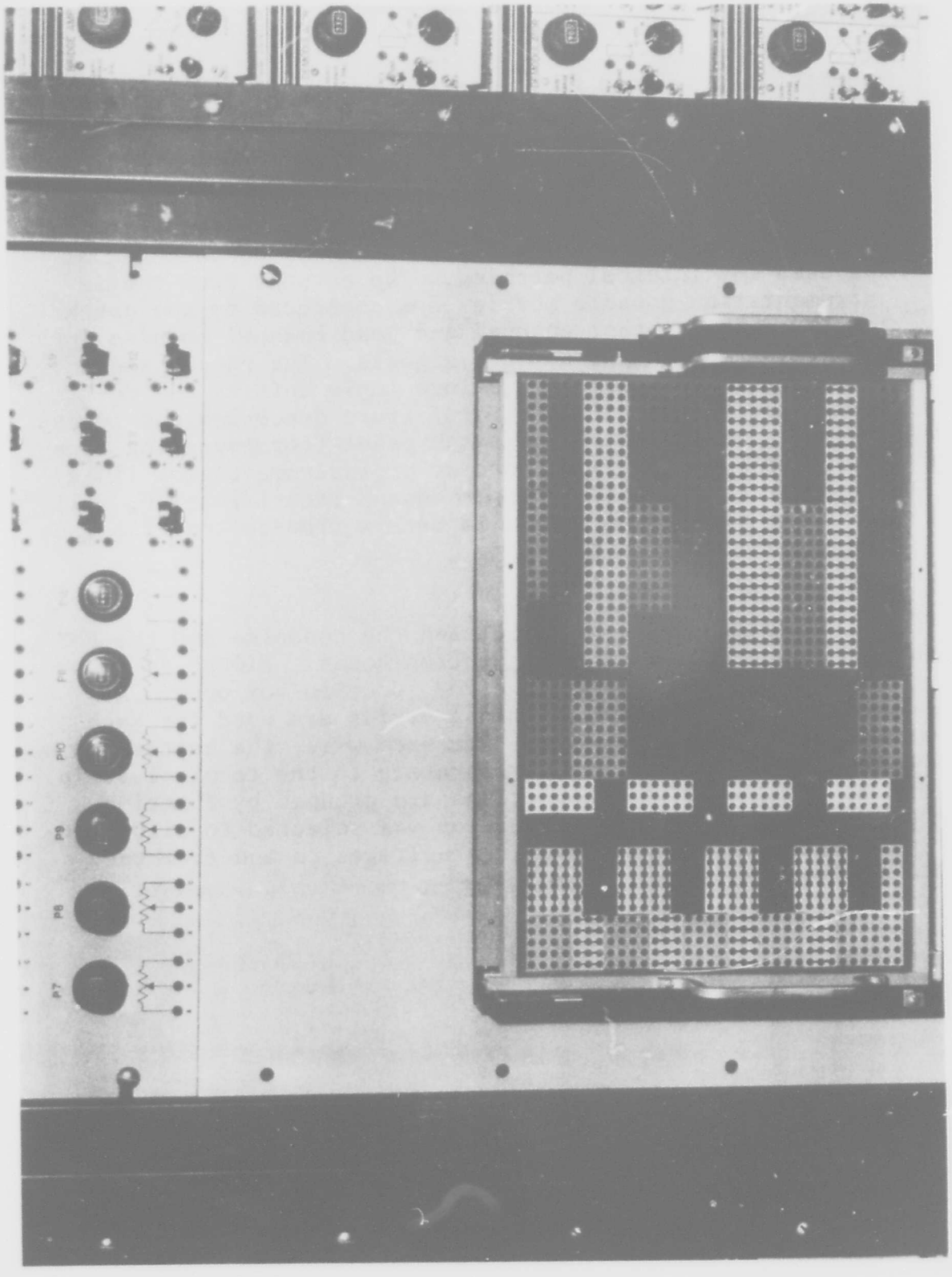

FIGURE 21 Simulator Patch and General Purpose Switch and Potentiometer Panel

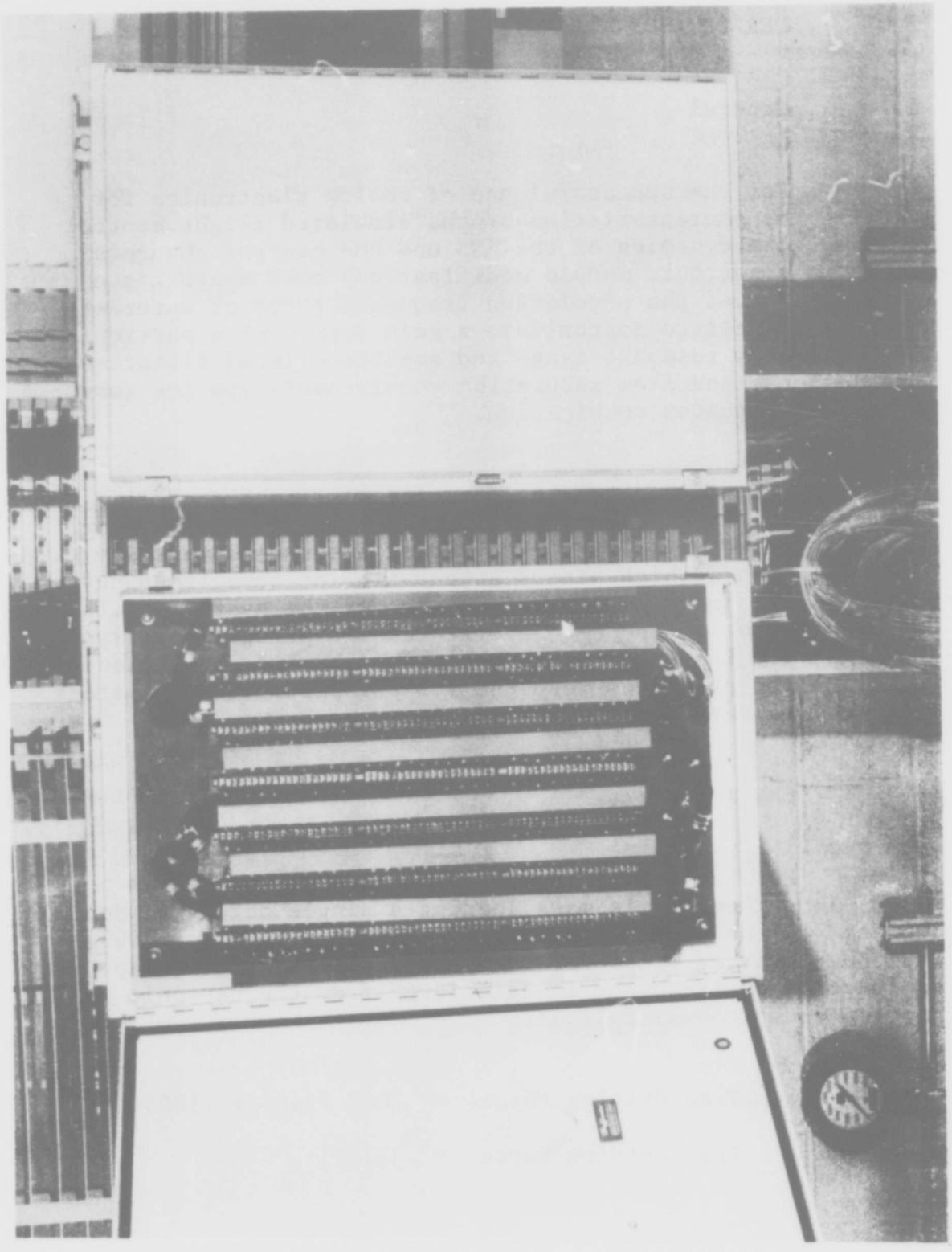

FIGURE 22 SMS and PMS Junction Boxes

2.0 PERFORMANCE ANALYSIS

2.1 General

For the successful use of analog electronics for varying the characteristics of the simulated flight control system, the dynamics of the SMS and PMS control channels (without electronic module modification) must approximate gain terms over the simulation frequency range of interest. The requirement to approximate a gain term over a particular frequency response range and amplitude level dictates the response and flow saturation requirements for the servovalve and actuator combination.

Secondary actuators for typical flight control systems have a frequency response which starts attenuating at some frequency below 20 Hz. Power actuators generally have a response which starts attenuating at some frequency below 5 Hz. The design requirements for the hybrid simulator were that the PMS and SMS have at least typical flight system response for its actuators. The following two subsections describe the predicted response for the particular actuators and servovalves used for the simulator.

2.2 SMS Actuators

For the secondary actuators, the drive area is .1885 in^2. The dynamic mass loading a single actuator when coupled to the coupling bar is .0373 # sec^2/in. For 2000 PSI peak driving pressure, the peak stroke limitation as a function of frequency is calculated from the harmonic motion equations as follows:

a. Peak driving force = 2000 #/in^2 x .1885 in^2

Peak driving force = 377 #

b. Available stroke

$$\hat{F} = m \hat{a}$$

Equation (a)

Where: $\hat{F}$ = peak driving force (377 #)

m = mass (.0373 # $sec.^2/in.$)

$\hat{a}$ = peak acceleration

For sinusoidal motion

$$\hat{a} = (2\pi f)^2 \hat{x}$$

Equation (b)

Where: f = frequency in Hz

$\hat{x}$ = peak stroke

c. Combining the preceding equations (a) and (b) substituting in the values:

$$\left[f^2 \hat{x} = 255.9\right]$$

Equation (c)

The stroke available as a function of frequency as limited by the available servovalve flow is also calculated from the harmonic motion equations.

a. Peak velocity $= \hat{\dot{x}} = 2\pi f \hat{x}$

Equation (d)

Where: f = frequency in Hz

$\hat{x}$ = peak stroke

b. Peak flow $= Q = A \hat{\dot{x}}$

Equation (e)

Where: A = actuator area ($.1885$ in.^{2})

$\hat{\dot{x}}$ = peak velocity

c. Combining equations (d) and (e) for a valve flow of 15 in.^{3}/sec. (available from a Moog Model 31 valve with 1000 PSI pressure drop across the valve):

$$\hat{Q} = A \hat{x} 2\pi f$$

$$\left[f \hat{x} = 12.66 \right]$$

Equation (f)

A plot of equation (c) for the mass limited deflection and equation (f) for the flow limited deflection (for the design actuator area, loading mass and servovalve) is shown in FIGURE 23.

Note that the peak stroke of the SMS actuator at high frequencies is limited by the available force rather than flow. In actual SMS use, the force limit does not occur. The coupling bar is used only with two or more actuators attached to it. increasing the driving force available to accelerate the coupling bar mass.

2.3 PMS Actuators

For the primary actuators, the drive area is .982 $in.^2$ The dynamic mass loading of a single actuator when coupled solidly to the output member and supporting frame is .0957 # $sec.^2$/ in. For 2000 PSI peak driving pressure, the peak stroke limitation as a function of frequency is calculated from the harmonic motion equations as follows:

a. Peak driving force = 2000 #/$in.^2$ x .982 $in.^2$

b. Peak driving force = 1964 #

b. Available stroke

$$\hat{F} = m \hat{a}$$

Equation (a)

Where: $\hat{F}$ = peak driving force (1964 #)

m = mass (.957 # $sec.^2$/in.)

$\hat{a}$ = peak acceleration

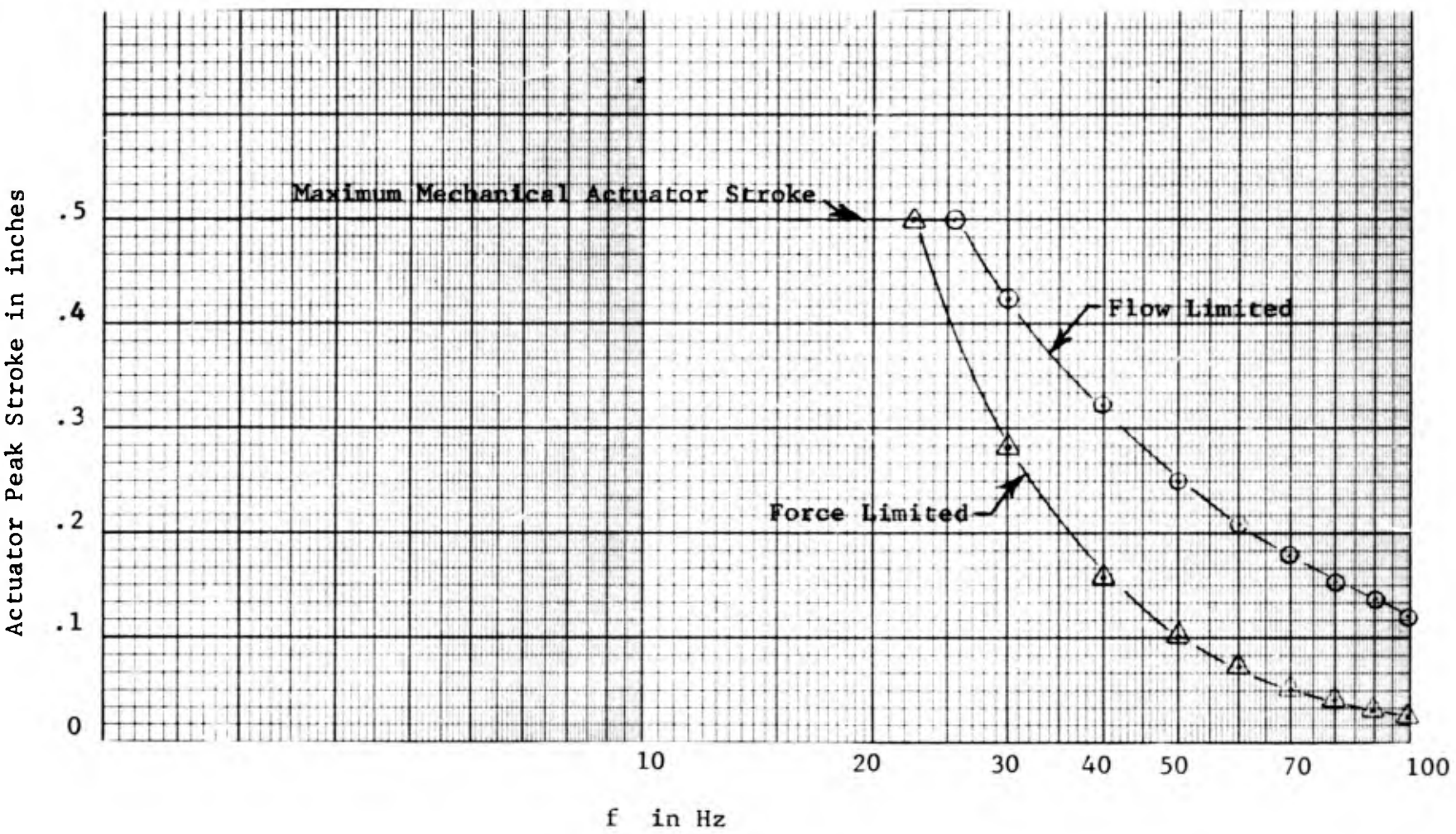

FIGURE 23 SMS Actuator Response

For sinusoidal (harmonic) motion $\hat{a} = (2\pi f)^2 \hat{x}$

Where: f = frequency in Hz

$\hat{x}$ = peak stroke

c. Combining equations a and b and substituting in the PMS parameter values:

$$\left[f^2 \hat{x} = 519.96\right]$$

Equation (c)

The stroke available as a function of frequency as limited by the available servovalve flow is also calculated from the harmonic motion equations.

a. Peak velocity = $\hat{\dot{x}} = 2\pi f \hat{x}$

Equation (d)

Where: f = frequency in Hz

$\hat{x}$ = peak stroke

b. Peak flow = Q = $A \hat{\dot{x}}$

Equation (e)

Where: A = actuator area ($.982 \text{ in}^2$)

$\hat{\dot{x}}$ = peak velocity

c. Combining equations (d) and (e) for a valve flow of 31 $in.^3/sec.$ (available from a Moog Model 32 valve with 1000 PSI pressure drop across the valve):

$$\hat{Q} = A \hat{x} 2\pi f$$

$$\left[f \hat{x} = 5.02 \right]$$

Equation (f)

A plot of equation (c) for the mass limited deflection and equation (f) for the flow limited deflection (for the design PMS actuator area, loading mass and servovalve) is shown in FIGURE 24.

As shown in FIGURE 24, the PMS control actuators are flow, rather than force limited. This is a direct result of using commercial cylinders with a drive area of .982 $in.^2$ This was the smallest available drive area with the 1 in. diameter piston rod (required for column stiffness). A .5 $in.^2$ drive area actuator would more closely match the flow and force limit boundaries. However, the PMS actuators used will meet the 5 Hz "no attenuation" requirement for the simulator. In addition, the maximum stroke of the PMS control actuator can be limited electrically to any selected value. For example, at an electrical stroke limit of $\pm$ .5 inches, the apparent frequency response with no saturation will be above 10 Hz.

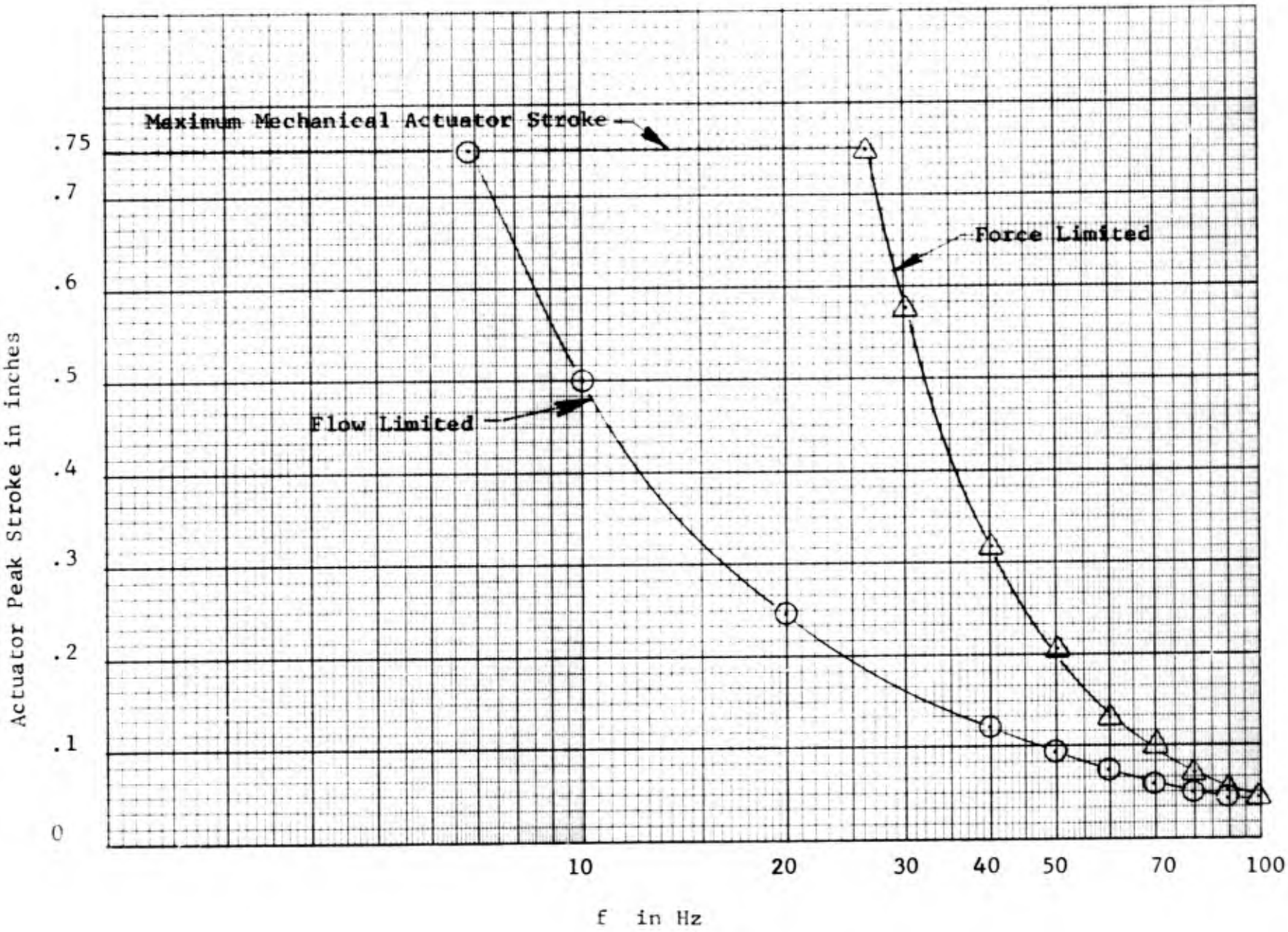

FIGURE 24 PMS ACTUATOR RESPONSE

2.4 PMS Control Actuator and Surface Member Frequency Response

To predict the frequency response for the PMS control actuators before actual hardware testing, a mathematical model of a PMS control channel was developed. This model was then evaluated by computer program for response of the surface member and actuator position for different settings of the compliance couplings and several actuator position loop gains. The mechanical diagram for the PMS which was used for writing the force equations is the following:

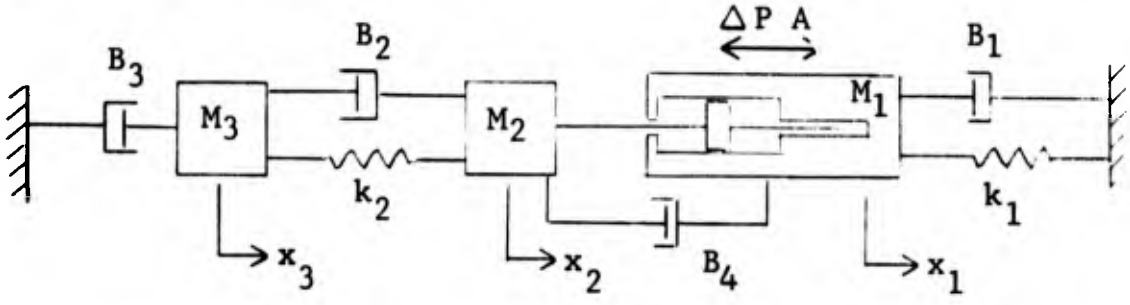

Where: M_1 = Mass of actuator body (.0642 # sec^2/in.)

M_2 = Mass of surface member (.0295 # sec^2/in.)

M_3 = Mass load elements (.0512 # sec^2/in.)

x_1 = Control actuator body motion

x_2 = Control actuator piston motion

x_3 = Surface member motion

k_1 = Actuator to structure spring rate (5,000 to 200,000#/in.)

k_2 = Actuator piston to surface spring rate (5,000 to 200,000 #/in.)

B_1 = Damping of body to structure motion

($.2534 \sqrt{k_1}$ # sec./in.)

B_2 = Damping of control actuator piston to surface motion

($.0172 \sqrt{k_2}$ # sec./in.)

B_3 = Damping of surface motion to structure (.03 # sec./in.)

B_4 = Damping of actuator piston to actuator body (.03 # sec./in.)

A = Actuator drive area

ΔP = Differential pressure across actuator piston

The values of B_1 and B_2 were selected to give a damping ratio of .05 for the resonance of M_1 and M_2 on k_1 and k_2 respectively. Damping values for B_3 and B_4 are selected to be low values of damping in order to emphasize any peaking in the response which might be masked by a high damping value.

From the mechanical diagram, the force equations are:

$$\left[M_1 S^2 + (B_1 + B_4) S + k_1\right] x_1 - B_4 S x_2 = -\Delta P A$$

Equation (a)

$$-B_4Sx_1 + \left[M_2S^2 + (B_2 + B_4)S + k_2\right] x_2 - (B_2S + k_2)x_3 = \Delta P\ A$$

Equation (b)

$$-(B_2S + k_2)x_2 + \left[M_3S^2 + (B_2 + B_3)S + k_2\right]\ x_3 = 0$$

Equation (c)

In addition to the preceding force equations, the following actuator flow demand equation is used for the math model of the PMS actuator:

$$Q_i = AS\ (x_2 - x_1) + C_3S\ \Delta P\ \ +\ \ C_4\ \Delta P$$

Equation (d)

Where:

- A = Actuator area (.982 $in.^2$)
- C_3 = $\frac{V}{4\ \beta}$ (2.45 x 10^{-5} $in.^4/\#$)
- V = Volume of fluid in actuator (1.5 $in.^3$)
- β = Bulk Modulus of oil (150,000 $\#/in.^2$)
- C_4 = Leakage coefficient (0)
- x_2 = Actuator piston motion relative to structure
- x_1 = Actuator body motion relative to structure
- Q_i = Flow from valve

The output flow of the control valve (for small signal levels) is described by the equation:

$$Q_i = C_5 \; x_{sp} - C_6 \Delta P$$

Equation (e)

Where: Q_i = Output flow

C_5 = Flow gain coefficeint (2688 $in.^3$ amp./sec.)

C_6 = Load sensitivity coefficient (.00128 $in.^5/\#sec.$)

In addition to the preceding equations (a) through (e), the frequency response of the Moog 32 valve under full input current conditions was approximated and used in the computer simulation. The approximation technique used was a straight line approximation of phase and amplitude based on measured test data from the valve manufacturer.

For the PMS simulation, equations (a) through (e) and the servovalve response approximation were solved simultaneously by the digital computer. Open and closed loop frequency response plots were made for several values of coupling spring rates and loop gains.

In the response plots described in the following paragraphs, the actuator motion plots show actuator piston motion relative to the actuator body. The plots of surface motion are for surface motion relative to the mounting structure. The actuator motion plots are significant since the actuator piston motion relative to the body is used as a feedback signal for the PMS actuators. The surface motion response plots were made to show the PMS system output response capability.

The plots are titled "unloaded" since the motion equations solved assume that the load actuator is by-passed.

FIGURES 25 and 26 show the open loop actuator and surface responses with the springs k_1 and k_2 adjusted to 50,000 #/in. Note that on FIGURE 25 the actuator phase angle reaches-180 degrees at approximately 85 Hz and the magnitude shows no peaking at high frequencies. This indicates that frequency response flat to above 50 Hz is feasible for the PMS actuator at that spring setting. FIGURE 26 for the surface response shows that the motion of the surface follows the actuator motion well to above 80 Hz.

FIGURES 27 through 32 show the actuator and surface response for a loop gain of 376 and three different settings of the k_1 and k_2 . These figures illustrate the general effect of k_1 and k_2 variation on the closed loop response.

FIGURES 27 and 28 show the frequency response with k_1 and k_2 adjusted to 5,000 #/in. This is the minimum value for the spring rates available from the present PMS hardware. Note on the frequency response of the actuator shown in FIGURE 27 that the amplitude response is flat to above 40 Hz. The phase lag gradually increases to 50 degrees at 45 Hz. In the frequency region of 0 to 10 Hz, the response is essentially that of a gain term. FIGURE 28 shows the surface response with the low spring rates. The response is essentially flat out to 20 Hz. The small peaks at 25 and 70 Hz are the resonances of the PMS masses on the coupling springs.

These two figures represent the PMS closed loop response with the minimum coupling between the actuator, surface and the mounting structure.

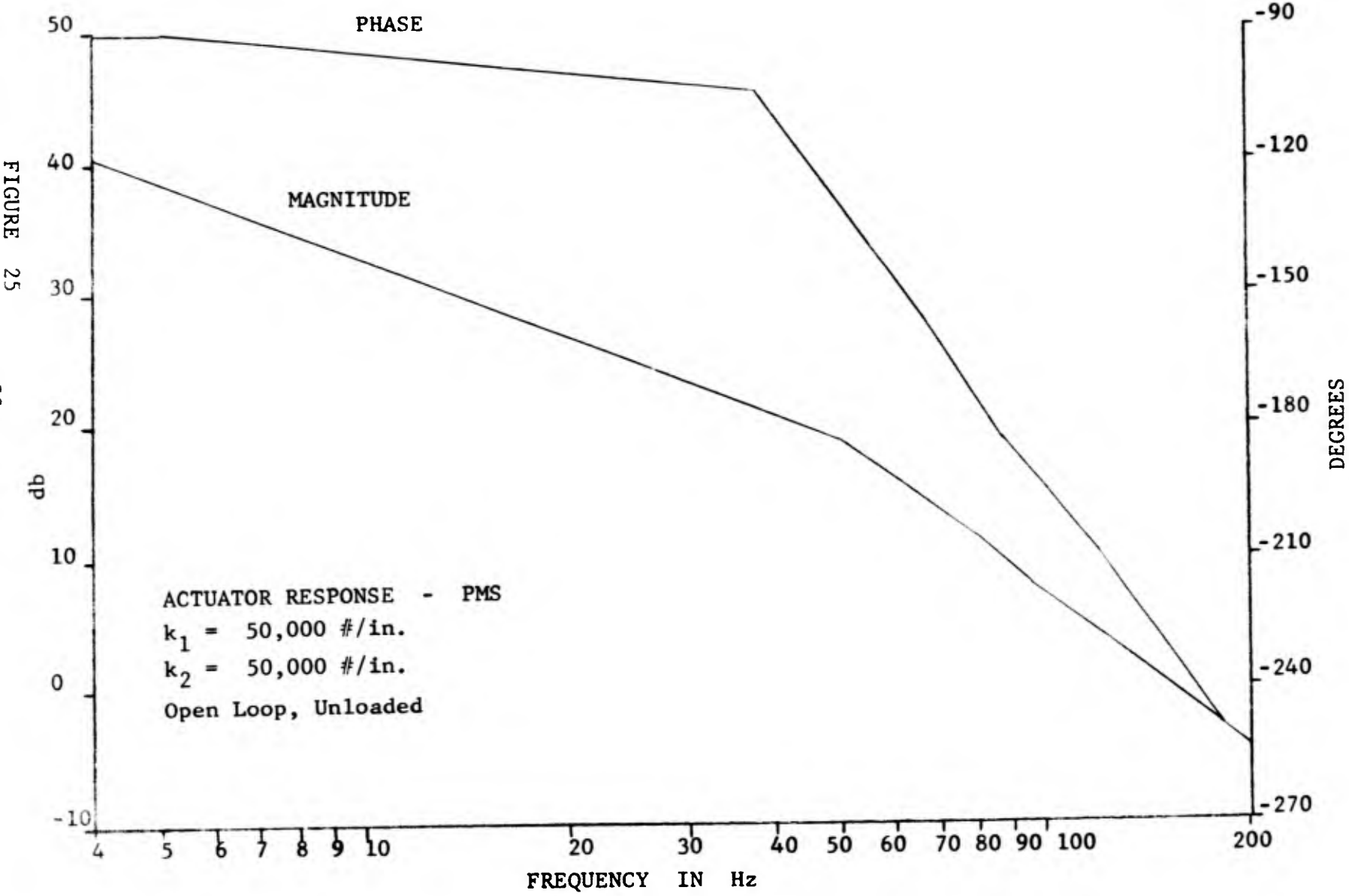
PHASE
MAGNITUDE
50
40
30
20
10
0
-10
db
-90
-120
-150
-180
-210
-240
-270
DEGREES
ACTUATOR RESPONSE - PMS
k_1 = 50,000 #/in.
k_2 = 50,000 #/in.
Open Loop, Unloaded
4 5 6 7 8 9 10 20 30 40 50 60 70 80 90 100 200
FREQUENCY IN Hz

FIGURE 25

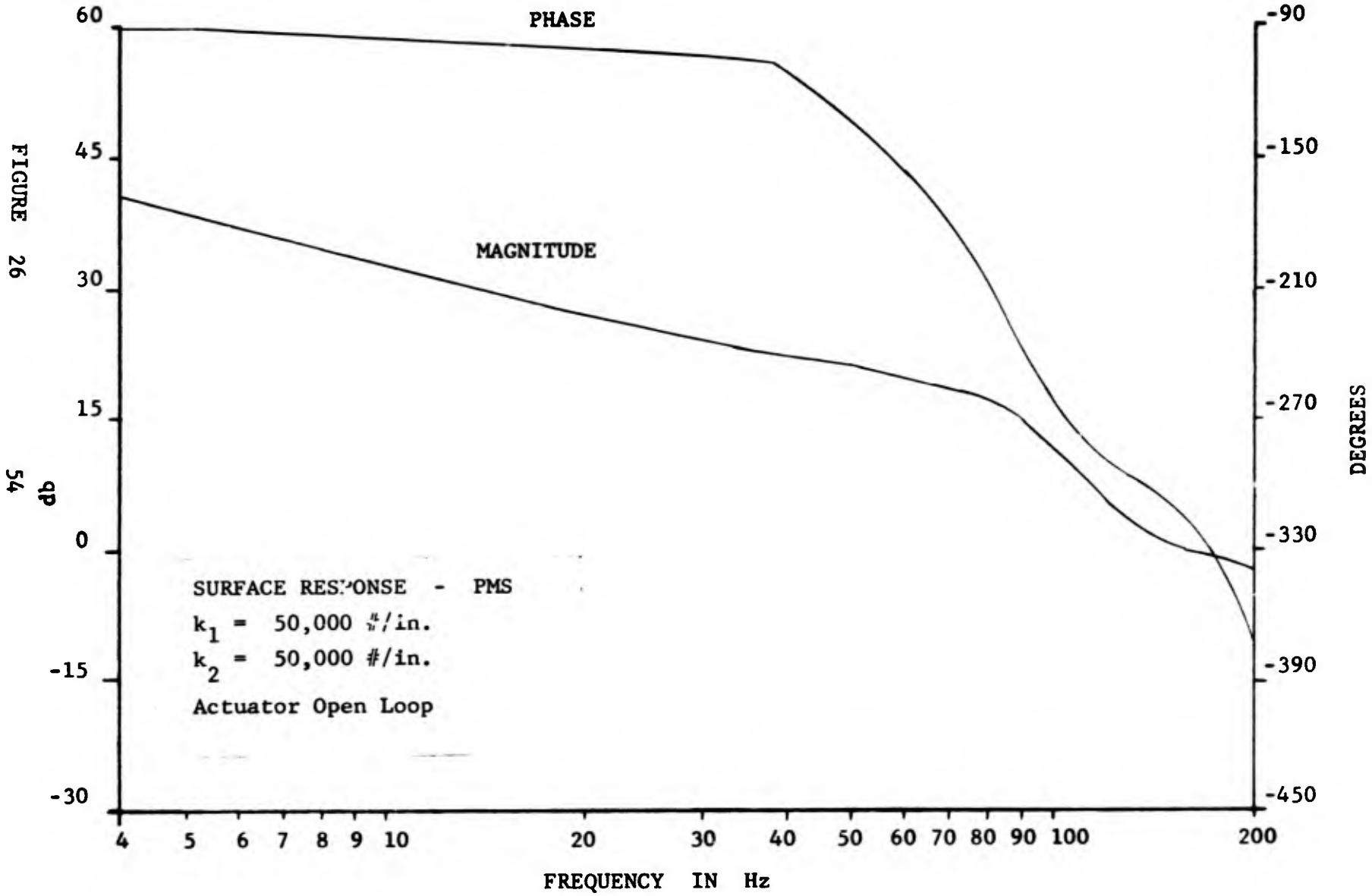
PHASE
MAGNITUDE
60
45
30
15
0
-15
-30
dB
-90
-150
-210
-270
-330
-390
-450
DEGREES
4
5
6
7
8
9
10
20
30
40
50
60
70
80
90
100
200
FREQUENCY IN Hz
SURFACE RESPONSE - PMS
k_1 = 50,000 #/in.
k_2 = 50,000 #/in.
Actuator Open Loop

FIGURE 26

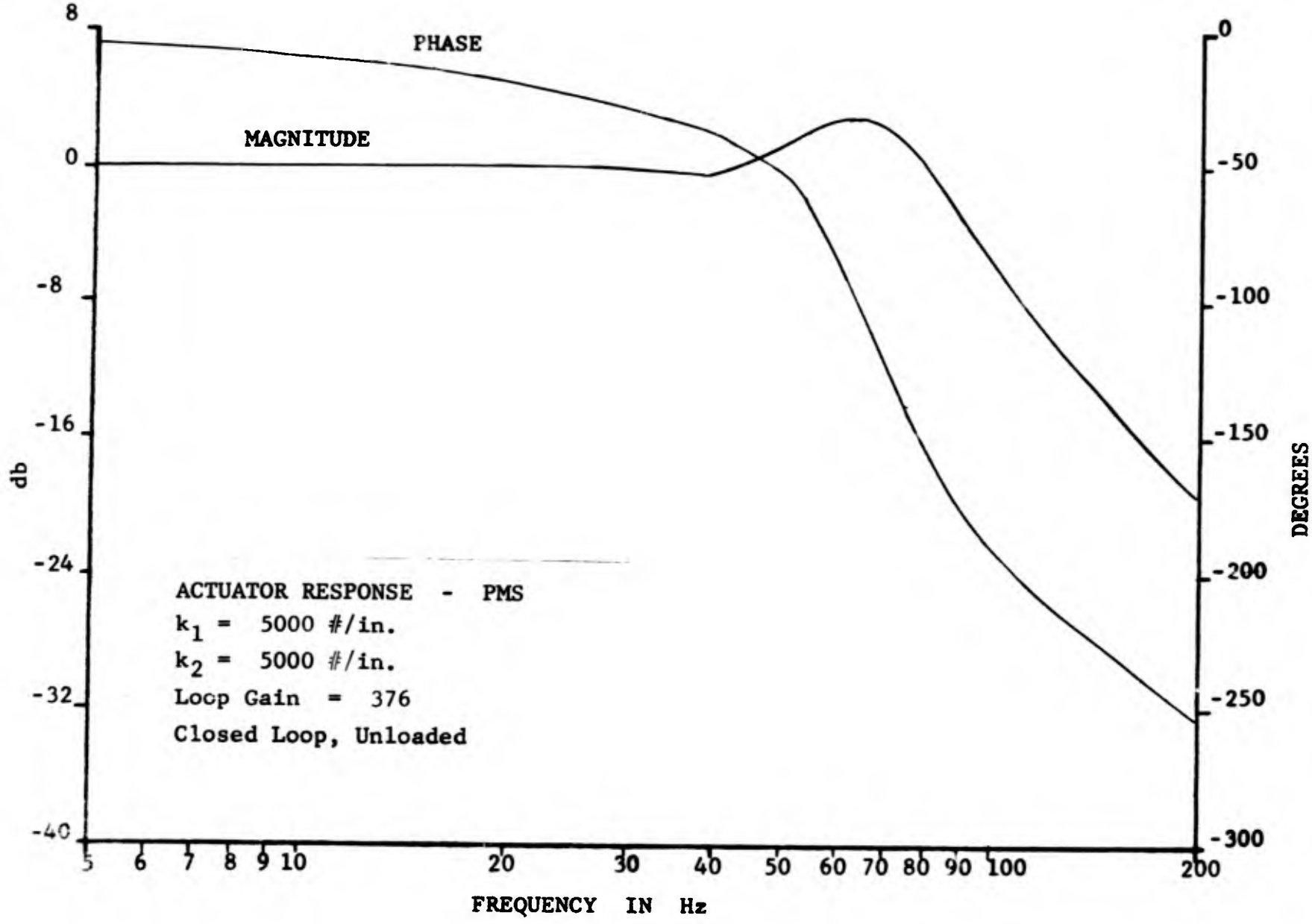
PHASE
MAGNITUDE
8
0
-8
-16
-24
-32
-40
db
0
-50
-100
-150
-200
-250
-300
DEGREES
5 6 7 8 9 10 20 30 40 50 60 70 80 90 100 200
FREQUENCY IN Hz
ACTUATOR RESPONSE - PMS
k_1 = 5000 #/in.
k_2 = 5000 #/in.
Loop Gain = 376
Closed Loop, Unloaded

FIGURE 27

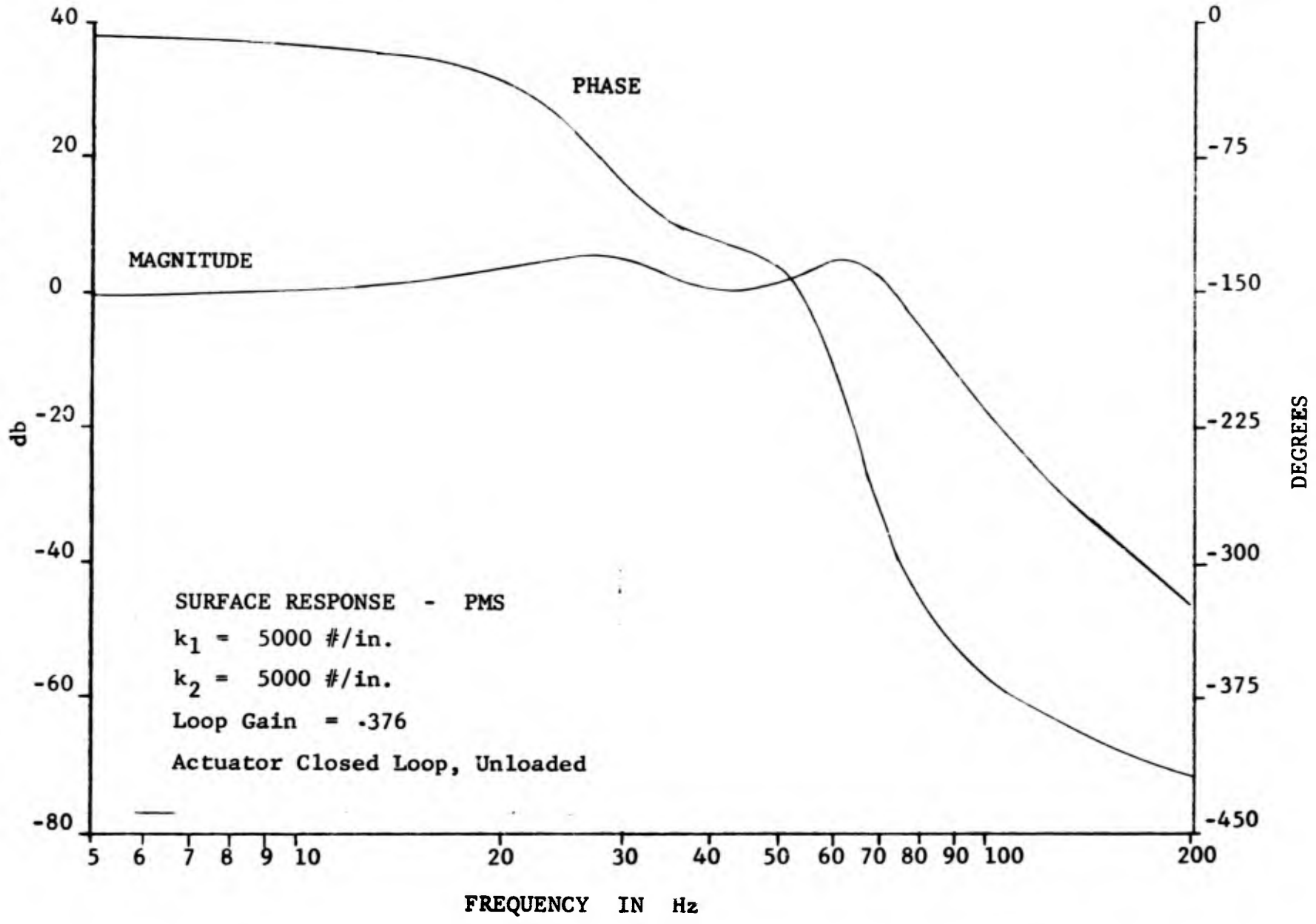
PHASE
MAGNITUDE
40
20
0
-20
-40
-60
-80
db
0
-75
-150
-225
-300
-375
-450
DEGREES
SURFACE RESPONSE - PMS
k_1 = 5000 #/in.
k_2 = 5000 #/in.
Loop Gain = .376
Actuator Closed Loop, Unloaded
5 6 7 8 9 10 20 30 40 50 60 70 80 90 100 200
FREQUENCY IN Hz

FIGURE 28

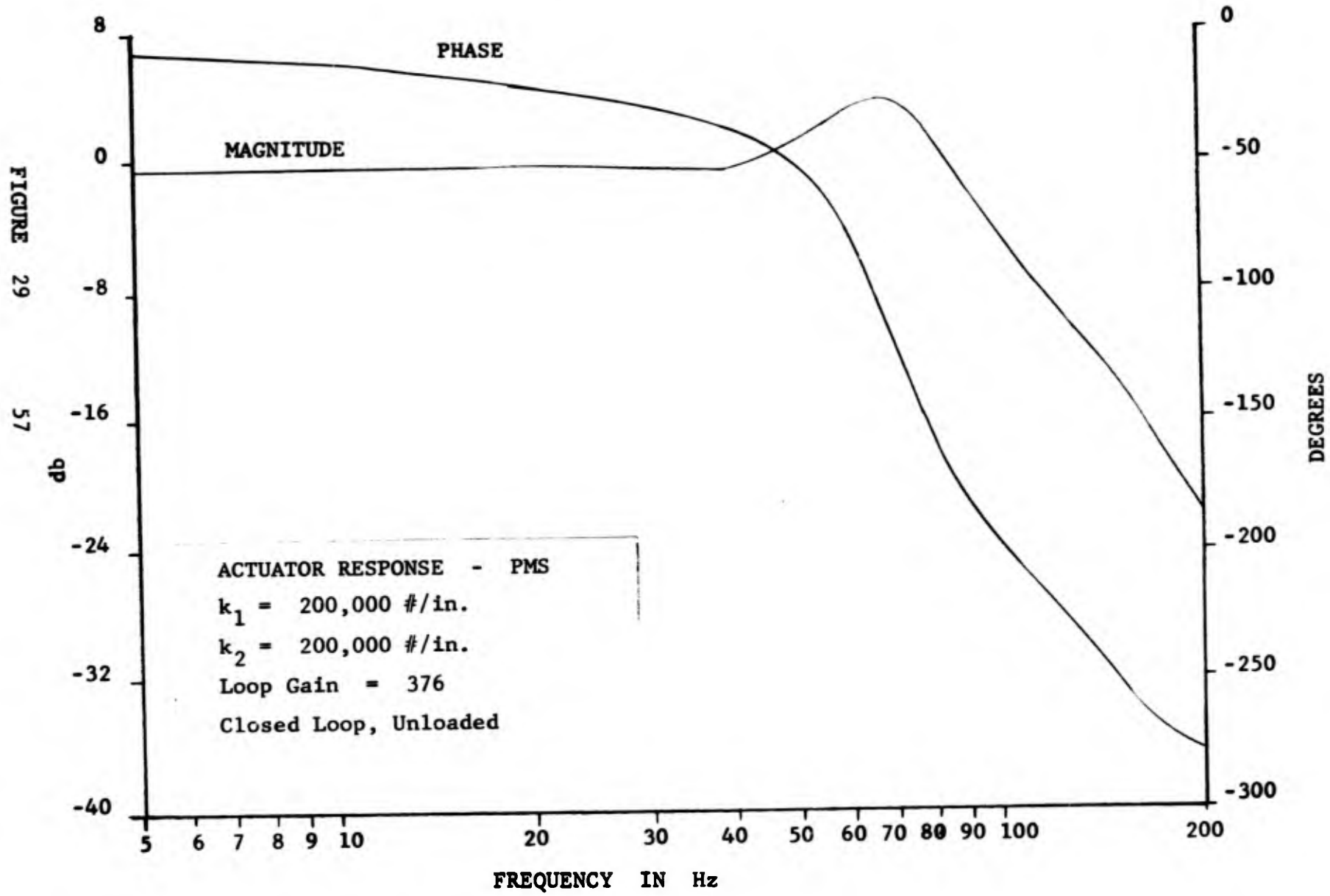
PHASE
MAGNITUDE
8
0
-8
-16
-24
-32
-40
db
0
-50
-100
-150
-200
-250
-300
DEGREES
5 6 7 8 9 10 20 30 40 50 60 70 80 90 100 200
FREQUENCY IN Hz
ACTUATOR RESPONSE - PMS
k_1 = 200,000 #/in.
k_2 = 200,000 #/in.
Loop Gain = 376
Closed Loop, Unloaded

FIGURE 29

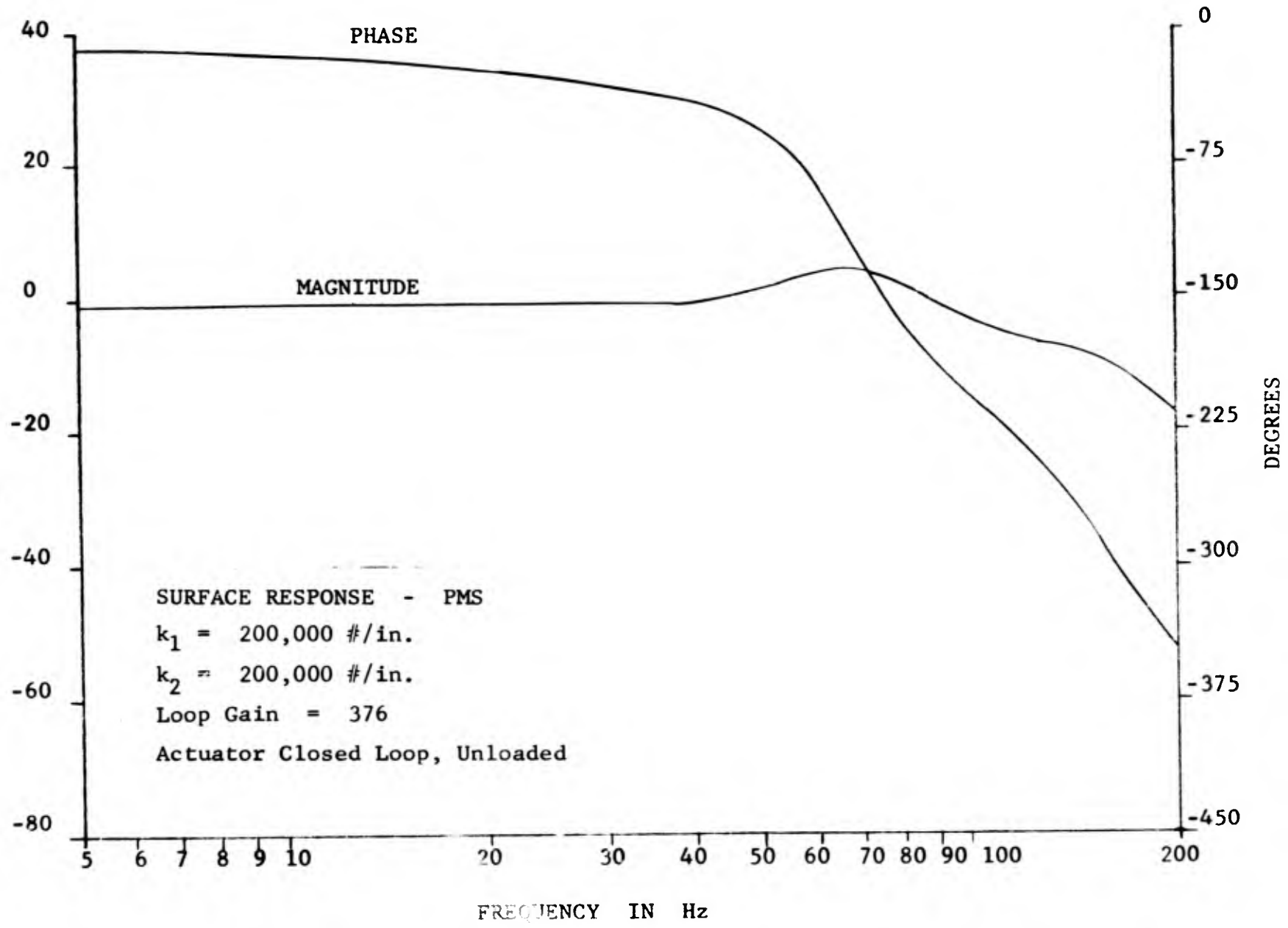
PHASE
MAGNITUDE
40
20
0
-20
-40
-60
-80
db
0
-75
-150
-225
-300
-375
-450
DEGREES
SURFACE RESPONSE - PMS
k_1 = 200,000 #/in.
k_2 = 200,000 #/in.
Loop Gain = 376
Actuator Closed Loop, Unloaded
5 6 7 8 9 10 20 30 40 50 60 70 80 90 100 200
FREQUENCY IN Hz

FIGURE 30

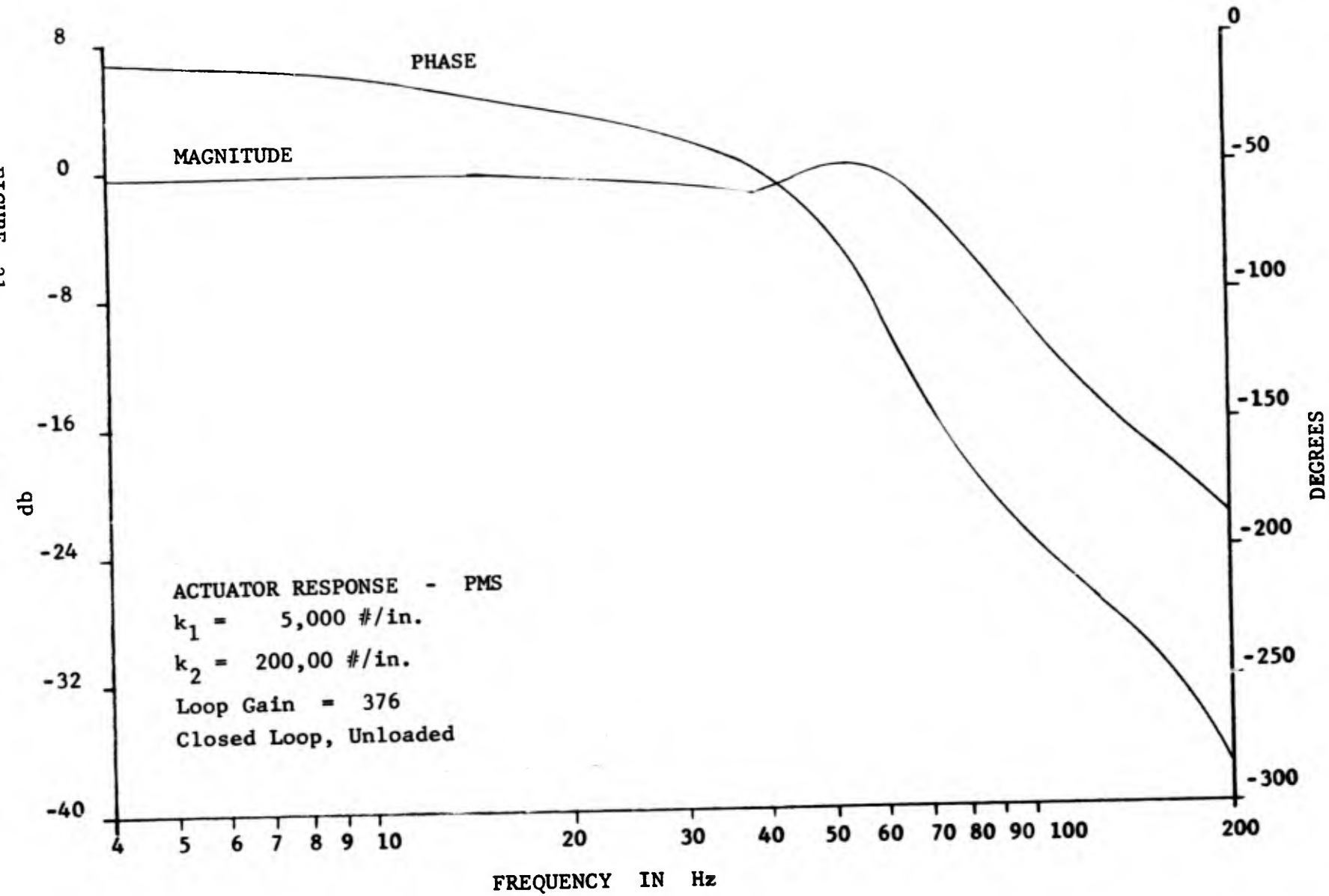
PHASE
MAGNITUDE
8
0
-8
-16
-24
-32
-40
db
0
-50
-100
-150
-200
-250
-300
DEGREES
ACTUATOR RESPONSE - PMS
k_1 = 5,000 #/in.
k_2 = 200,00 #/in.
Loop Gain = 376
Closed Loop, Unloaded
4 5 6 7 8 9 10 20 30 40 50 60 70 80 90 100 200
FREQUENCY IN Hz

FIGURE 31

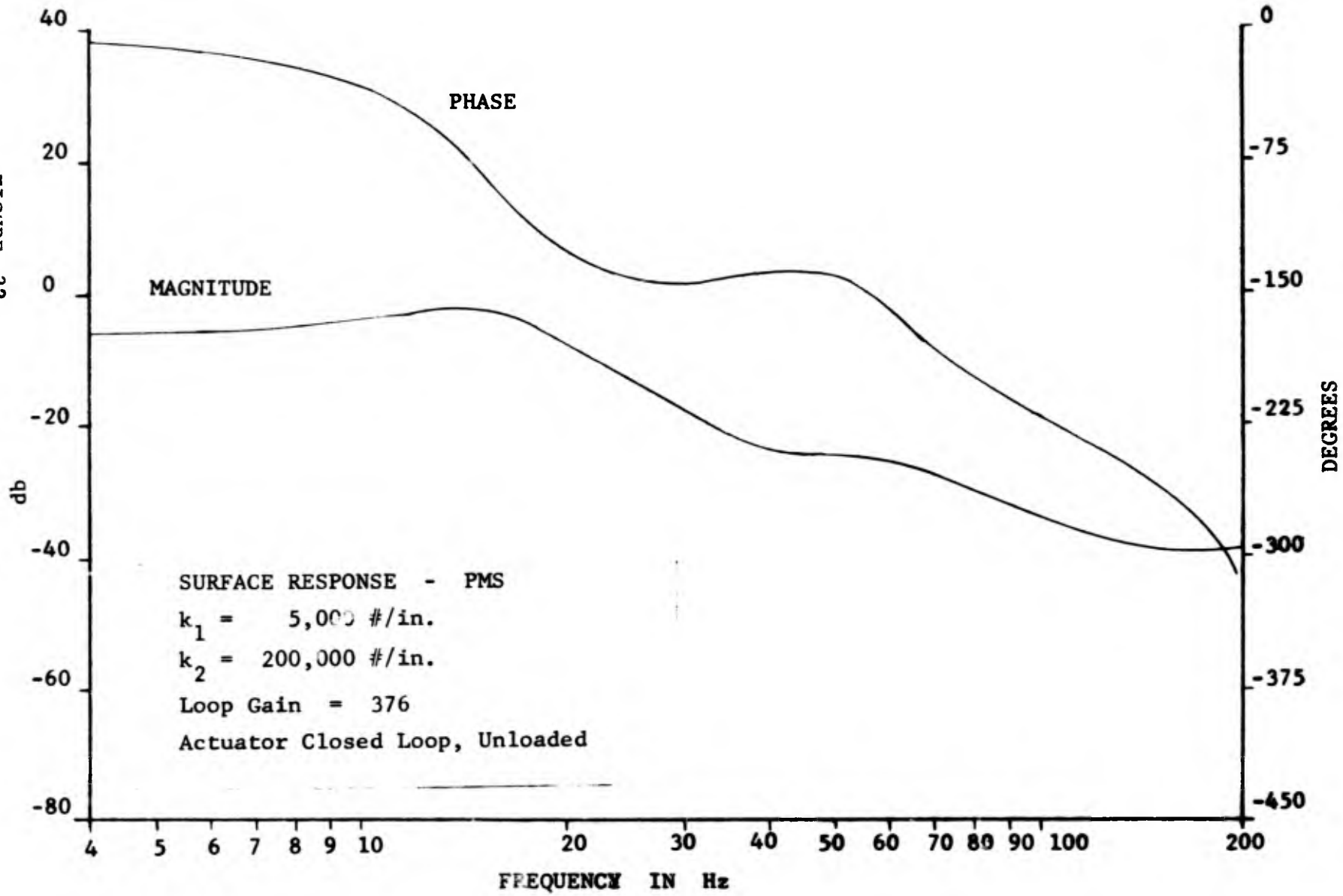
PHASE
MAGNITUDE
SURFACE RESPONSE - PMS
k_1 = 5,000 #/in.
k_2 = 200,000 #/in.
Loop Gain = 376
Actuator Closed Loop, Unloaded
40
20
0
-20
-40
-60
-80
db
0
-75
-150
-225
-300
-375
-450
DEGREES
4 5 6 7 8 9 10 20 30 40 50 60 70 80 90 100 200
FREQUENCY IN Hz

FIGURE 32

FIGURES 29 and 30 show the frequency response of the actuator and surface for k_1 and k_2 adjusted to 200,000 #/in. This is the maximum coupling stiffness between the surface, actuator and structure. The actuator response shows mild peaking at about 70 Hz. The magnitude of actuator response is flat to 40 Hz and the phase lag does not reach 50 degrees until 48 Hz. The phase lag for frequencies below 20 Hz is less than 20 degrees. As might be expected from the stiff coupling between the surface, actuator and structure, the surface motion follows the actuator piston to body motion up to a frequency of 40 Hz.

FIGURES 31 and 32 show the frequency response of the actuator and surface for k_1 = 5,000 #/in. and k_2 = 200,000 #/in. As might be expected, the actuator response is relatively unaffected by the low coupling stiffness to the structure. This is because the feedback signal for the actuator is piston motion relative to the actuator body, not piston motion relative to the structure. Surface motion, however, is significantly affected by the low actuator body to structure coupling stiffness. For this condition, the frequency response of the surface is flat up to only 10 Hz and the phase lag reaches 50 degrees by approximately 12 Hz.

FIGURE 33 shows actuator response with a mass load of approximately 19 times the minimum surface member mass. The actuator response demonstrates mild peaking at 55 Hz due to increase surface mass. The amplitude response remains flat to 40 Hz. The phase lag is less than 25^{o} up to 18 Hz. Since 200,000 #/in. coupling spring rates are used, the surface response will follow the actuator response up to 40 Hz.

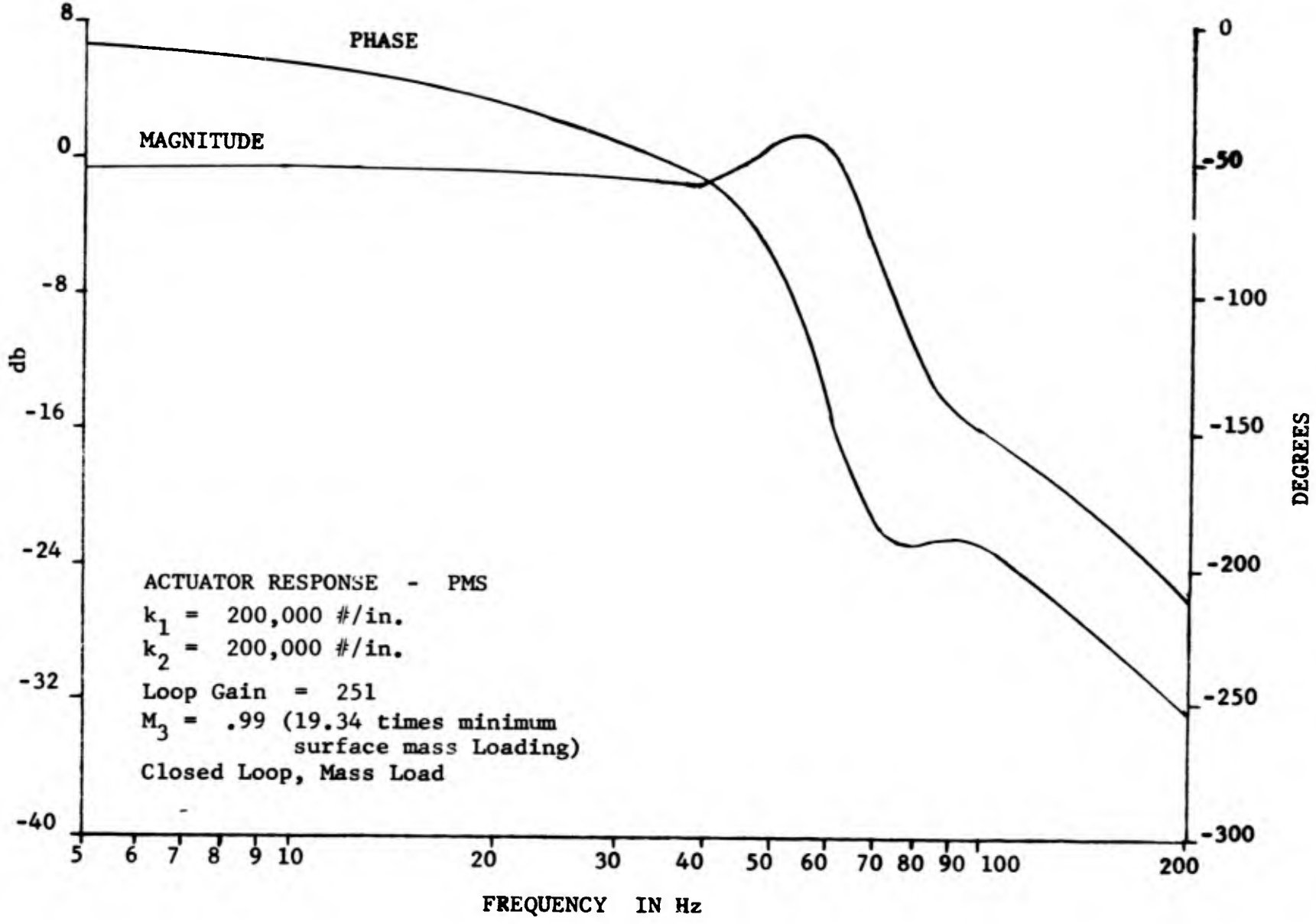
PHASE
MAGNITUDE
8
0
-8
-16
-24
-32
-40
db
0
-50
-100
-150
-200
-250
-300
DEGREES
ACTUATOR RESPONSE - PMS
k_1 = 200,000 #/in.
k_2 = 200,000 #/in.
Loop Gain = 251
M_3 = .99 (19.34 times minimum surface mass Loading)
Closed Loop, Mass Load
5 6 7 8 9 10 20 30 40 50 60 70 80 90 100 200
FREQUENCY IN Hz

FIGURE 33

3.0 TESTING PROCEDURE

3.1 General

The objective of the testing performed on the hybrid simulator was to record the performance characteristics of the simulator elements. The testing included input-output measurements of individual electronic elements as well as measurement of the load and control channel characteristics.

The instrumentation used in measuring and recording the input-output characteristics of the simulator elements was the following:

a. A Bafco, Inc. frequency response analyzer

b. An Esterline Angus x,y,y', recorder

c. A Brush Model 200 strip chart recorder

d. A Wavetec Model 144 function generator

e. Tektronix Model 7613 oscillocope

These five instruments were connected to the hybrid simulator using the simulator patch panel.

3.2 Specific

3.2.1 Control Channel Electronics

The control channel electronics include the

following plug-in modules:

1. Servo driver
2. Summing amplifier
3. Limiter
4. Deadband
5. Second order filter

For all five of the control channel modules, the frequency response was measured using the Bafco, Inc. frequency response analyzer and the x,y,y', plotter. To measure the servo driver response, an SMS valve having a coil resistance of 400 ohms was used as a valve load. During all of the response measurements, the output waveforms were monitored using the Tektronix Model 7613 oscilloscope. For the non-linear modules of deadband and limiter, the frequency response was measured at amplitude settings where the non-linearities did not affect the output waveforms. For the non-linear modules, the x,y,y', plotter and the Wavetec function generator were used to record the non-linear amplitude dependent characteristics at selected module settings. The second order filter response characteristics were measured at different damping settings for selected natural frequencies.

3.2.2 Instrumentation Electronics

The instrumentation electronics include the following plug-in modules:

1. Bridge amplifier
2. D.C. amplifier
3. Demodulator

For the bridge amplifier and the D.C. amplifier, the Bafco frequency response analyzer and x,y,y', recorder were used to measure and record the frequency response. For the D.C. amplifier, the response is a function of the amplifier gain and was measured at selected gain range settings. The demodulator frequency response was measured by the Bafco by modulating the 5000 Hz carrier signal from the simulator LVDT excitation electronics.

3.2.3 Logic Module Electronics

The Logic Module electronics include the following sections:

1. First Order Lag Filter Module
2. Comparator Module
3. Time Delay Module
4. Failure Indication and Reset Module

The Bafco and x,y,y', recorder were used to measure and record the First Order Lag Filter Module frequency response. The frequency response was measured at selected potentiometer settings corresponding to the break frequency of the filter. All four sections of the filter were measured and recorded. The performance of the comparator and time delay sections was measured and recorded using the Wavetec function generator and the Model 200 Brush strip chart recorder. The First Order Lag Filter Module was adjusted for a break frequency of 1000 Hz during the comparator and time delay performance measurements. A ramp input was applied to one of the four monitor voltage inputs. The input voltage, the output of the First Order Lag Filter Module, the ouput of the Comparator Module and the output of the Time Delay Module were recorded on the strip chart. The time and amplitude response was recorded for different settings of the comparator and delay time.

The measurements were repeated for all four monitor voltage inputs.

Operation of the Failure Indication and Reset Module was verified by visual observation. Proper operation was established by injecting failures with the failure logic test button and observing the failure indication lights.

3.2.4 SMS Failure Transfer Time

To establish the minimum transfer time using the Logic Module and the SMS solenoid bypass valves, the Logic Module was connected to SMS control channels 1 and 2. The model 200 Brush strip chart recorder was used to record the input to the control channels and the output position of the control actuators. The Wavetec function generator was used to command both control channels. A loss of signal was created in one channel and the time response record used to establish the transfer time after the failure detection level threshold was reached. For this measurement, the time delay was set to its minimum value and the first order lag break frequency was set to 1000 Hz.

3.2.5 SMS Control Channel Performance

The Bafco, Inc. frequency response analyzer and the Esterline Angus x,y,y', recorder were used to measure the frequency response of the SMS control channels. For the response measurements, the demodulated outputs of the LVDT position transducers for the SMS channels were used as feedback signals. The frequency response of an uncoupled single channel at different loop gain settings was recorded. The frequency response for the various loop gains was measured at 10% input amplitude. The frequency response of a single

channel at a loop gain of 638 and an input amplitude of 25% and 100% was recorded to establish saturation response envelope.

The frequency response of two, three and four SMS channels coupled together was also recorded at a high loop gain setting for the coupled channels. The gain used for these response measurements was the highest gain setting obtainable without causing ringing when a step input was used to drive the control channels. No stability compensation was used in the control loops.

The x,y,y', recorder and the Wavetec function generator were used to measure and record the SMS control channel position linearity. The function generator was used to generate a low frequency full amplitude sinusoidal input for the control channels and the x,y,y', recorder was used to record the demodulated output of each channel's position LVDT vs. input voltage. To measure the SMS actuator friction, the Wavetec was used to generate a low frequency full amplitude sinusoidal input for the control channels. The x,y,y', recorder was used to record the output of each control actuator's differential pressure transducer vs. the input voltage.

3.2.6 PMS Performance

To measure the PMS frequency response, the Bafco frequency response analyzer and x,y,y' recorder were used. The PMS channels were run uncoupled. Both low level (10% input) and high level (100% input) frequency response measurements were made. The compliance members for the frequency response runs were adjusted to their minimun compliance positions. The loop gain was adjusted to the maximum setting without instability. No compensation was used in the control loops.

To measure and record the PMS position linearity, the Wavetec function generator and x,y,y' recorder were

used. The function generator was used to drive the PMS control channels with a low frequency sinusoidal input. The x,y,y', recorder was used to record the demodulated output voltage of the actuator position LVDT (measuring piston motion relative to the actuator body) vs. the input voltage.

3.2.7 Load Channel Performance

The same test procedure was used for both the SMS and PMS load channel performance measurements. The Bafco response analyzer and the x,y,y', recorder were used to measure and record the PMS and SMS frequency response. Two types of load frequency response were run. The first type of response was made with a "blocked" load condition (with the control actuator connected to the load actuator and commanded to a neutral position). This frequency response indicates small motion response capability of the load channels. The second type of frequency response run on each load channel was with the load channels commanded to "0" load pressure and the control actuator for the respective channel commanded to a large position amplitude. This frequency response indicated the ability of the load channels to produce the commanded load independent of the amplitude of motion.

This frequency response indicates the sensitivity of the load channel output to the amplitude of motion that the control channels can produce over the frequency range of interest.

The load frequency response measurements were made with the load control loop gains set at the maximum gain with stable operation. The PMS compliance members were adjusted to their minimum compliance positions during the load channel performance tests.

The load force linearity for the load control channels was measured and recorded with the Wavetec

function generator and Esterline Angus x,y,y', recorder. The Wavetec function generator was used to generate a low frequency sinusoidal input into the load control channel inputs. The x,y,y', recorder was used to record the output voltage of the differential pressure transducers connected across each load actuator piston area vs. the input voltage into the load channel.

4.0 TEST RESULTS

4.1 General

The test results presented in this section are examples of the results recorded in performing the test procedure described in the preceding section. The single channel SMS characteristics used for illustration are the results recorded on the SMS channel 3 load and control channel performance. The PMS performance results presented are the measurements taken on channel 1 of the PMS. The test results are presented in the the same order as the test procedure description.

4.2 Control Channel Electronics Performance Results

The performance characteristics of the control channel electronics are presented as follows:

1. FIGURE 34 - Summing Amplifier Frequency Response
2. FIGURE 35 - Servo Amplifier Frequency Response
3. FIGURE 36 - Limiter Frequency Response
4. FIGURE 37 - Limiter Output Characteristics
5. FIGURE 38 - Dead Band Frequency Response
6. FIGURE 39 - Dead Band Output Characteristics
7. FIGURE 40 - Second Order Filter Characteristics

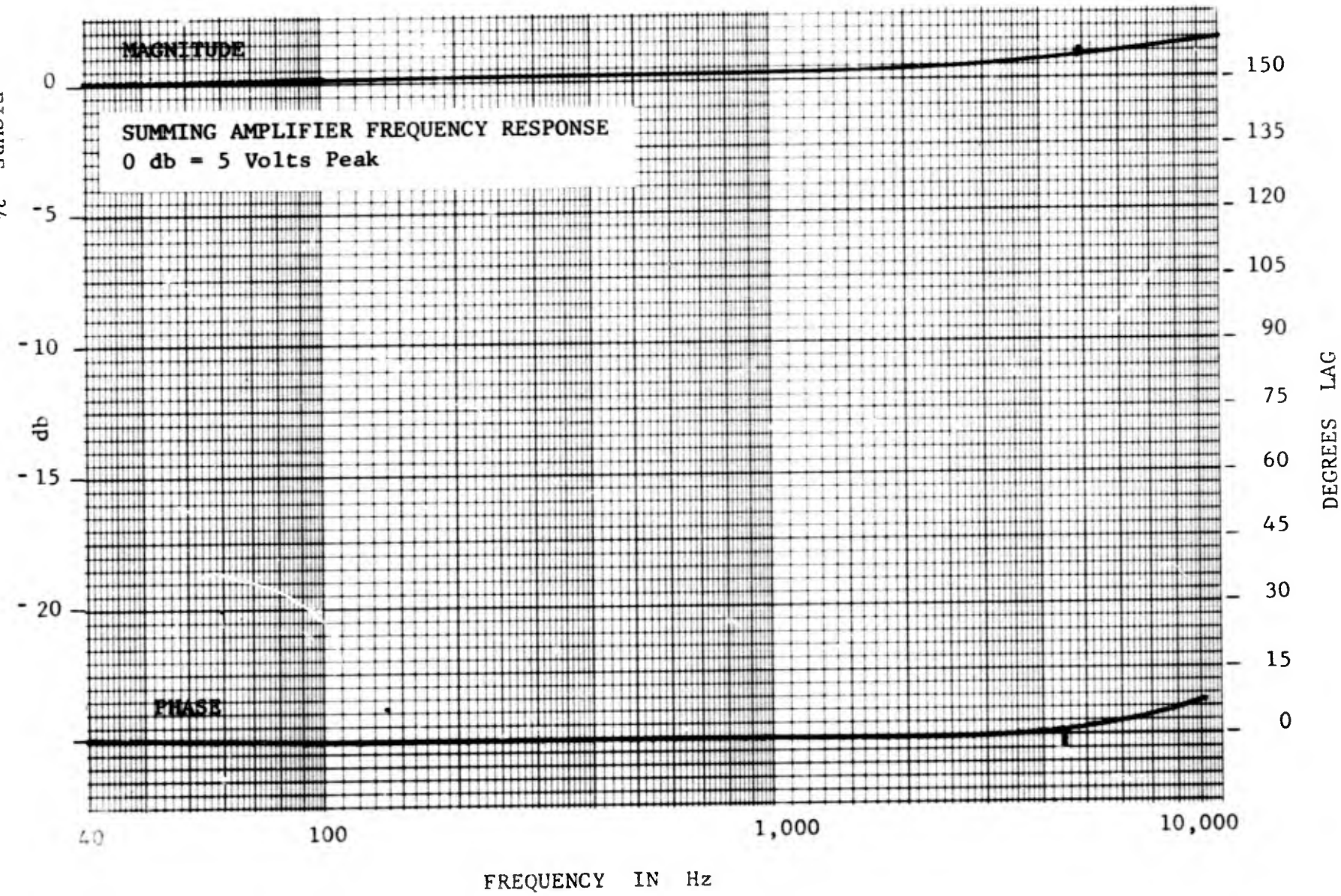
MAGNITUDE
SUMMING AMPLIFIER FREQUENCY RESPONSE
0 db = 5 Volts Peak
PHASE
0
-5
-10
-15
-20
db
150
135
120
105
90
75
60
45
30
15
0
DEGREES LAG
40
100
1,000
10,000
FREQUENCY IN Hz

FIGURE 34

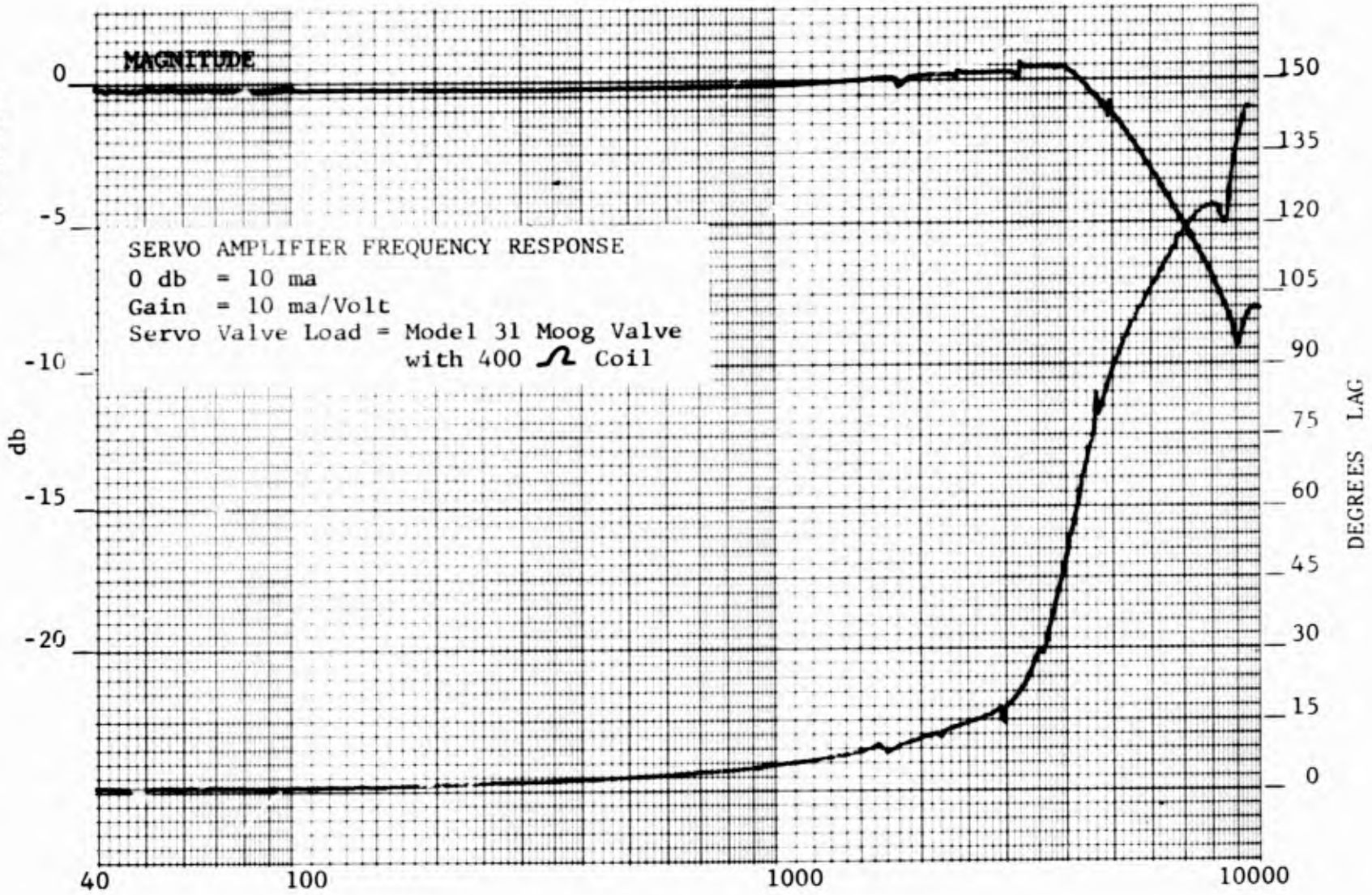
MAGNITUDE
SERVO AMPLIFIER FREQUENCY RESPONSE
0 db = 10 ma
Gain = 10 ma/Volt
Servo Valve Load = Model 31 Moog Valve
with 400 Ω Coil
0
-5
-10
-15
-20
db
150
135
120
105
90
75
60
45
30
15
0
DEGREES LAG
40
100
1000
10000
FREQUENCY IN Hz

FIGURE 35

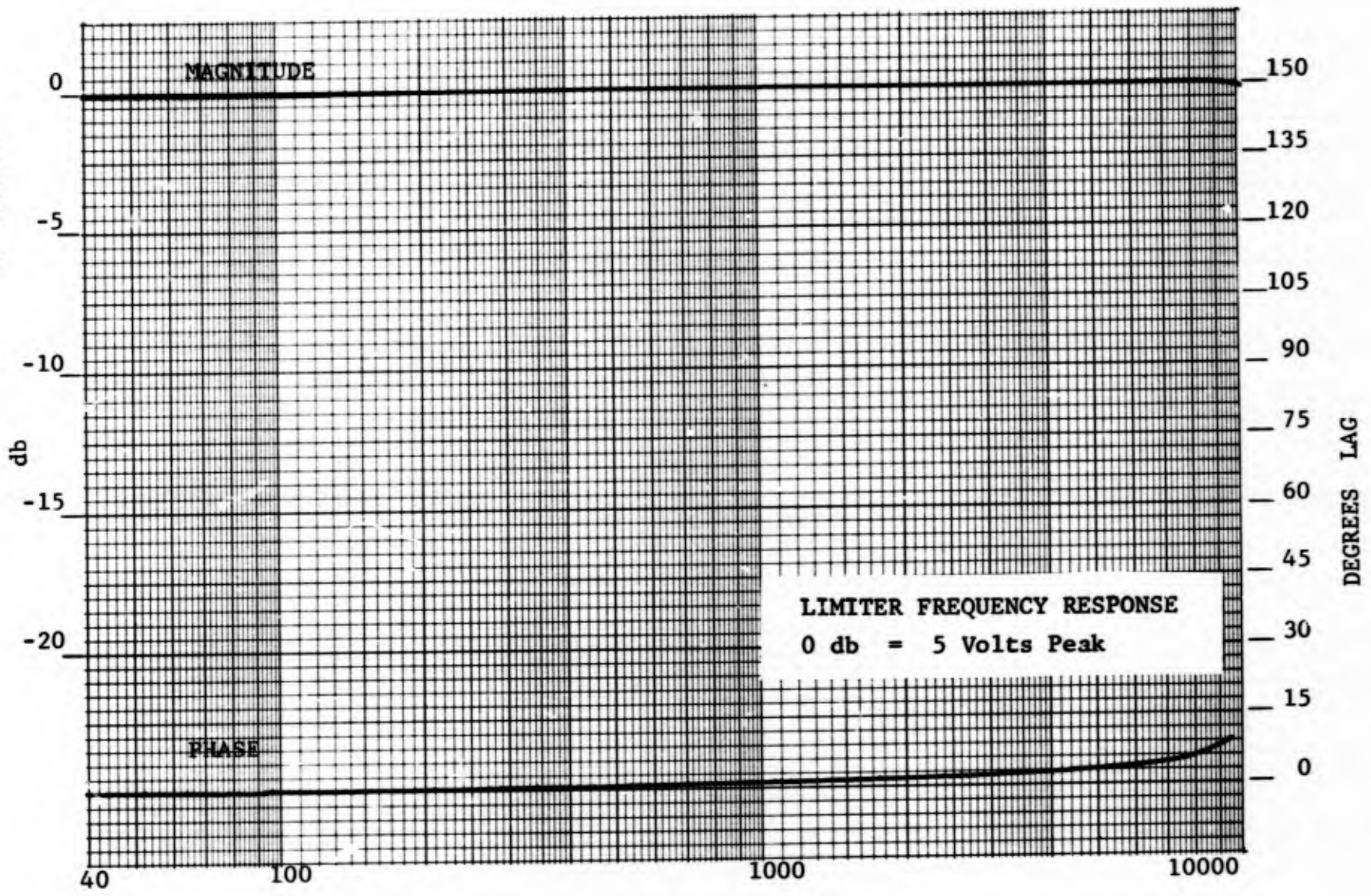
MAGNITUDE
PHASE
0
-5
-10
-15
-20
db
150
135
120
105
90
75
60
45
30
15
0
DEGREES LAG
LIMITER FREQUENCY RESPONSE
0 db = 5 Volts Peak
40
100
1000
10000
FREQUENCY IN Hz

FIGURE 36

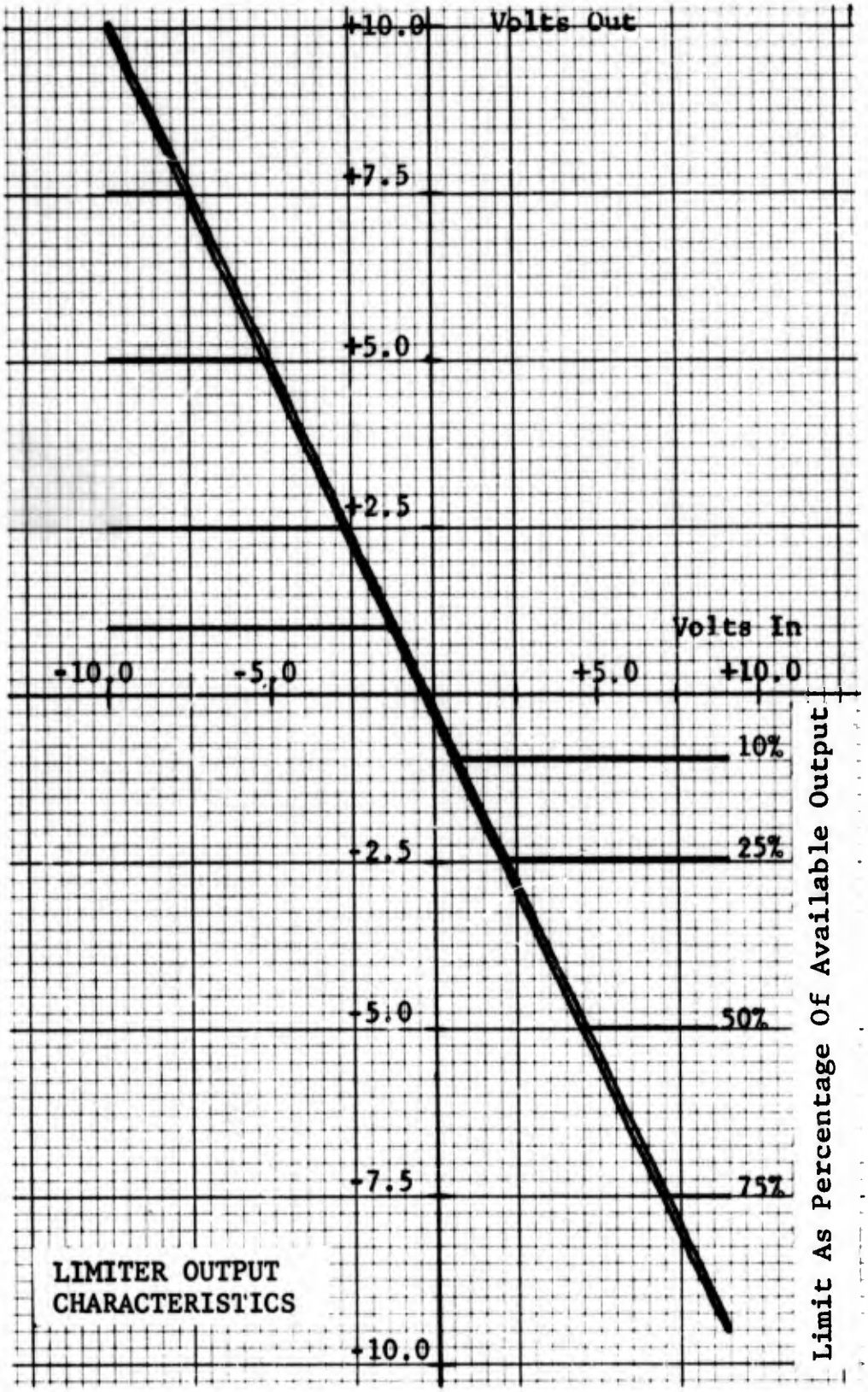
+10.0
Volts Out
+7.5
+5.0
+2.5
Volts In
+10.0
-5.0
+5.0
+10.0
10%
25%
-2.5
-5.0
50%
-7.5
75%
LIMITER OUTPUT
CHARACTERISTICS
-10.0
Limit As Percentage Of Available Output

FIGURE 37

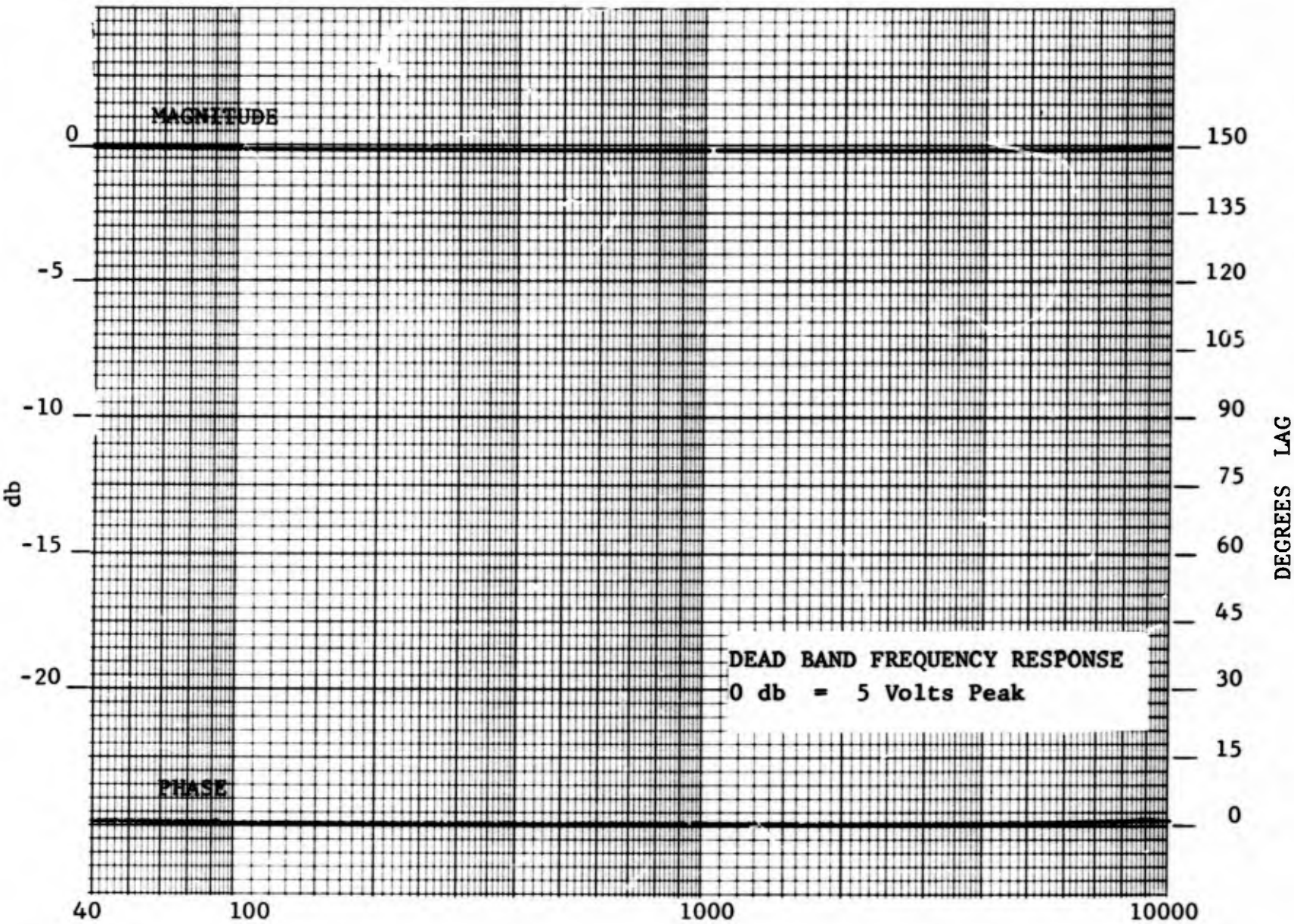
MAGNITUDE
PHASE
0
-5
-10
-15
-20
db
150
135
120
105
90
75
60
45
30
15
0
DEGREES LAG
DEAD BAND FREQUENCY RESPONSE
0 db = 5 Volts Peak
40
100
1000
10000
FREQUENCY IN Hz

FIGURE 38

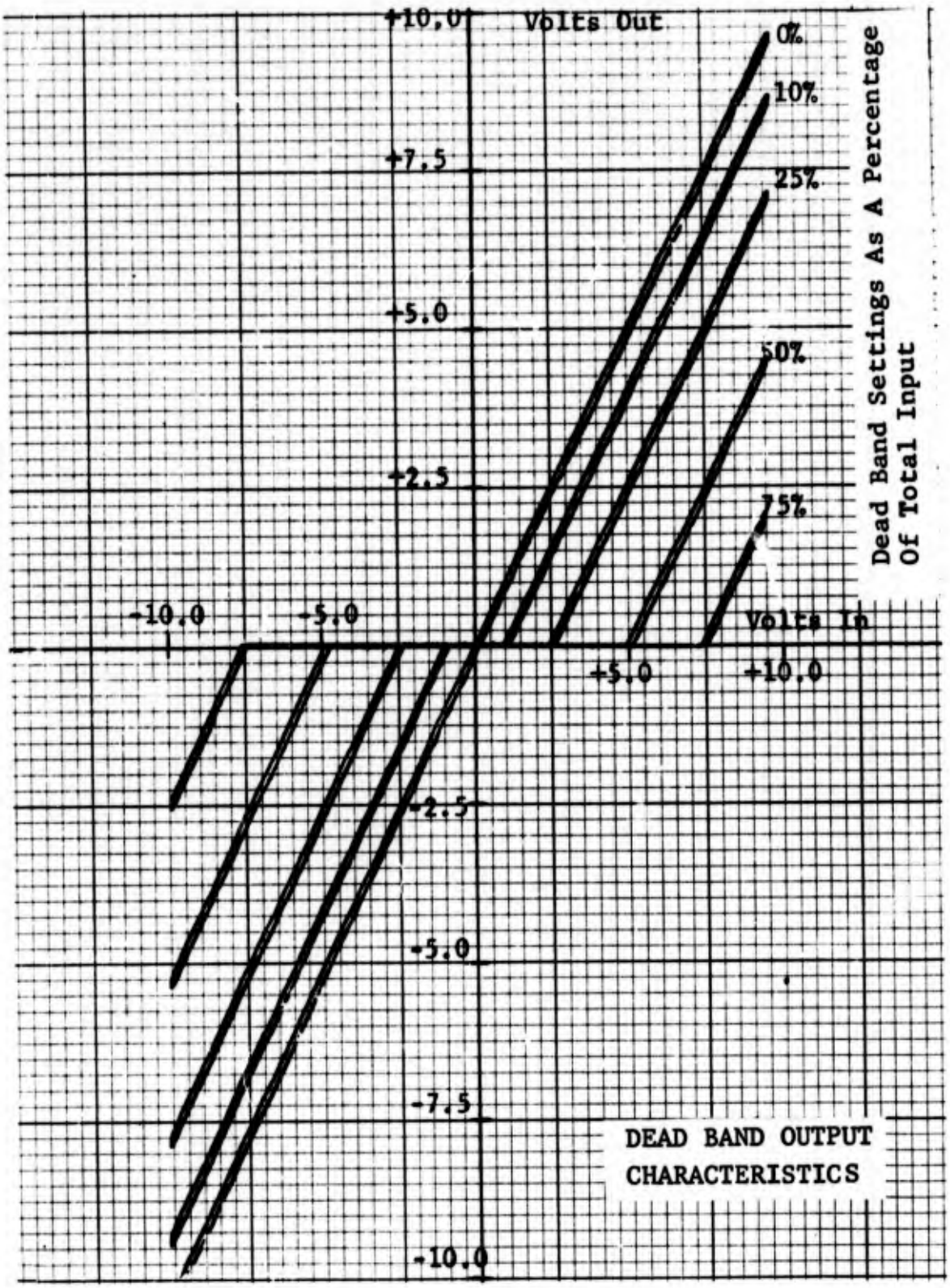
+10.0
Volts Out
0%
10%
25%
50%
75%
+7.5
+5.0
+2.5
-10.0
-5.0
Volts In
+5.0
+10.0
-2.5
-5.0
-7.5
-10.0
Dead Band Settings As A Percentage Of Total Input
DEAD BAND OUTPUT CHARACTERISTICS

FIGURE 39

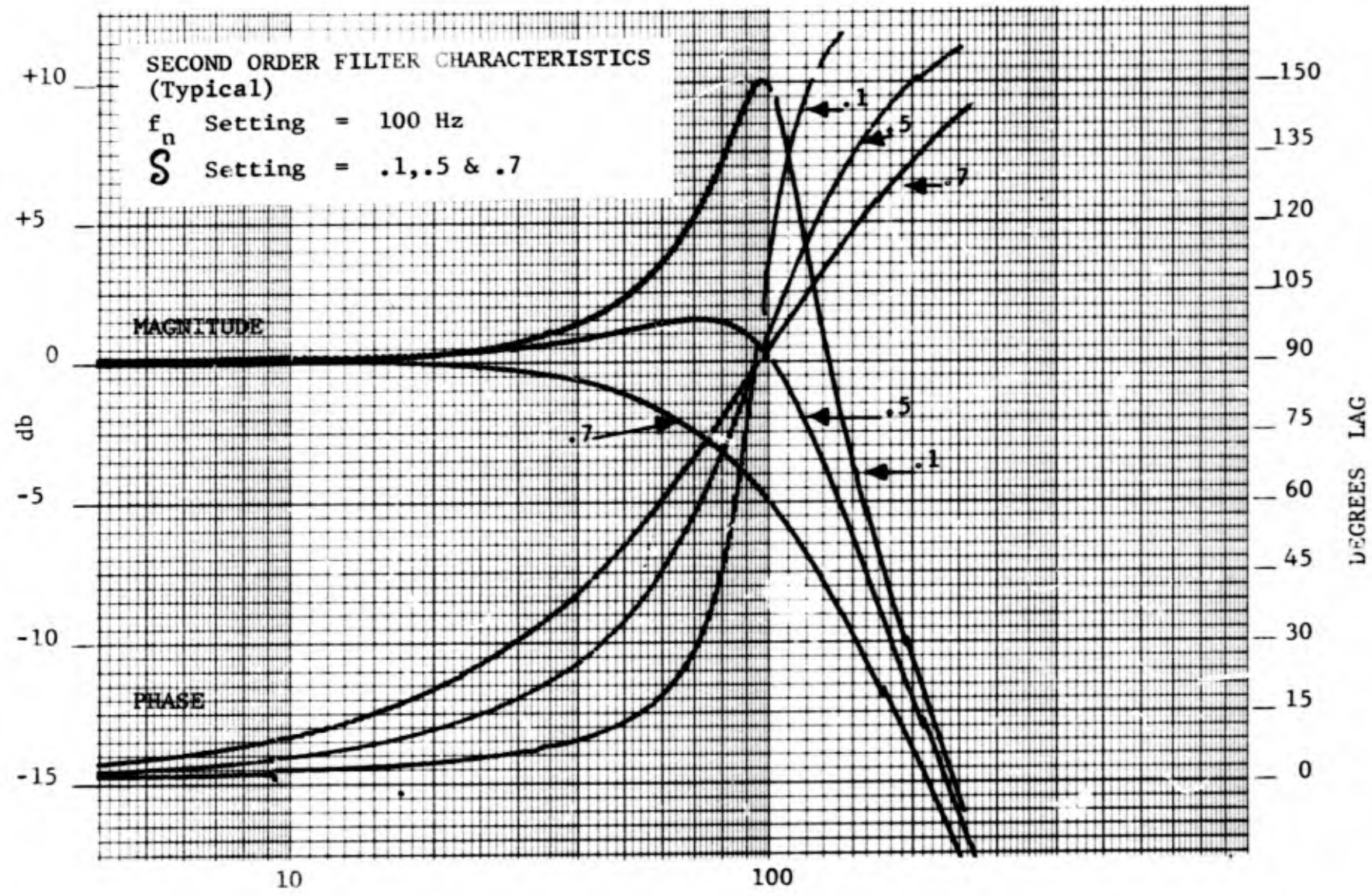
SECOND ORDER FILTER CHARACTERISTICS
(Typical)
f_n Setting = 100 Hz
S Setting = .1,.5 & .7
+10
+5
0
-5
-10
-15
db
MAGNITUDE
PHASE
.1
.5
.7
.7
.5
.1
150
135
120
105
90
75
60
45
30
15
0
DEGREES LAG
10
100
FREQUENCY IN Hz

FIGURE 40

FIGURES 34, 36 and 38 show that the frequency response of the summing amplifier, limiter and dead band modules have flat frequency response and zero phase shift at all frequencies below 5000 Hz. The servo amplifier response as shown in FIGURE 35 with a valve load has flat frequency response (note that this is a valve current to input voltage response) at all frequencies below 1000 Hz. This response is more than sufficient to allow ignoring the dynamics of these electronic modules in setting up the SMS and PMS simulations.

The characteristics of the limiter output as shown in FIGURE 37 show that the limiter has the sharp corner characteristics desired for simulating mechanical limits. The apparent hysteresis shown on the figure is generated by the x,y,y' recorder and not the limiter electronics.

The characteristics of the dead band as shown in FIGURE 39 show that the dead band module provides symetrical dead band thresholds as designed with linear unity gain outside the dead band amplitude level. The apparent hysteresis shown on the figure exists in the x,y,y', plotter and not in the electronics.

The response of the second order filter as shown in FIGURE 40 match the classical frequency response plots for a second order transfer function. This plot is representative of the filter characteristics for different natural frequencies and damping settings and indicates that the filter is operating as expected from the design calculations.

4.3 Instrumentation Electronics Performance

The performance characteristics of the instrumentation modules are presented on the figures as follows:

1. FIGURE 41 - Demodulator Frequency Response

2. FIGURE 42 - Bridge Amplifier Frequency Response

3. FIGURE 43 - D.C. Amplifier Frequency Response (Gain 10)

4. FIGURE 44 - D.C. Amplifier Frequency Response (Gain 1000)

As shown on FIGURE 41, the frequency response of the demodulator exhibits a flat response with less than 10 degrees phase shift for frequencies below 200 Hz. This is more than adequate for the demodulation of the position LVDT's used on the SMS and PMS. The response roll off above 200 Hz is caused by the carrier frequency filtering used in the demodulator module.

As shown on FIGURE 42, the frequency response of the bridge amplifier shows no amplitude attenuation or phase shift below 10,000 Hz. This extended response allows using the differential pressure tranducers and the bridge amplifiers as effective force measuring instrumentation for the PMS and SMS loading channels.

As shown in FIGURES 43 and 44, the frequency response of the D.C. amplifier is a function of the amplifier gain position used. The most limited response (occurring at 1000 gain position) exceeds the requirements for use with the hybrid simulator.

4.4 Logic Module Performance

The performance characteristics of the Logic Module and the SMS minimum transfer time are presented in FIGURES 45 through 49 as follows:

1. FIGURE 45 - Logic First Order Lag Filter Response

2. FIGURES 46 to 49 - Failure Logic Time and Amplitude Characteristics

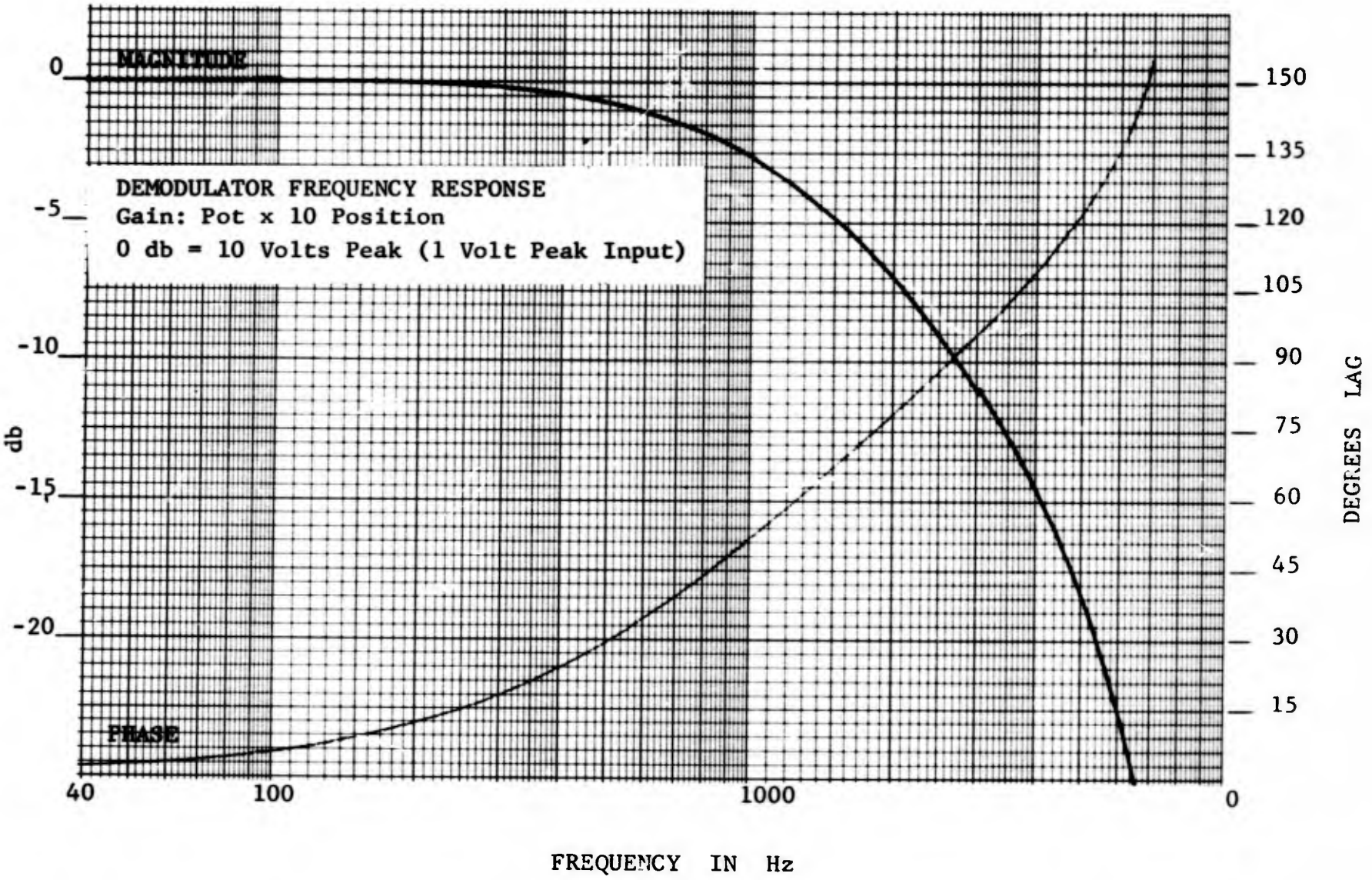
DEMODULATOR FREQUENCY RESPONSE
Gain: Pot x 10 Position
0 db = 10 Volts Peak (1 Volt Peak Input)
MAGNITUDE
PHASE
0
-5
-10
-15
-20
db
150
135
120
105
90
75
60
45
30
15
DEGREES LAG
40
100
1000
0
FREQUENCY IN Hz

FIGURE 41

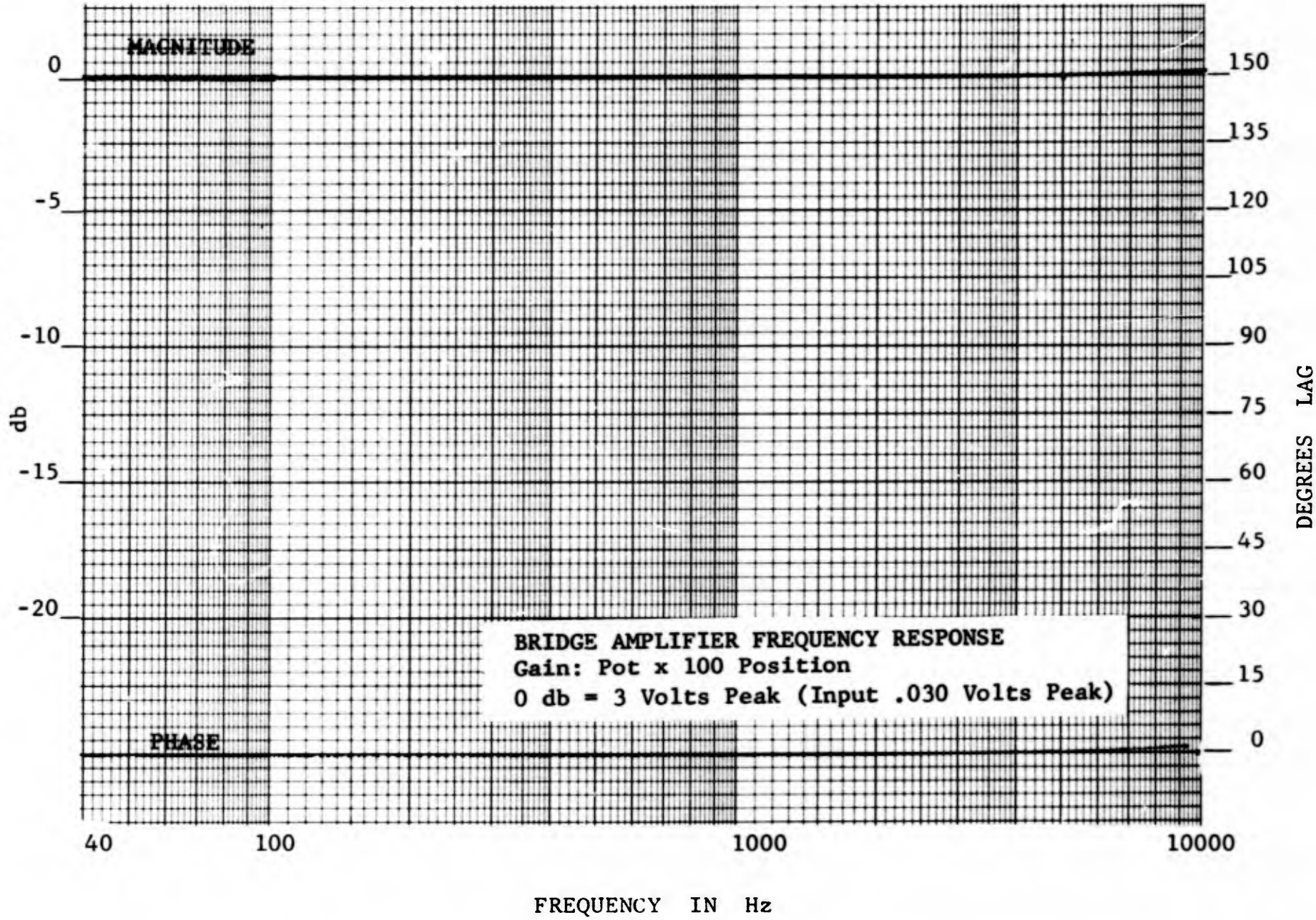
MAGNITUDE
0
-5
-10
-15
-20
db
150
135
120
105
90
75
60
45
30
15
0
DEGREES LAG
BRIDGE AMPLIFIER FREQUENCY RESPONSE
Gain: Pot x 100 Position
0 db = 3 Volts Peak (Input .030 Volts Peak)
PHASE
40
100
1000
10000
FREQUENCY IN Hz

FIGURE 42

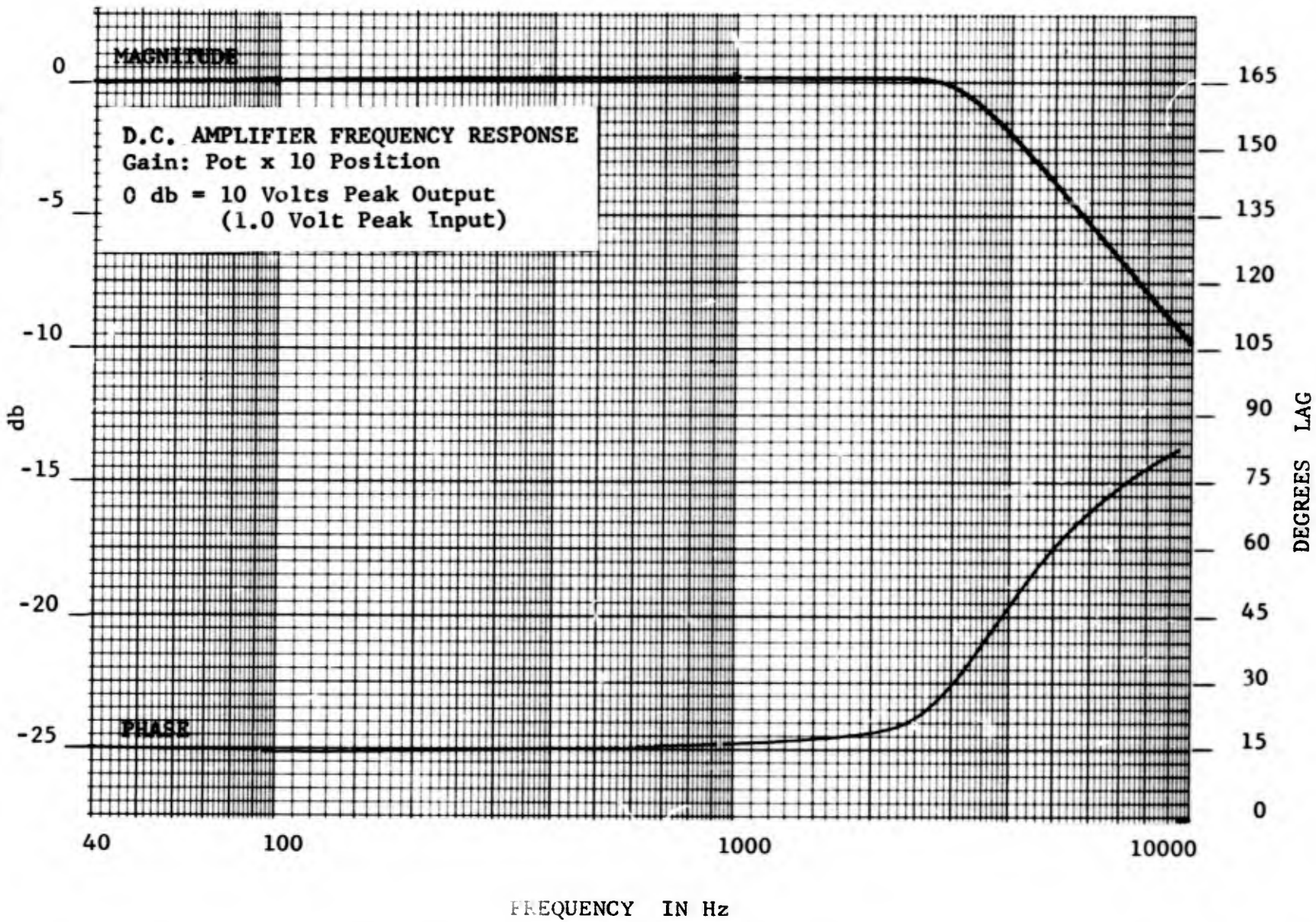
MAGNITUDE
D.C. AMPLIFIER FREQUENCY RESPONSE
Gain: Pot x 10 Position
0 db = 10 Volts Peak Output
(1.0 Volt Peak Input)
PHASE
0
-5
-10
-15
-20
-25
db
165
150
135
120
105
90
75
60
45
30
15
0
DEGREES LAG
40
100
1000
10000
FREQUENCY IN Hz

FIGURE 43

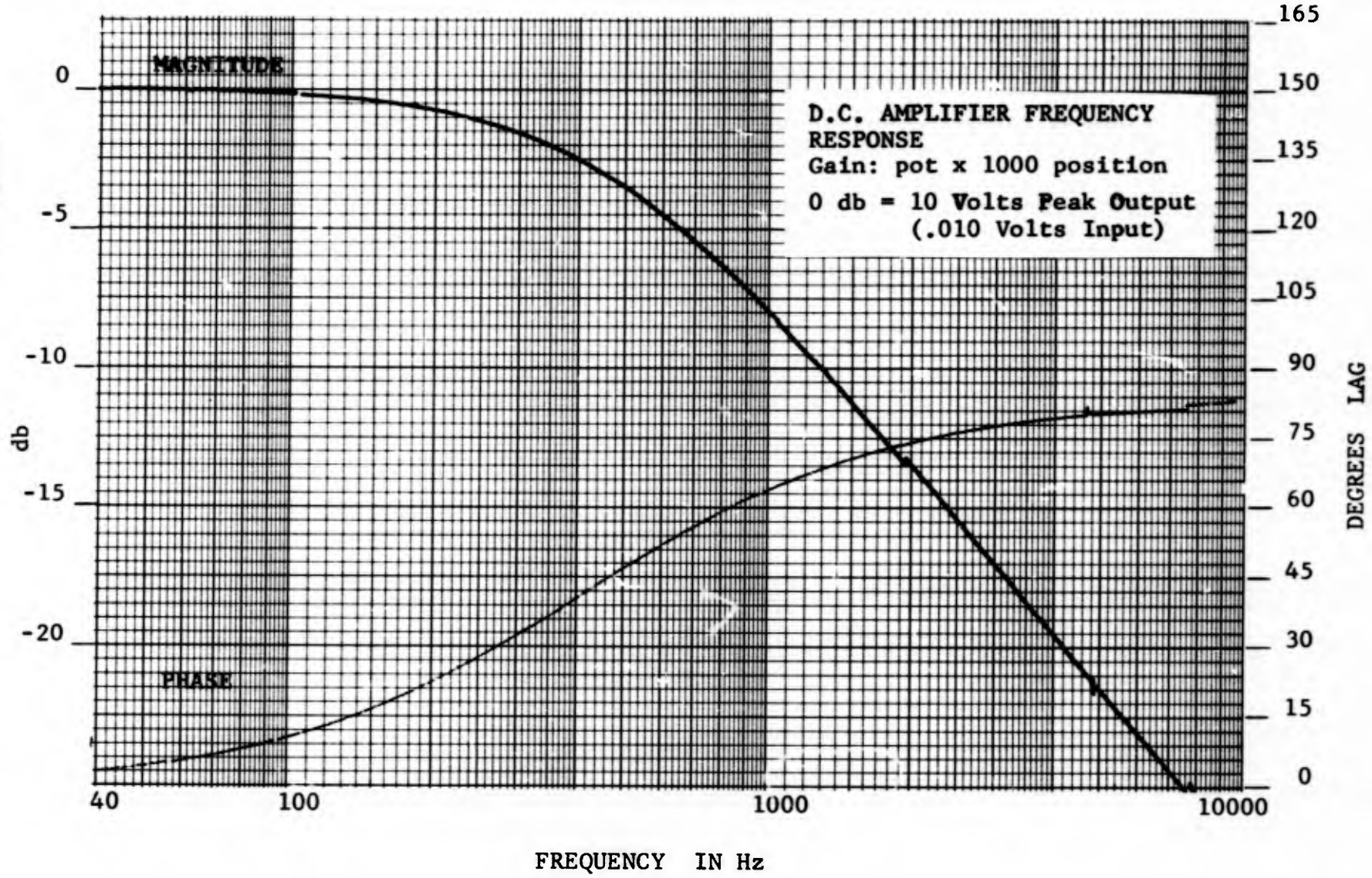
MAGNITUDE
PHASE
D.C. AMPLIFIER FREQUENCY RESPONSE
Gain: pot x 1000 position
0 db = 10 Volts Peak Output
(.010 Volts Input)
0
-5
-10
-15
-20
db
165
150
135
120
105
90
75
60
45
30
15
0
DEGREES LAG
40
100
1000
10000
FREQUENCY IN Hz

FIGURE 44

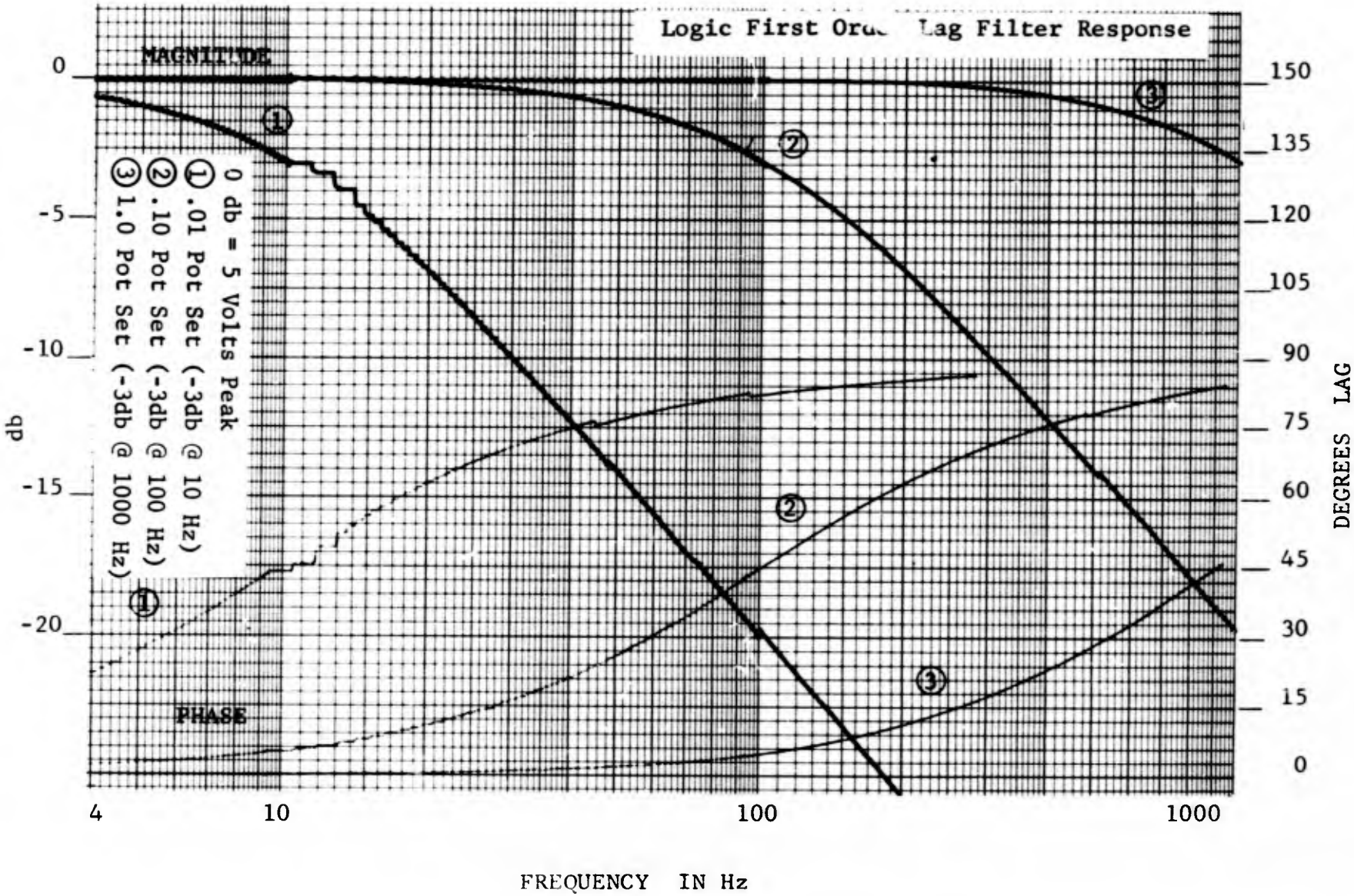
Logic First Order Lag Filter Response
MAGNITUDE
PHASE
0 db = 5 Volts Peak
① .01 Pot Set (-3db @ 10 Hz)
② .10 Pot Set (-3db @ 100 Hz)
③ 1.0 Pot Set (-3db @ 1000 Hz)
0
-5
-10
-15
-20
db
150
135
120
105
90
75
60
45
30
15
0
DEGREES LAG
4
10
100
1000
FREQUENCY IN Hz

FIGURE 45

FAILURE LOGIC TIME AND AMPLITUDE CHARACTERISTIC

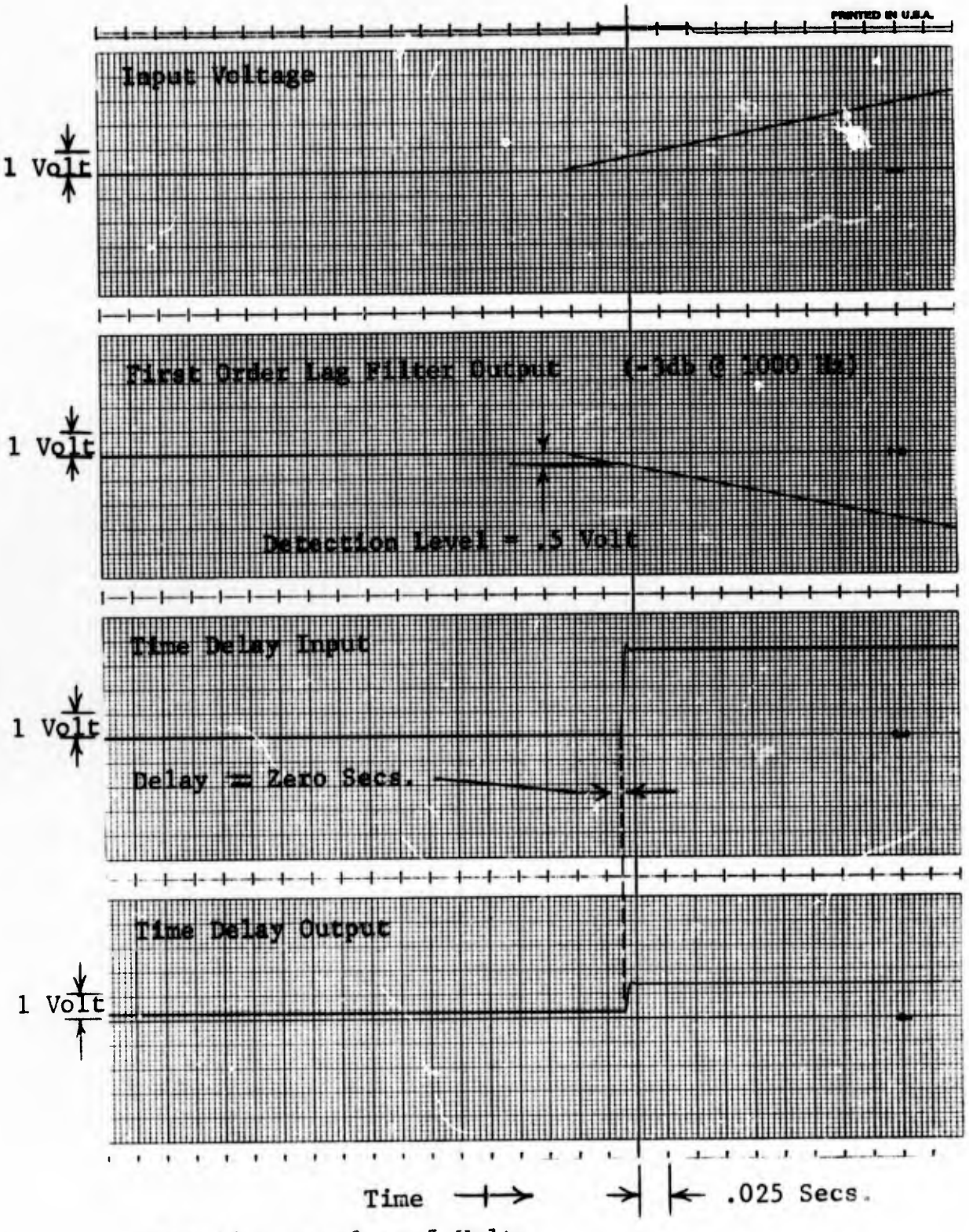

Detection Level = .5 Volts
Time Delay = 0 Secs.

FIGURE 46

FAILURE LOGIC TIME AND AMPLITUDE CHARACTERISTIC

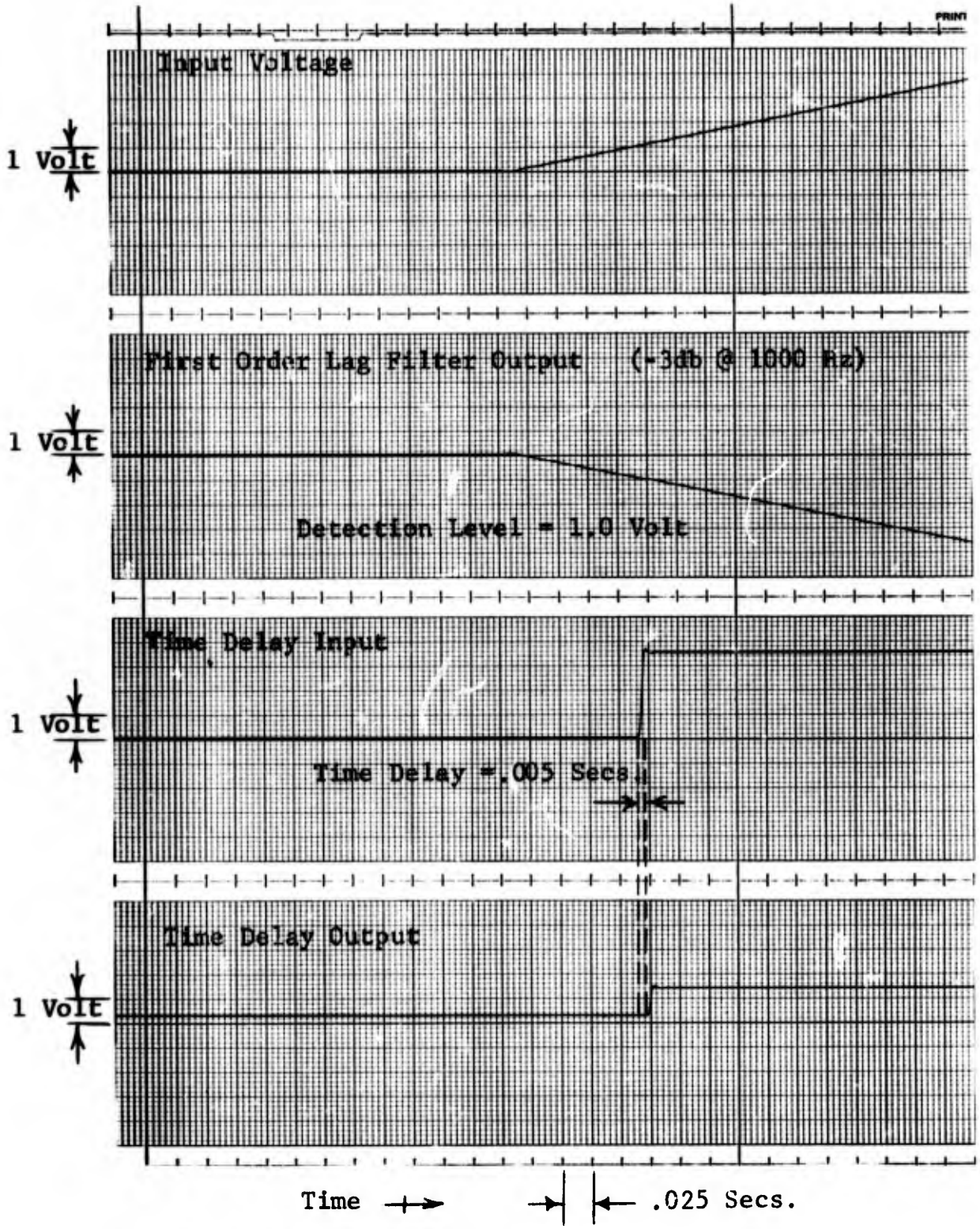

Detection Level = 1.0 Volt
Time Delay =.005 Secs.

FIGURE 47

FAILURE LOGIC TIME AND AMPLITUDE CHARACTERISTIC

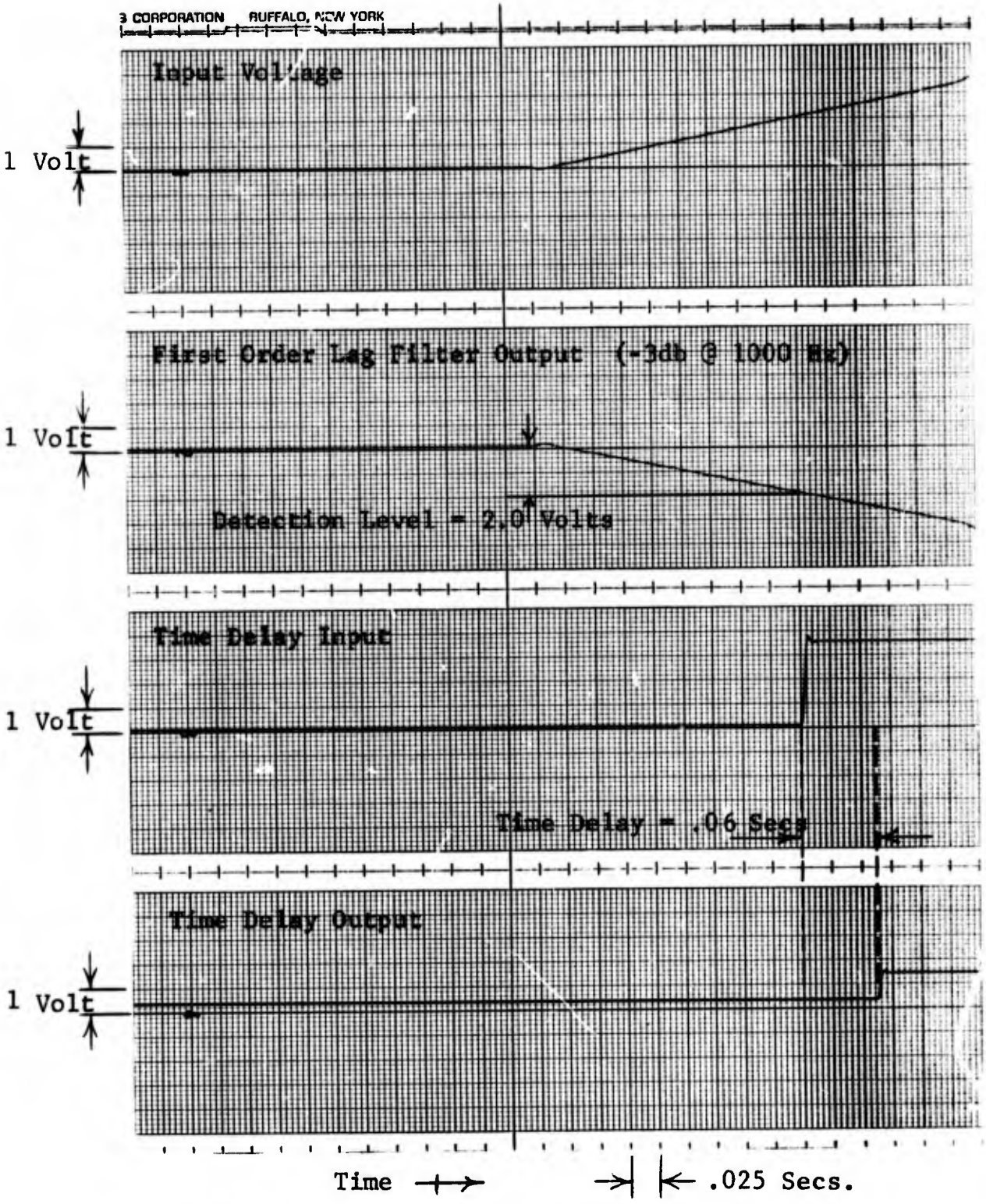

Detection Level = 2.0 Volt
Time Delay = .060 Secs.

FIGURE 48

FAILURE LOGIC TIME AND AMPLITUDE CHARACTERISTIC

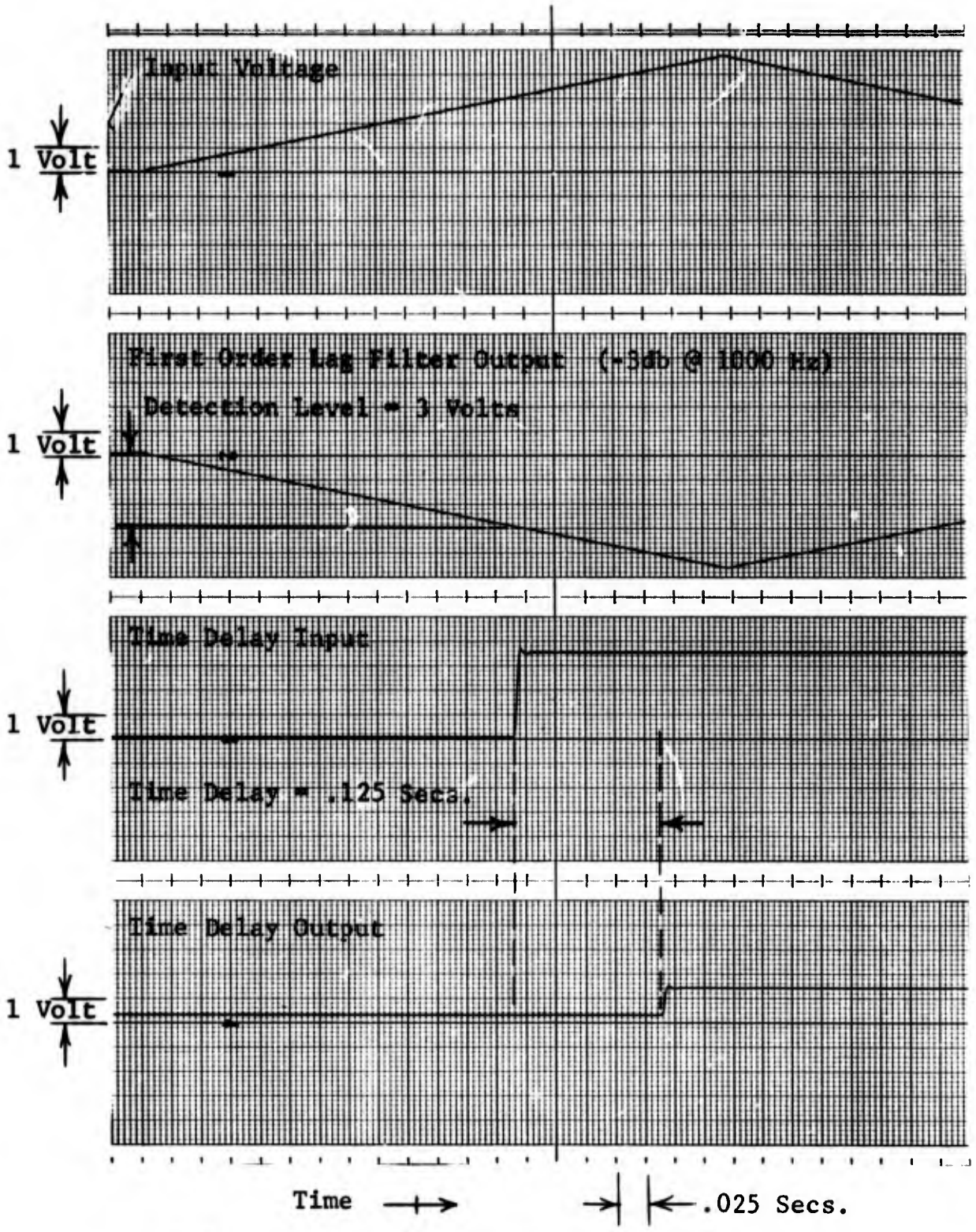

Detection Level = 3 Volts
Time Delay = .125 Secs.

FIGURE 49

The response of the lag filter as shown on FIGURE 45 illustrates the filter characteristics for three different break frequency settings. For all three settings, the phase and amplitude characteristics correspond to a first order lag (with -3 db amplitude corresponding to a 45 degree phase lag). The response agrees with the expected design performance. The "staircase" effects on curve (1) from 10 to 20 Hz is characteristic of the Bafco, Inc frequency response analyzer and is not caused by the lag filter electronics.

FIGURES 46 through 49 show the time and amplitude characteristics for different settings of the comparator threshold and the time delay. Note that the measured time delay is adjustable from 0 secs. to .125 secs. The range of time delay is variable within the time delay module. The range as tested is greater than the 0 to 100 millisecond delay used as a design objective.

4.5 SMS Failure Transfer Time

The transfer time for the SMS and logic unit as shown in FIGURE 50 indicates that .008 secs. is the minimum transfer time with the solenoid bypass mechanization used in the SMS actuators. This transfer time is consistent with simulating state-of-the-art control channel transfer mechanization characteristics.

4.6 SMS Control Channel Performance

Typical single channel and coupled channel frequency response for the SMS control channels is shown in FIGURES 51 through 55 as follows:

1. FIGURE 51 - SMS Frequency Response (25% and 100% input)

SMS FAILURE TRANSFER TIME

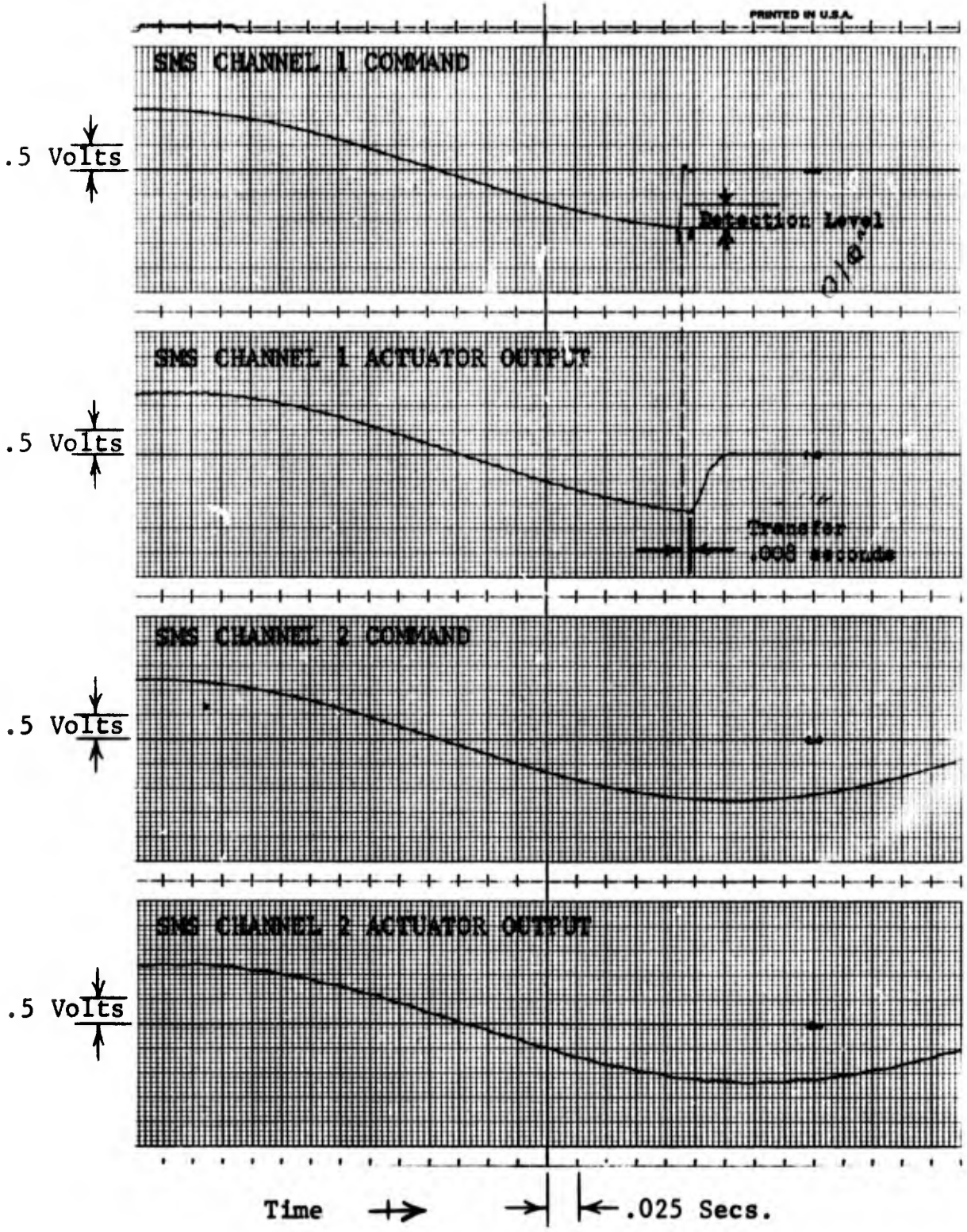

FIGURE 50

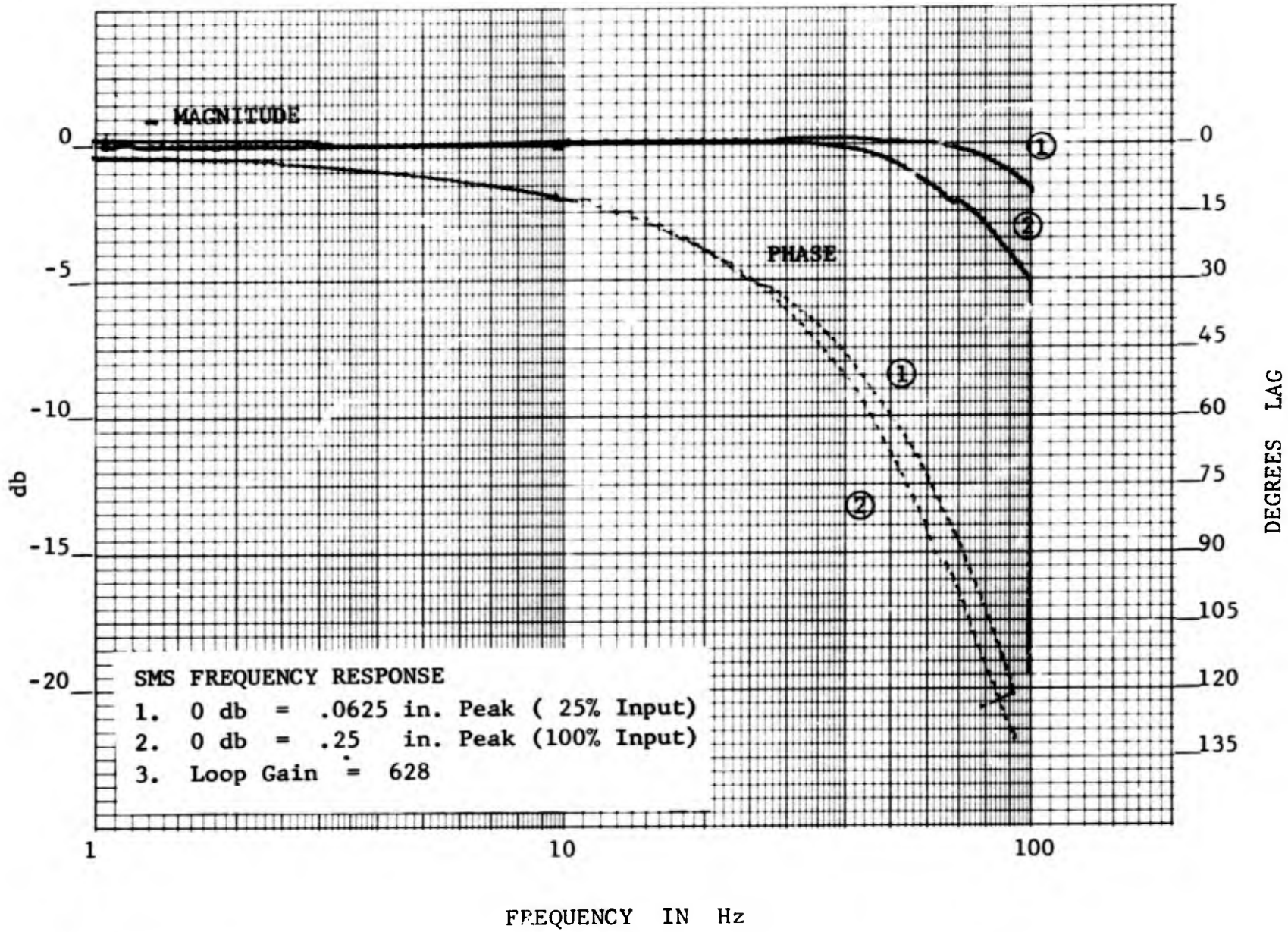
MAGNITUDE
PHASE
0
-5
-10
-15
-20
db
0
15
30
45
60
75
90
105
120
135
DEGREES LAG
1
10
100
FREQUENCY IN Hz
SMS FREQUENCY RESPONSE
1. 0 db = .0625 in. Peak (25% Input)
2. 0 db = .25 in. Peak (100% Input)
3. Loop Gain = 628

FIGURE 51

2. FIGURE 52 - SMS Single Channel Frequency Response (loop gains of 15.7, 157 and 628)

3. FIGURE 53 - SMS Frequency Response- Channels 2 & 3 Coupled

4. FIGURE 54 - SMS Frequency Response- Channels 2,3 & 4 Coupled

5. FIGURE 55 - SMS Frequency Response- Channels, 1,2,3 & 4 Coupled

FIGURE 51 shows the amplitude saturation characteristics of a single SMS control channel at a loop gain of 628. As indicated by curve (2) (100% input) on the figure, no amplitude sensitivity occurs at any frequency below 50 Hz. This demonstrates that for simulations having control channel frequency response requirements below 50 Hz, the amplitude effects of the basic SMS control actuator may be ignored. The 50 Hz "saturation effect" frequency exceeds the 20 Hz minimum design objective by a comfortable margin. Note that the frequency response of the single channel is only 1 1/2 db down at 100 Hz. The actuator dynamic effects below 20 Hz are minimal (no amplitude attenuation at all below 50 Hz and only 24 degrees phase lag at 20 Hz). This performance meets the design objective of $\pm$ 1 db small signal frequency response to 60 Hz.

FIGURE 52 shows the frequency response of an SMS single channel at three different loop gains. The loop gain change was accomplished by changing the servo driver gain. Note that at low loop gains (curve 1) the position and phase accuracy show minor variations caused by the low loop gain. This figure does illustrate the ability to vary the SMS control channel frequency response as desired. Curves 2 and 3 have the phase and amplitude characteristics of a first order lag. Curve 1 has characteristics of a second order system with a natural frequency of 100 Hz and a damping ratio of .7.

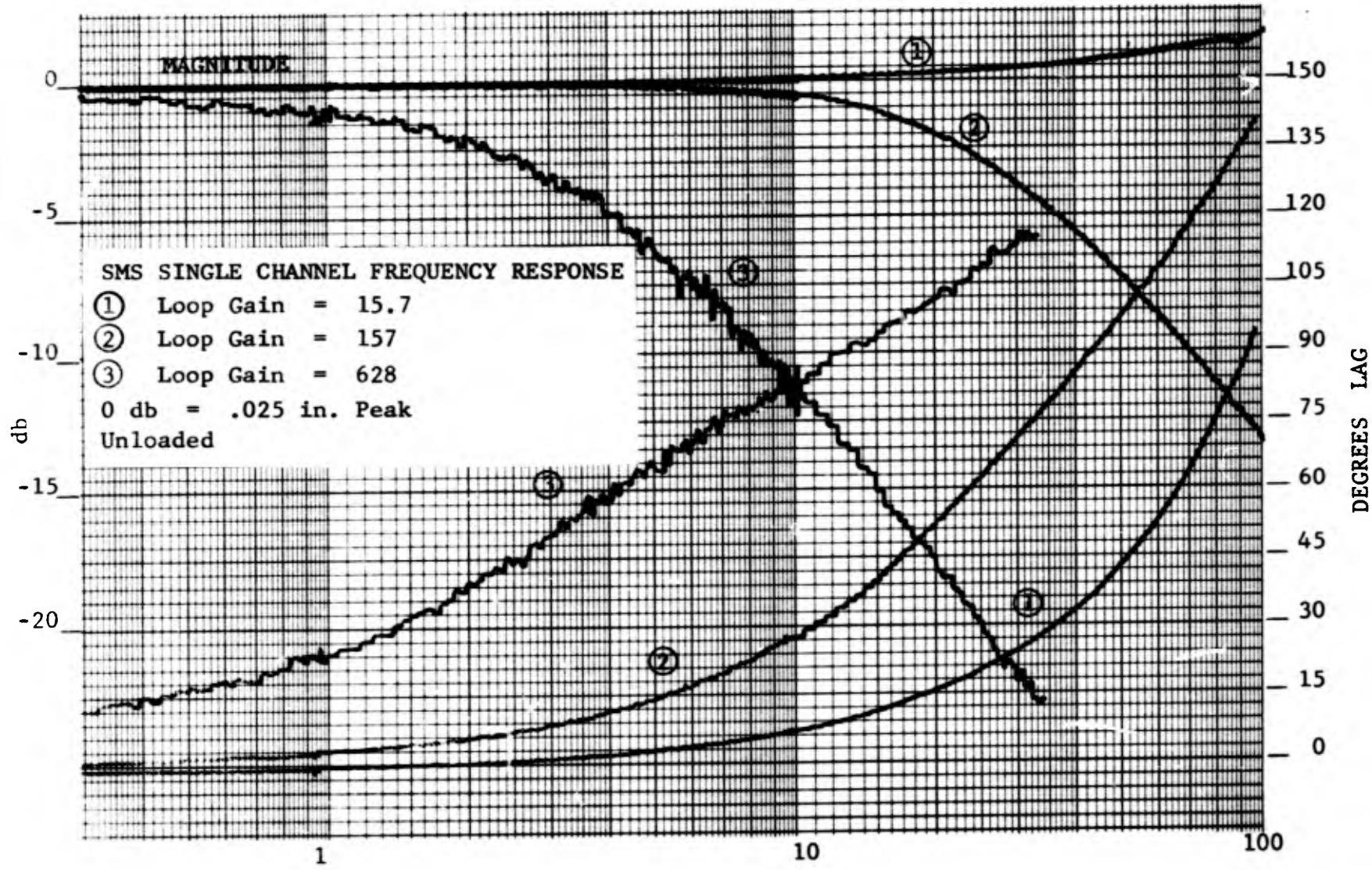
MAGNITUDE
SMS SINGLE CHANNEL FREQUENCY RESPONSE
① Loop Gain = 15.7
② Loop Gain = 157
③ Loop Gain = 628
0 db = .025 in. Peak
Unloaded
0
-5
-10
-15
-20
db
150
135
120
105
90
75
60
45
30
15
0
DEGREES LAG
1
10
100
FREQUENCY IN Hz

FIGURE 52

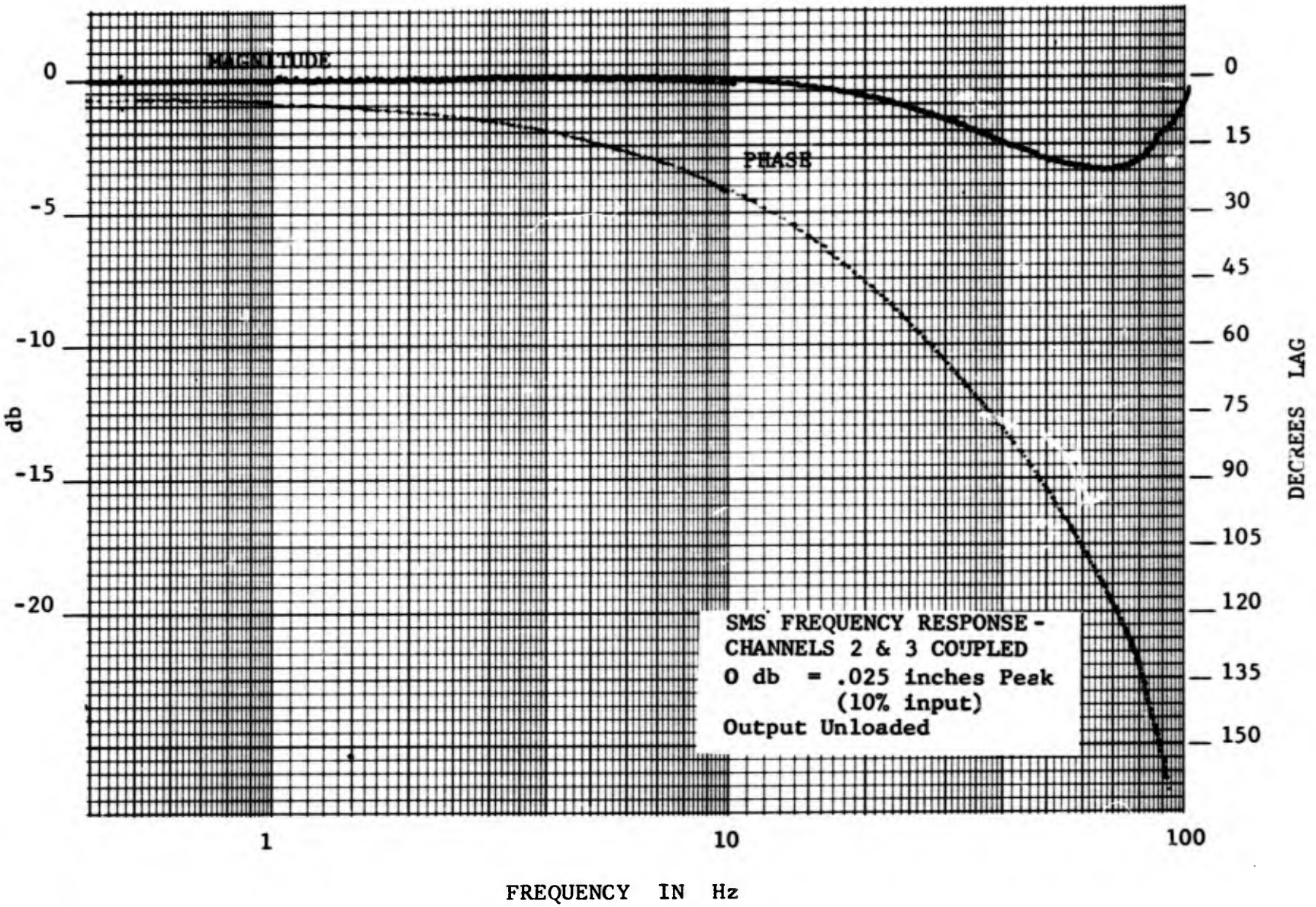
MAGNITUDE
PHASE
0
-5
-10
-15
-20
db
0
15
30
45
60
75
90
105
120
135
150
DEGREES LAG
1
10
100
FREQUENCY IN Hz
SMS FREQUENCY RESPONSE -
CHANNELS 2 & 3 COUPLED
O db = .025 inches Peak
(10% input)
Output Unloaded

FIGURE 53

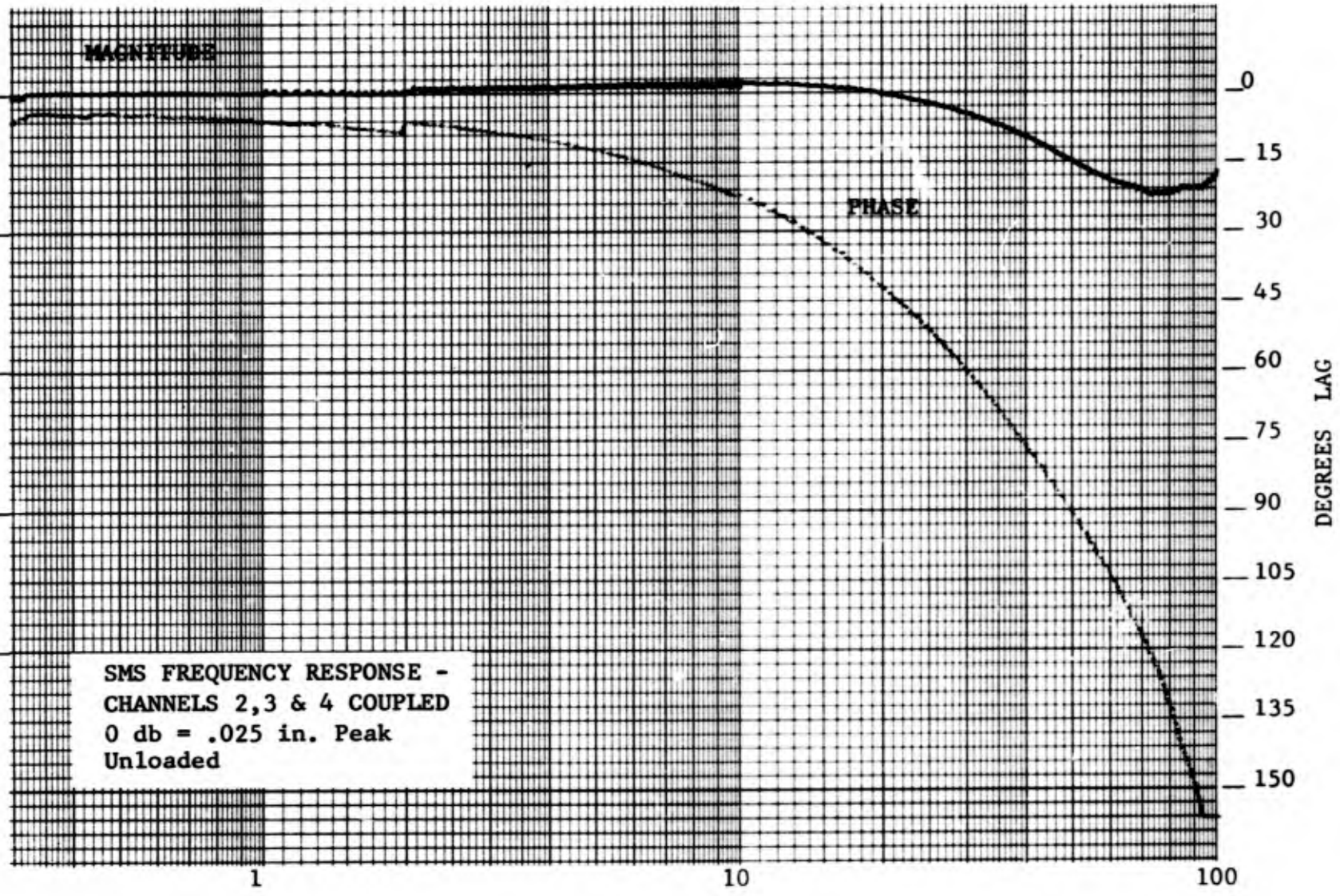
MAGNITUDE
PHASE
0
-5
-10
-15
-20
db
0
15
30
45
60
75
90
105
120
135
150
DEGREES LAG
SMS FREQUENCY RESPONSE -
CHANNELS 2,3 & 4 COUPLED
0 db = .025 in. Peak
Unloaded
1
10
100
FREQUENCY IN Hz

FIGURE 54

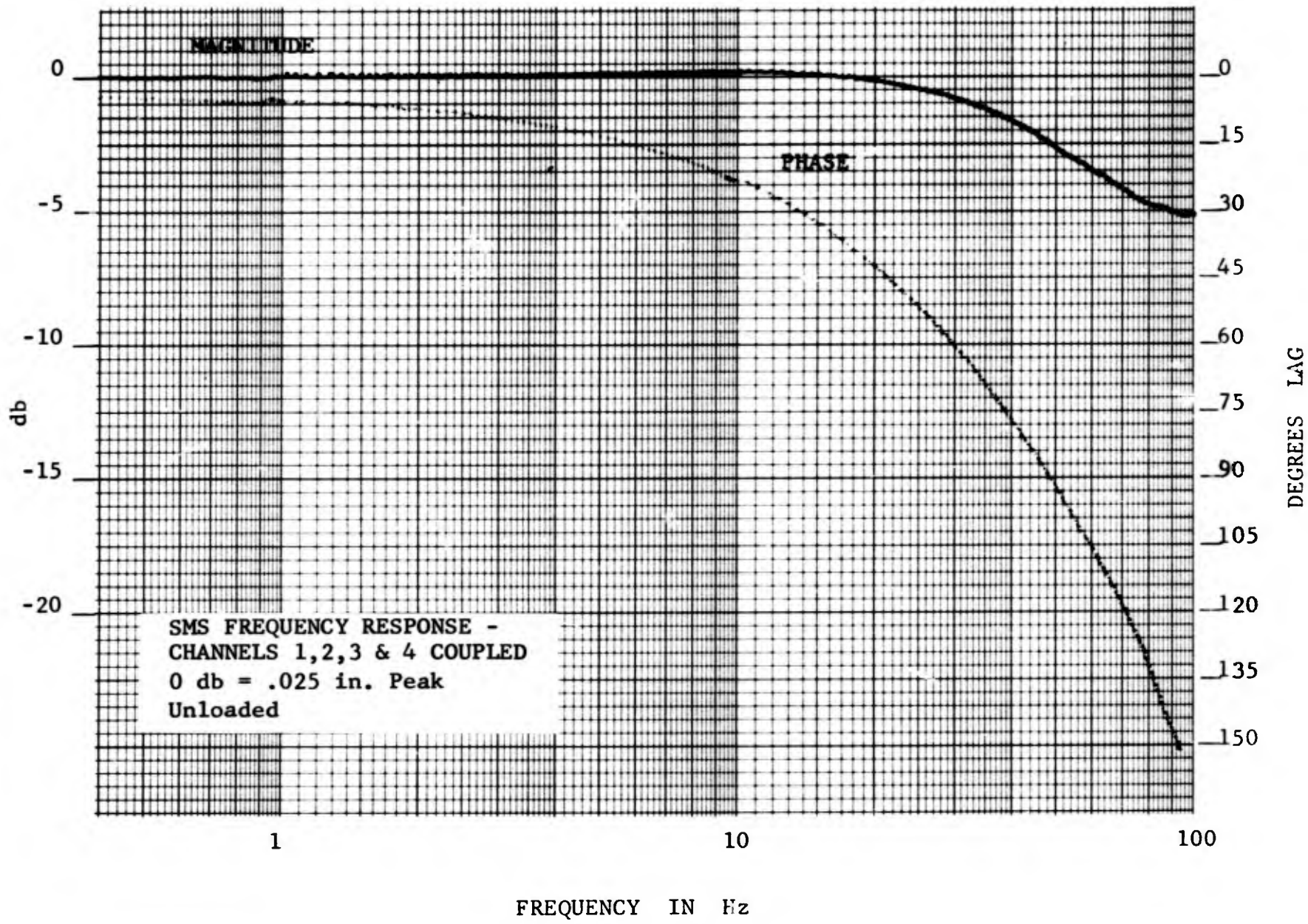
MAGNITUDE
PHASE
0
-5
-10
-15
-20
db
0
15
30
45
60
75
90
105
120
135
150
DEGREES LAG
SMS FREQUENCY RESPONSE -
CHANNELS 1,2,3 & 4 COUPLED
0 db = .025 in. Peak
Unloaded
1
10
100
FREQUENCY IN Hz

FIGURE 55

FIGURES 53, 54 and 55 shows the frequency response with the SMS channels coupled together. The loop gains for each channel were adjusted to produce a frequency response which was attenuated by 3 db at 80 Hz. Note the resonant peak shown on FIGURE 53 with channels 2 & 3 coupled together. This is the resonance of the coupling bar mass on the spring rate of the control actuators. With additional actuators, the actuator stiffness is increased and the resonant frequency of the coupling bar mass and actuator stiffness is increased. FIGURES 54 and 55 demonstrate this. Note that the frequency response of the SMS channels is unaffected by the coupling of actuators together, indicating that the four channels track each other accurately. This is important from the standpoint of simulating force sharing redundancy mechanizations. To evaluate performance degradation with channel mismatch, it is first necessary to have four channels which do not exhibit a force fight condition when coupled together.

FIGURE 56 illustrates the SMS position output linearity of the SMS control actuators at a loop gain of 376. The curve reveals no observable non-linearity.

FIGURE 57 indicates the breakout and running friction typical of the SMS actuators. As shown on the figure, the maximum pressure differential across the SMS actuator piston is approximately 50 PSI. This level is 1.67% of the available drive pressure differential.

4.7 PMS Control Channel Performance

The performance characteristics of the PMS control channels are indicated in the following figures:

1. FIGURE 58 - PMS Frequency Response
2. FIGURE 59 - Primary Position Linearity

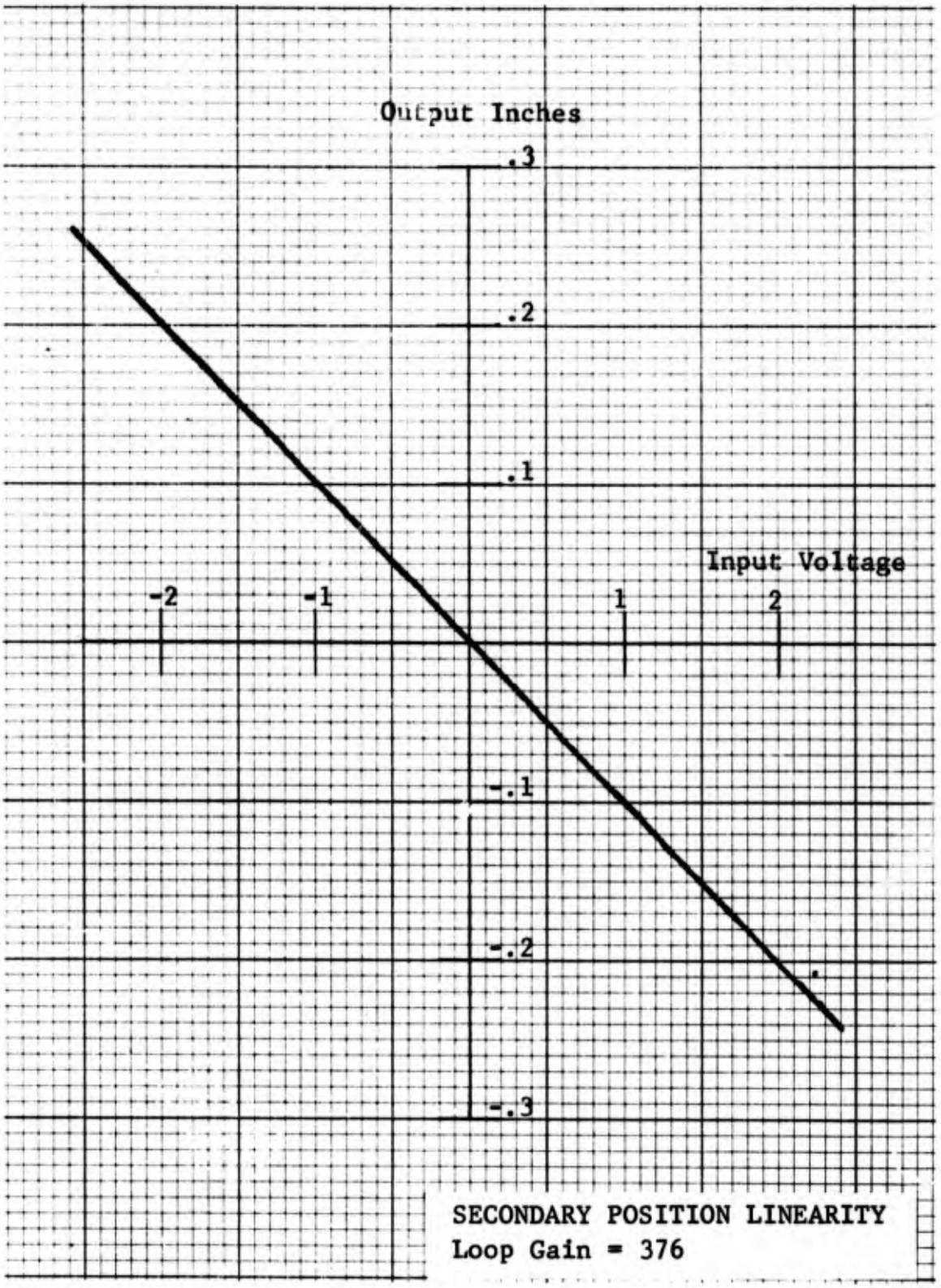
Output Inches
.3
.2
.1
-.1
-.2
-.3
Input Voltage
-2
-1
1
2
SECONDARY POSITION LINEARITY
Loop Gain = 376

FIGURE 56

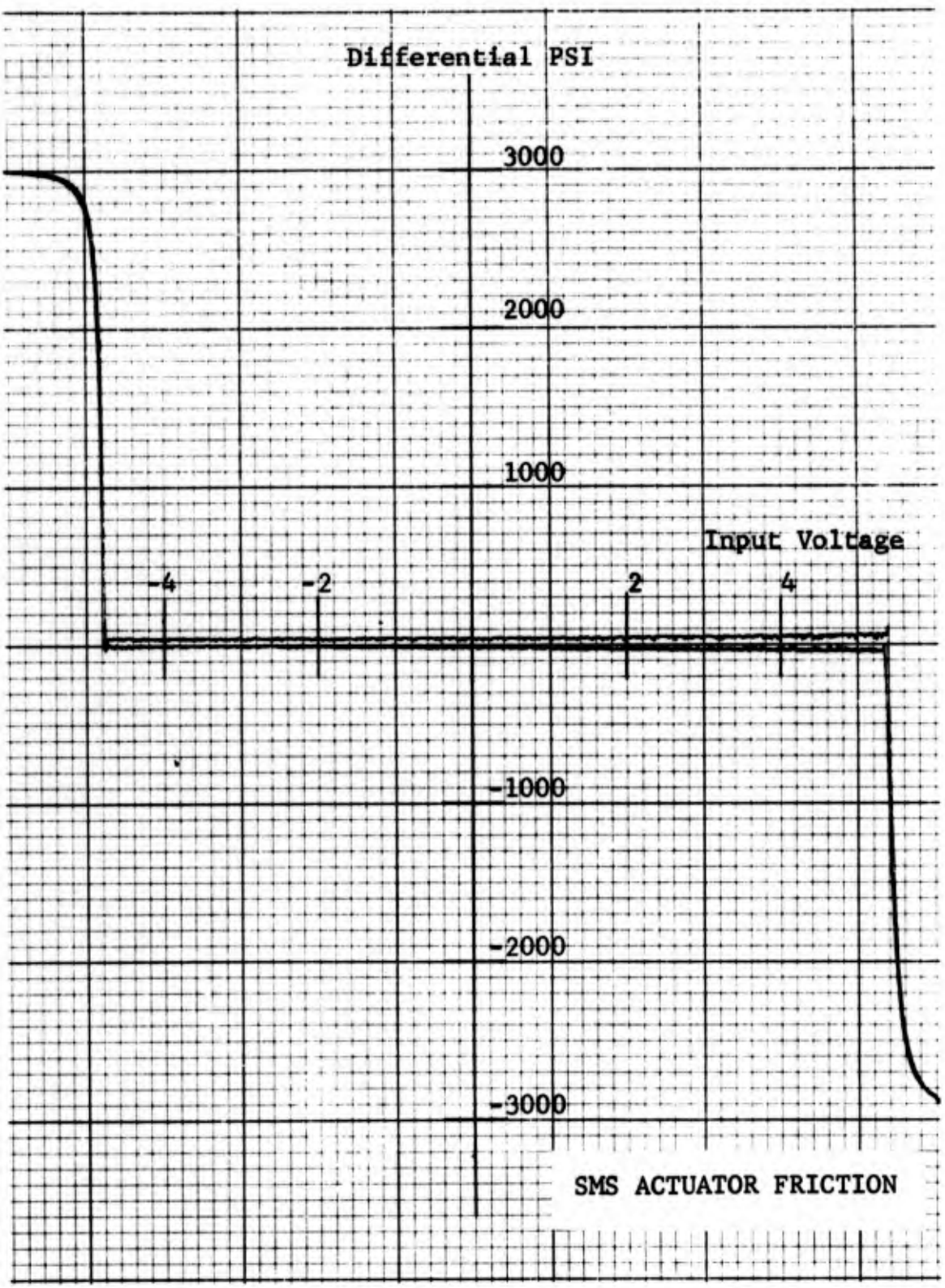
Differential PSI
3000
2000
1000
Input Voltage
-4
-2
2
4
-1000
-2000
-3000
SMS ACTUATOR FRICTION

FIGURE 57

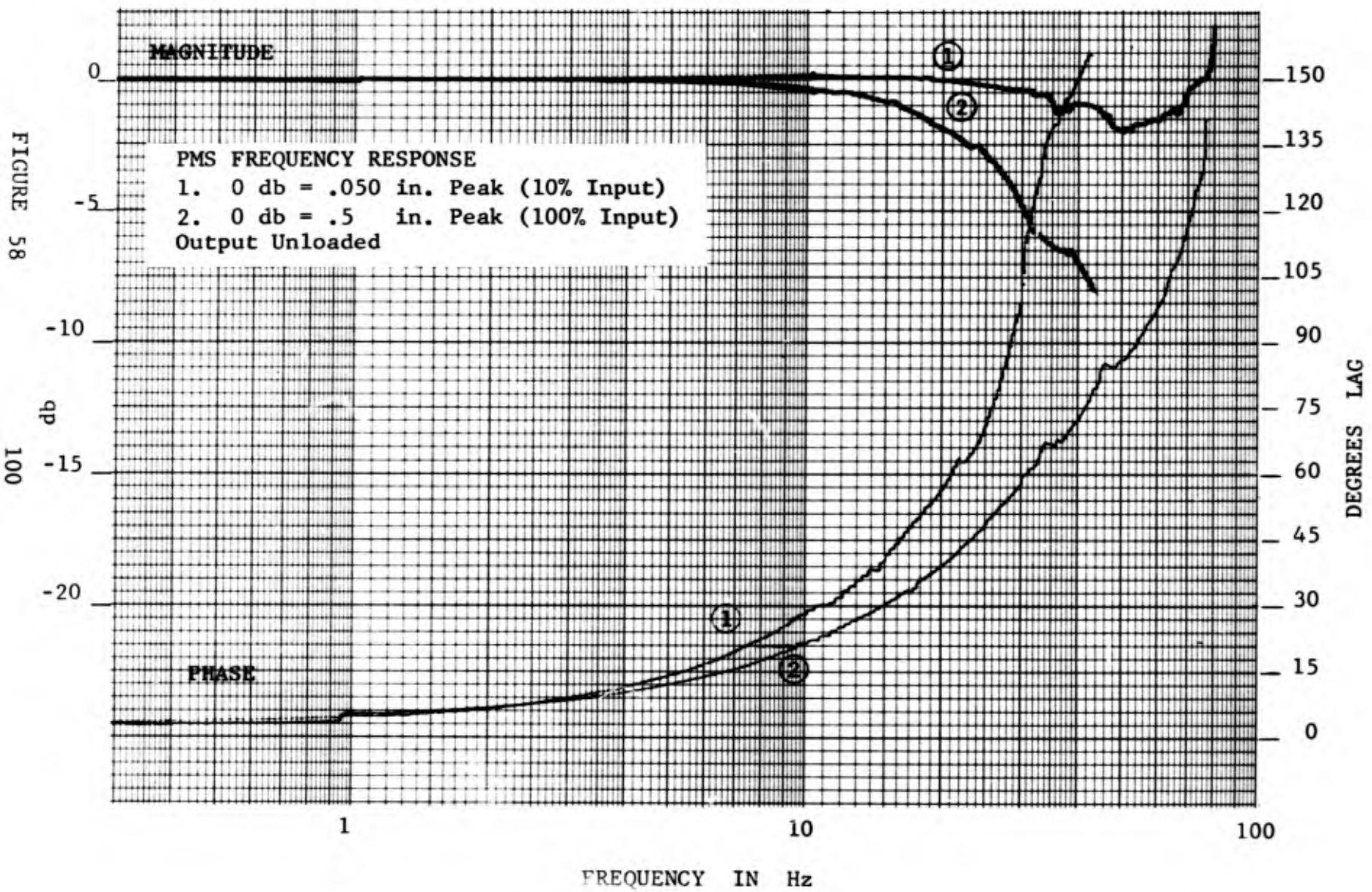

FIGURE 58

100

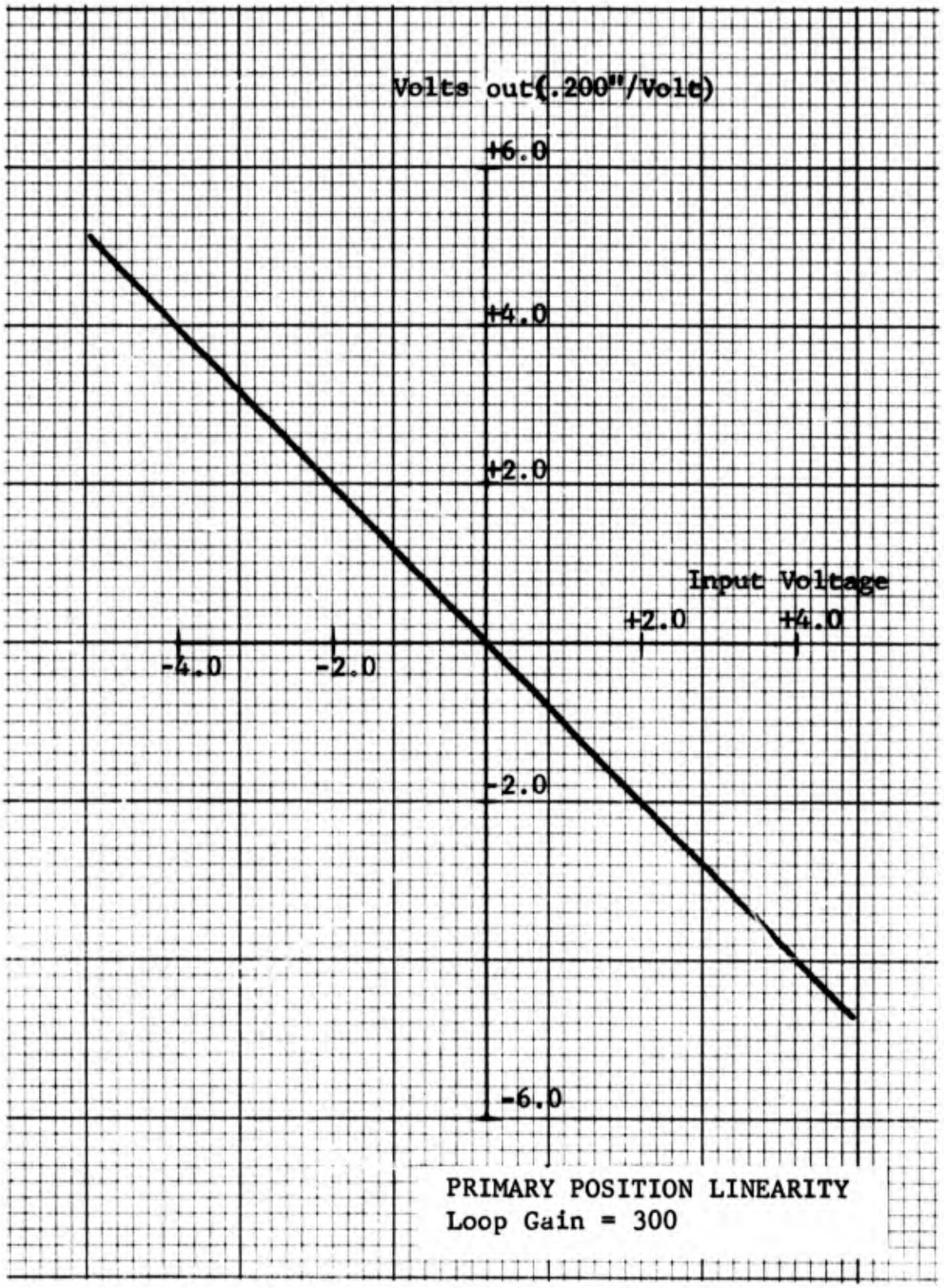
Volts out(.200"/Volt)
+6.0
+4.0
+2.0
Input Voltage
+2.0
+4.0
-4.0
-2.0
-2.0
-6.0
PRIMARY POSITION LINEARITY
Loop Gain = 300

FIGURE 59

The PMS frequency response shown in FIGURE 58 shows the small signal and maximum signal frequency response. The small signal frequency response is flat $\pm$ 1 db to 86 Hz. The full amplitude frequency response shows 1 db of attenuation due to amplitude saturation effects at 20 Hz. These measurements exceed the design value requirements of "small signal frequency response to 5 Hz" by a comfortable margin.

The primary position linearity plot of FIGURE 59 shows no observable non-linearity for the control actuator output at the loop gain used.

4.8 Load Channel Performance Results

The performance of the SMS load channels is indicated in the following figures:

1. FIGURE 60 - SMS Load Frequency Response (blocked load)
2. FIGURE 61 - SMS Load Frequency Response (0 load command)
3. FIGURE 62 - SMS Load Actuator Output V.S. Command

The blocked load SMS load response shown on FIGURE 60 indicates that for small amplitudes of motion, the load channel maintains both high and low load force response $\pm$ 1 db to 55 Hz. The load channel response is flat and with low phase shift to 20 Hz. This will adequately meet the small motion load requirements for all SMS simulations.

FIGURE 61 shows the ability of the SMS load channels to maintain the commanded load over the dynamic

DEGREES LAG
0
15
30
45
60
75
90
105
120
135
150
db
0
5
10
15
20
MAGNITUDE
PHASE
1
10
100
FREQUENCY IN Hz
SMS LOAD FREQUENCY RESPONSE
1. 0 db = 2500 PSI Peak
2. 0 db = 300 PSI Peak
Load Actuator Driving Control Actuator
Having 0 Position Command
Actuators Not Connected To Coupling Beam

FIGURE 60

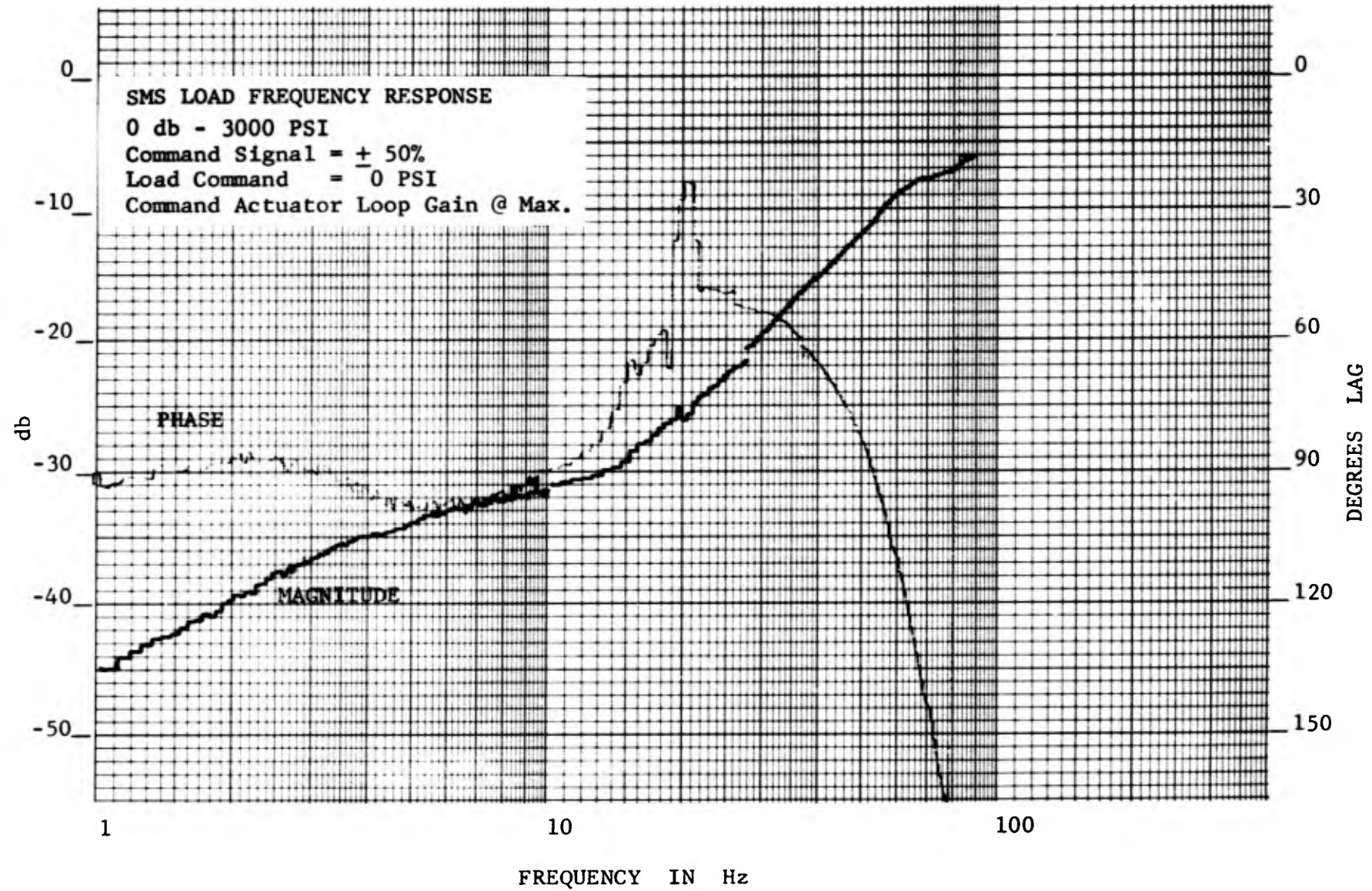

FIGURE 61
104

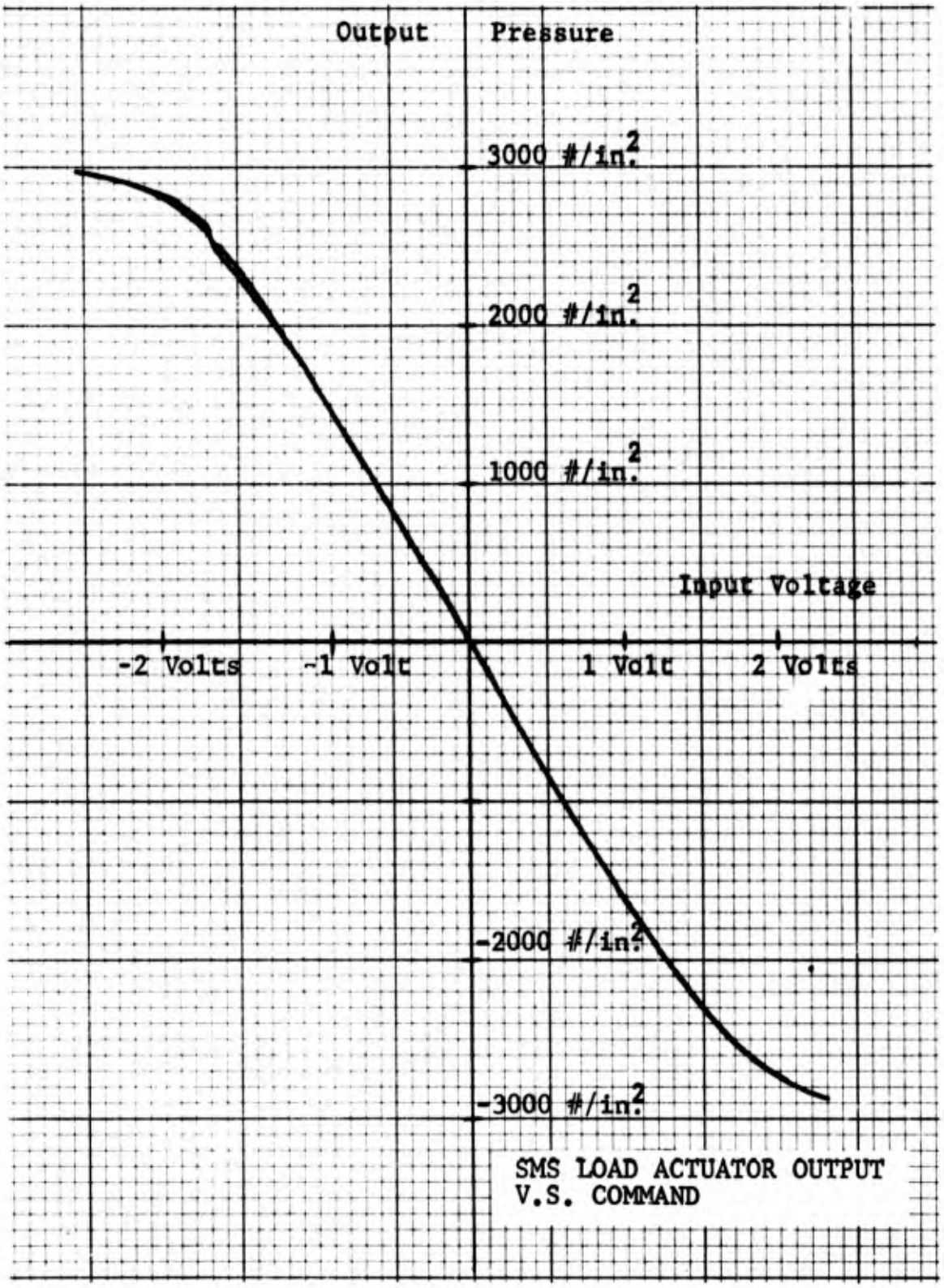
Output Pressure
3000 #/in.2
2000 #/in.2
1000 #/in.2
Input Voltage
-2 Volts
-1 Volt
1 Volt
2 Volts
-2000 #/in.2
-3000 #/in.2
SMS LOAD ACTUATOR OUTPUT
V.S. COMMAND

FIGURE 62

range of the SMS control actuators at an input level of 50%. Note that below 10 Hz the maximum load pressure error (the difference between the commanded "0" pressure and the actual output pressure) is less than 100 PSI (-30 db relative to 3000 PSI). The phase angle characteristic at low frequencies is caused by the leakage flow past the load actuator pistons. This leakage gives a 90 degree phase lag at frequencies below 10 Hz. At higher frequencies (where the flow to supply the compliance effects of the actuator exceeds the piston leakage flow) the phase lag reduces to zero. The low frequency phase lag can be reduced to zero by installing piston seals on the SMS load actuator pistons.

FIGURE 62 shows the SMS load output force linearity. For commanded loads to 70% of the maximum load, the load actuators exhibit linear load output characteristics. This is consistent with the normal characteristics of a load actuator control system.

The PMS load control channel performance characteristics are indicated on the following figures:

1. FIGURE 63 - PMS Load Frequency Response
2. FIGURE 64 - PMS Load Linearity

FIGURE 63 shows the "blocked load" PMS load frequency response at two different peak load levels of 300 # and 1500 #. The load response for both of these drive conditions is flat within 1 db to 30 Hz. The phase angle at 10 Hz is -18 degrees. These measurements indicate that the PMS load actuator will be adequate for the PMS simulations.

FIGURE 64 shows the PMS output load linearity for a pressure range of $\pm$ 1500 PSI. The figure shows

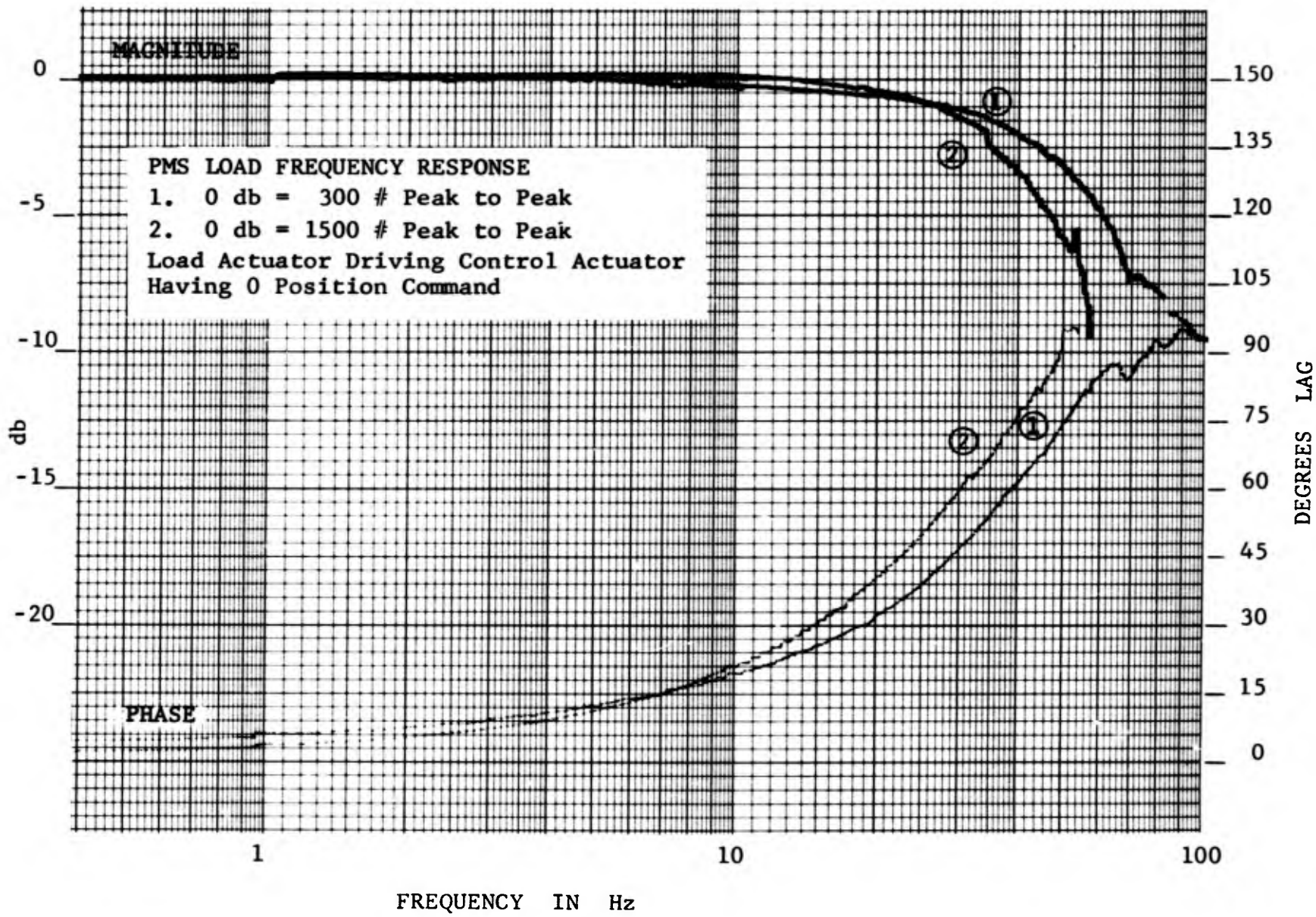
MAGNITUDE
PMS LOAD FREQUENCY RESPONSE
1. 0 db = 300 # Peak to Peak
2. 0 db = 1500 # Peak to Peak
Load Actuator Driving Control Actuator
Having 0 Position Command
PHASE
0
-5
-10
-15
-20
db
150
135
120
105
90
75
60
45
30
15
0
DEGREES LAG
1
10
100
FREQUENCY IN Hz

FIGURE 63

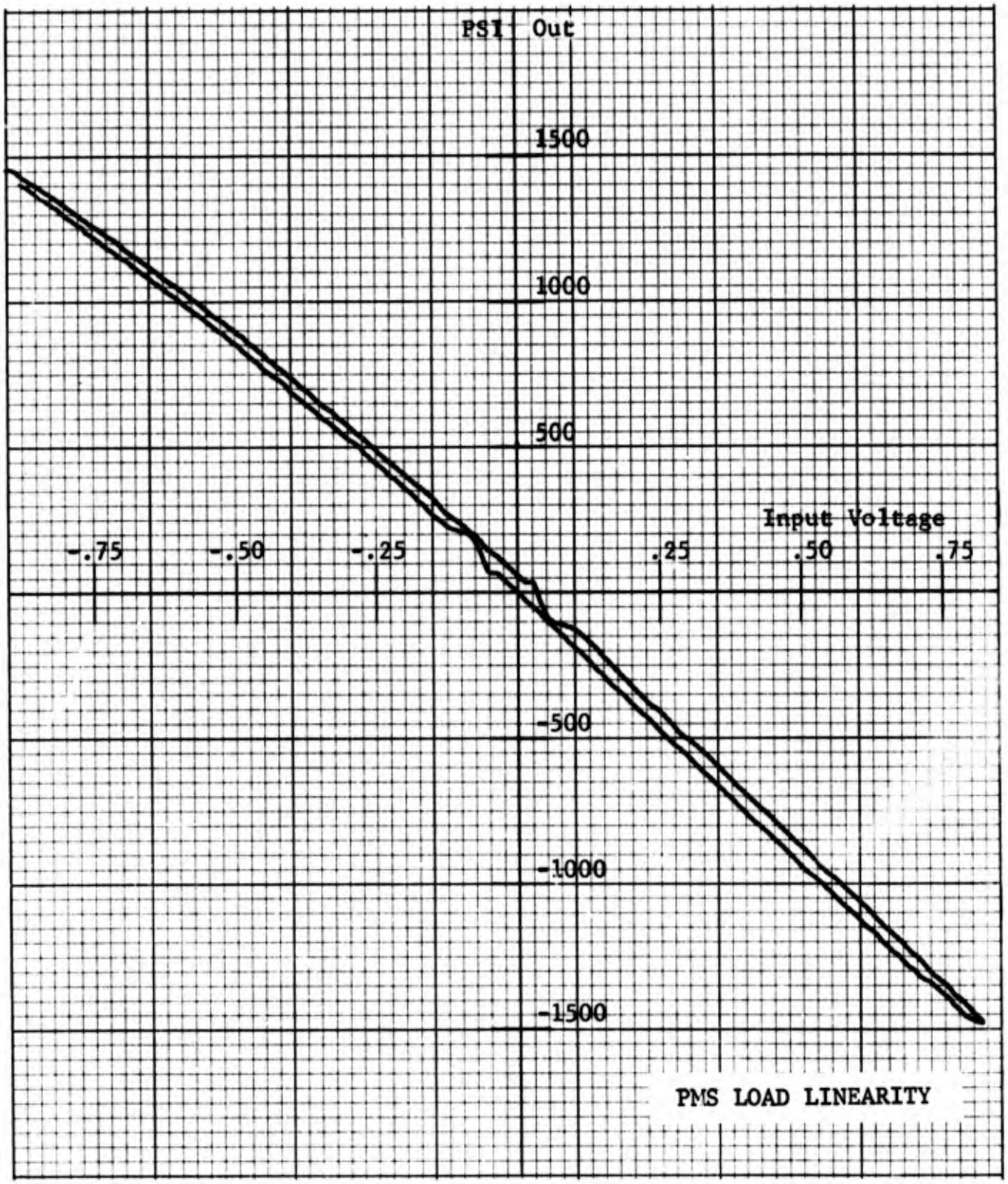
PSI Out
1500
1000
500
-500
-1000
-1500
-.75
-.50
-.25
.25
.50
.75
Input Voltage
PMS LOAD LINEARITY

FIGURE 64

some hysteresis for the output load characteristics. This hysteresis is caused by the piston seal friction for the PMS actuators and is also reflected on FIGURE 63 as the 3 degree phase lag at very low frequencies (less than 1 Hz). The slight non-linearities at +.05 and -.075 volts input are caused by the particular control valve for the channel measured and are a function of the valve lap conditions. The slight non-linearities and hysteresis are not sufficient to affect the load channel operation for the PMS simulations.

5.0 CONCLUSIONS AND RECOMMENDATIONS

From the test results, it is concluded that the elements of the hybrid simulator perform as designed. The response capability of the PMS and SMS exceeds their minimum requirements. Coupled operation of the SMS actuator channels is satisfactory with negligible force fight between channels. The response modifying electronics for the control and load channels work properly, allowing adequate variation of the SMS and PMS characteristics. The failure logic and transfer unit operates properly as designed. The minimum SMS failure detection and transfer time is .008 seconds (failure initiation to SMS actuator bypass). This is fast enough to allow duplication of the most rapid electromechanical transfer characteristics of state-of-the-art failure removal techniques. From the design and development effort, it is concluded that the hybrid simulator will allow convenient and accurate hardware simulation of state-of-the-art flight control systems.

To improve the operation of the hybrid simulator and/or correct items not possible to correct during the construction of the simulator, the following is recommended:

a. The PMS and SMS actuator return pressure to atmosphere piston rod seals should be replaced in order to reduce rod seal leakage.

b. The SMS load actuators should have seals installed on the pistons in order to improve the low frequency phase angle characteristics of the SMS load actuators.

c. The replacement digital dial drives received at the end of the contract should be installed on the electronic modules and the modules recalibrated.

d. Complete provisions for mechanically coupling PMS channels together.

SECTION III

FLUTTER SUPPRESSION TECHNIQUE INVESTIGATION

1. GENERAL

In order to better explain the particular approach to the surface flutter problem by using a particular technique, it is worthwhile first reviewing the flutter phenomena itself.

The term flutter is applied catagorically to oscillations of a flexible aerodynamic surface in a flow that is steady in the absence of the aerodynamic surface. If during all or part of the time of oscillation, the flow is separated, the flutter is called "stall flutter". Oscillation without the presence of flow separation is termed "classical flutter". Both types of flutter are discussed in the text "The Theory of Aeroelasticity" by Y.C. Fung of the University of California (Ref. 1). In addition, classical flutter has been recently researched by McDonnel Aircraft and the results published in AFFDL-TR-72-116 (Ref. 2). The particular method of modifying the actuator characteristics to prevent flutter agrees with the described physics of the flutter phenomenia as described in both these references.

1.1 Stall Flutter

"Stall flutter", which occurs at high angles of attack, resembles a forced vibration. If the speed of flow is gradually increased to beyond the stall flutter air speed at a high angle of attack, the intensity of flutter increases rapidly, reaches a maximum and then decreases to a practically flutter free condition. This is because at high angles of attack, the predominant frequency of the airstreams' vortex sheet over the aerodynamic surface becomes clearly defined. Stall flutter

---

1. Fung, Y.C., "The Theory of Aeroelasticity" Dover Publications, Inc., New York 1969
2. Triplett, W.E., et.al. "Active Flutter Suppression Systems for Military Aircraft, a Feasibility Study", AFFDL-TR-72-116, February 1973

is simply a reaction to the creation of these vortices in the wake. The stall flutter oscillation is predominately torsional. As a crude approximation, the flutter frequency is the same as the torsional natural resonant frequency in still air. Page 326 of Reference 1 states that "Stall flutter will occur when the aerodynamic work per cycle of pure pitch becomes positive and greater than the energy dissipated by the structure." The occurrence of stall flutter (as with classical flutter) can be analyzed by considering the energy extracted and returned to the airstream during one cycle of flutter motion. FIGURE 65 illustrates the work cycle equation for the lift vector L in torsional motion.

Stall Flutter

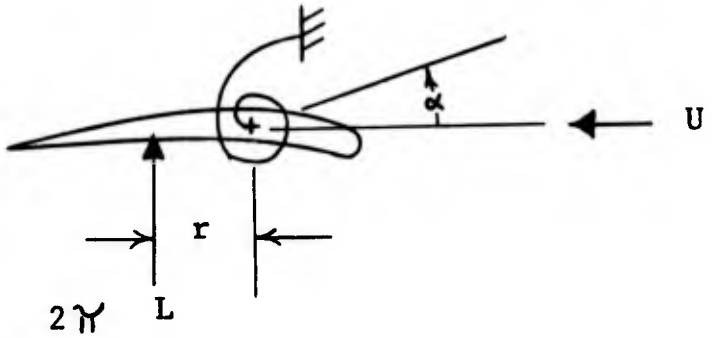

$$\text{Work/cycle} = \int_0^{\frac{2\pi}{\omega}} Lr(-\dot{\alpha})\cos\phi \, dt$$

Where: ϕ = the phase angle between the lift vector L and the torsional angle α at the frequency ω

L = lift vector (+ upwards)

α = angle of attack (+ counterclockwise)

r = distance between L and rotational centerline

U = airstream velocity

Note - Without integrating out, by inspection the work/cycle becomes positive when cos ϕ becomes negative.

FIGURE 65 - Stall Flutter Work/Cycle

Stall flutter occurs when the net aerodynamic work per cycle becomes positive (greater than the energy dissipated in the structure). As indicated in Reference 1, pages 321 and 322, the characteristics of stall flutter are:

a. Torsional motion predominates (where in classical flutter the torsional and bending strain are of the same order of magnitude, in stall flutter the magnitude of the bending motion becomes negligible in comparison to that in torsion).

b. The ratio of uncoupled bending and torsion resonant frequencies of the surface in still air has little effect on the stall flutter (whereas in classical flutter, there is a minimum airspeed where flutter occurs corresponding to when the torsional and bending resonant frequencies are the same).

1.2 Classical Flutter

Classical flutter occurs at low angles of attack and differs from stall flutter in that both torsional and bending motion of the aerodynamic surface in the airstream are inherent in the flutter phenomena. The flutter occurs because the speed of flow over the surface affects the amplitude and phase shift of the torsional motion in relation to the bending motion in such a way that energy is absorbed by the airfoil from the airstream. Since flutter is an oscillation induced by aerodynamic forces without any source of energy other than the airstream, flutter is possible only if the oscillating body (with mean position assumed constant) can extract energy from the airstream. The body in oscillation will be unstable if energy is gained from the airstream in completing a cycle. By way of further example, consider an airfoil performing only vertical oscillation (no torsional motion) with a constant peak amplitude H_o. Let the vertical displacement be described by the expression:

$$H = H_o \, e^{i\omega t}$$

Where: H = the instantaneous deflection (+ downward)
ω = the frequency of oscillation
t = time

The velocity of downward motion is $\dot{H} = i\omega H_o e^{i\omega t}$ (from differentiating the above expression with respect to time). If H were a constant, the downward motion would produce a lift force L_o on the airfoil of:

$$L_o = \tfrac{1}{2}\rho U^2 A \frac{dC_l}{d\alpha} H/U$$

Where: $\tfrac{1}{2}\rho U^2$ = the dynamic pressure
A, = the surface area of the airfoil
C_l = the coefficient of lift
α = the angle of attack

Since H varies with time, the instantaneous lift of the airfoil varies with time, both in magnitude and phase. Therefore the instantaneous lift L can be written in terms of the steady lift L_o as:

$$L = L_o \, r' e^{i\beta'}$$

Where: r' = the ratio of the absolute value of the instantaneous lift to the steady lift

β' = the phase angle by which the instantaneous lift leads the steady value at the frequency ω

When the airfoil moves through a distance dH, the work done by the lift vector L in terms of real variables is:

$$dW = -LdH = -LH\,dt$$

In terms of L and H (which are expressed in complex terms) these real variables are the real parts of the complex expression (the imaginary parts being used to indicate phase). Therefore,

$$dW = -\text{Real Part } (L) \cdot \text{Real Part } (\dot{H})\,dt$$

Integrating through a cycle of oscillation,

$$W = -\int_0^{\frac{\pi 2}{\omega}} \text{Real Part } (L) \cdot \text{Real Part } (\dot{H})\,dt$$

$$= -\tfrac{1}{2}\rho UA \frac{dC_1}{d\alpha} (\omega H_o)^2 r \int_0^{\frac{\pi 2}{\omega}} \sin(\omega t + \beta) \sin \omega t\,dt$$

$$= -\frac{\pi}{2} \rho \frac{dC_1}{d\alpha} \omega H_o^2 r \cos\beta$$

Therefore, for a constant dC_1/d_α, the gain of energy W by the airfoil from the airstream is proportional to - cos

For $-\frac{\pi}{2} < \beta < \frac{\pi}{2}$, W is negative and the airfoil will lose energy to the airstream.

This example shows the importance of the phase angle between applied aerodynamic force and the oscillatory motion. Pure bending flutter cannot occur. However, when a combination of the torsional and bending degrees are allowed, it is possible that a combination of phase relationships will allow the energy input to the airfoil

to be positive. The fundamental cause of classical flutter is that the airfoil, by adjusting its phase shift, extracts energy from the airstream.

The fact that the phase shift and amplitude ratio of the torsion and bending motions that follow a disturbance depend largely upon the airflow over the surface is of fundamental importance. It is this dependance on the airflow that causes flutter to occur at a certain critical speed.

FIGURE 66 from Reference 2 (pages 24 and 25) illustrates the variation in phasing between the torsional and bending motions for classical flutter and the relative effects on the work (energy) retained by the surface through each cycle of motion.

FIGURE 67 from Reference 1, page 222 shows a relief representation of the flutter phenomena. At zero airspeed, the lower amplitude peak is the bending frequency response of the surface. The upper peak is the torsional resonant frequency. With increasing airspeed, the flutter amplitude goes divergent at a finite airspeed. Note that the flutter frequency lies someplace between the bending and torsional resonance frequencies.

1.3 Technique Available to Raise The Airspeed At Which Flutter Occurs

In the case of stall flutter, the flutter occurs when the aerodynamic work per cycle in pure pitching motion becomes greater than the energy dissipated by the structure. Experiments and analysis show that the stall flutter speed can be increased by increasing the torsional stiffness and reducing the mass moment of inertia (Reference 1, page 326). This has the effect of increasing the resonant frequency of the free torsional oscillation. In addition, since stall flutter occurs when the energy (net) per cycle of pitch motion becomes positive (with the net energy input becoming greater than the energy absorbed by the surface), increasing the torsional

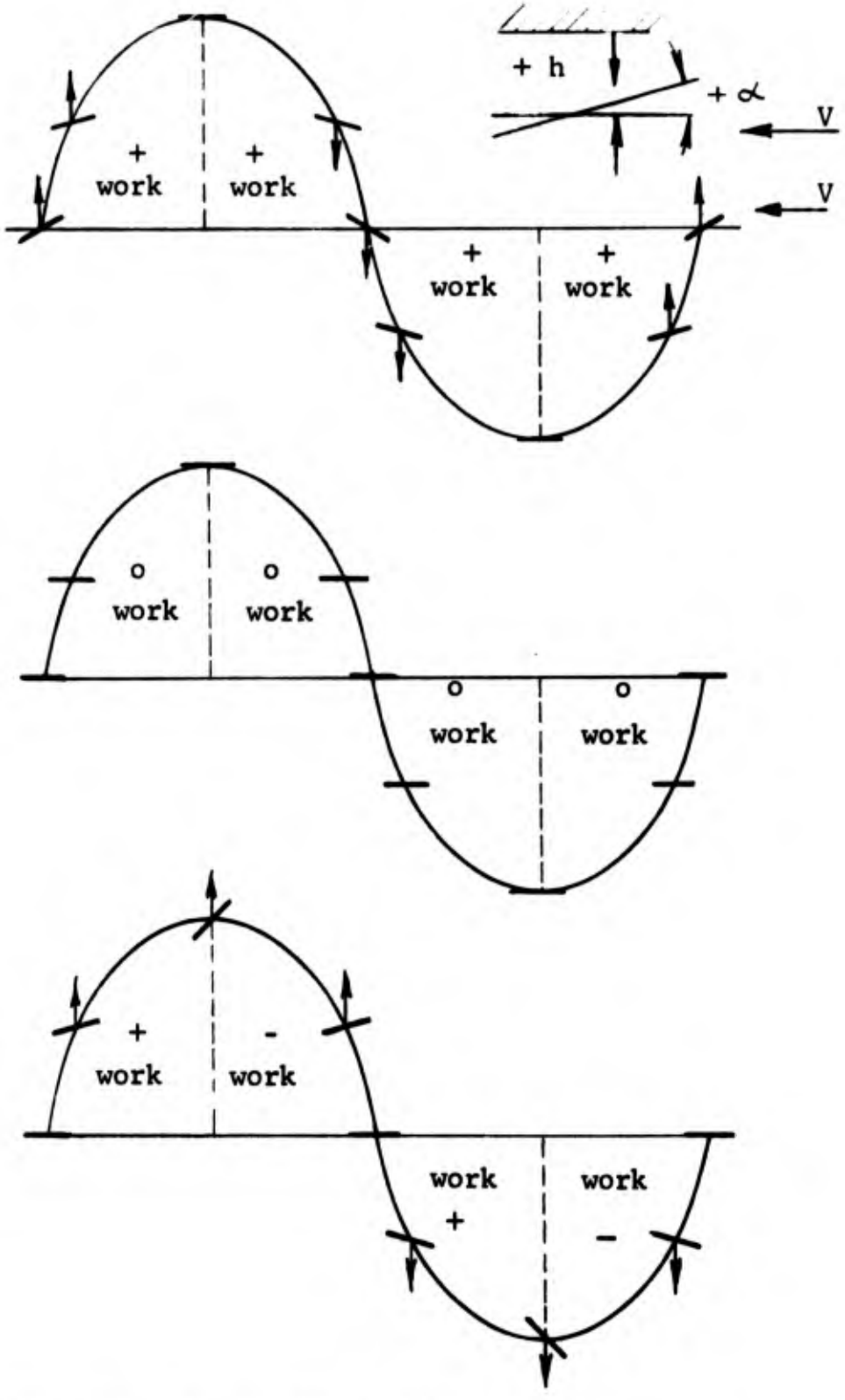

FIGURE 66 - Bending-Torsion Phasing Effects on Work/Cycle

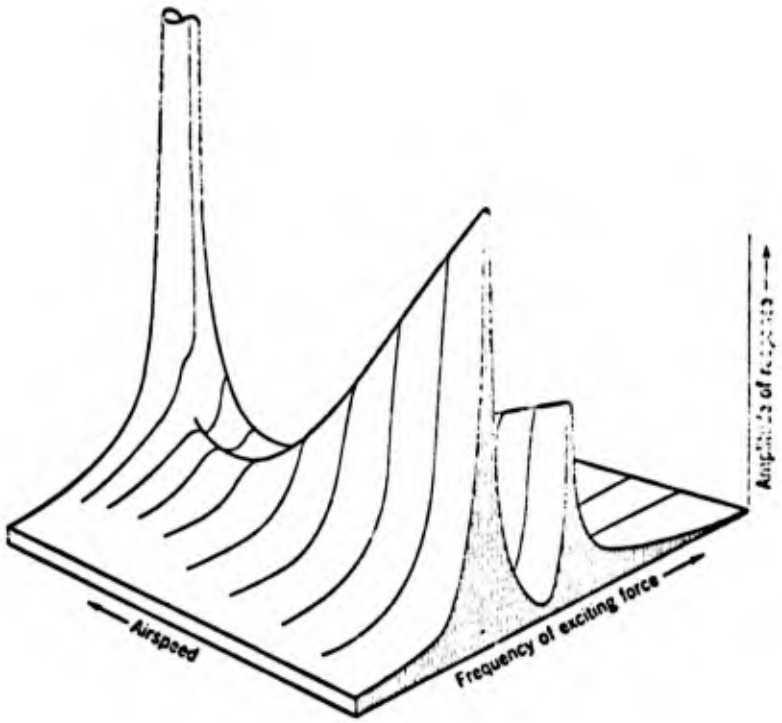

Relief map of the amplitude response of the vertical displacement of a wing subjected to a periodic exciting force acting on the elastic axis. Damping factor $g_h = g_\alpha = 0.05$

FIGURE 67 - Relief Representation of Flutter

damping of the airfoil motion will raise the stall flutter speed. For aerodynamic surfaces where the torsional stiffness is primarily determined by the control actuator, this damping can be accomplished by increasing the actuator damping characteristics.

For classical flutter, the bending and torsional motions at the flutter frequency are not in phase with each other. At the flutter frequency, the torsion motion lags the bending motion by 90^{o}. If either bending or torsion is suppressed, coupling will not occur. Notice, as shown in FIGURE 66 , when flutter occurs, the bending deflection peak and torsion deflection peak are 90^{o} out of phase. When the bending strain is at a maximum, the torsional strain is at a minimum. From an energy standpoint, this indicates that there is a periodic transfer of potential energy (stored energy) from a bending to a torsional mode of deflection. Suppression of the bending-torsion flutter of an airfoil can be accomplished by several methods as follows:

a. Changing the phase relationships between the bending and torsional motions.

b. Increasing the torsional (or bending) stiffness to eliminate one mode of motion.

c. Increasing the damping of the torsional and/or bending motions (Reference 2, pages 88 and 94).

The conventional way of increasing the flutter speed is to improve the stiffness of the airfoil. For slab type surfaces (like the F-4 and F-111 horizontal tail) the torsional stiffness is primarily determined by the control actuator. The technique of increasing the torsional stiffness is used to raise the resonant frequency. The higher the torsional resonant frequency, the higher the airspeed necessary to produce the driving force amplitude and frequency to cause flutter. Note that the actuator stiffness at resonance, not below, is the stiffness

that is important from a flutter standpoint. Techniques that increase actuator stiffness below resonance will have no effect on flutter suppression. In fact, to be effective, the stiffness value must be maintained out past the resonant frequency desired. For slab type surfaces, increasing the stiffness has generally been accomplished by increasing the actuator size --- particularly the drive area since the oil column stiffness generally dominates the actuator stiffness value. This is an actual stiffness increase by increasing the size of the actuator and carries with it weight and power consumption penalties.

The technique which is discussed in the following analysis for flutter suppression is improving the actuator damping. The mechanization for improving the damping of the actuator (in order to absorb energy in the torsional mode and suppress the amplitude rise at torsional resonance) is based upon using negative pressure feedback to create a damping effect over the flutter frequency range. Since for a slab type surface, the torsional spring rate is primarily determined by the actuator stiffness, application of this load pressure feedback to the actuator serves to damp both the actuator motion and the torsional motion of the surface. As indicated on page 88 of Reference 2, this will have the effect of stabilizing the flutter. However, since the damping affects the phase relationships of the bending-torsion motions, there theoretically may be some situations where adding damping may not result in a flutter stability increase. However, having the capability of adding damping with very little added weight is very attractive from the point of actuator size and flow requirements. In addition, with heavy damping (a damping ratio of .7 or greater) of the torsional motion over the flutter frequency region, the effect of the damping can be sufficient to suppress torsional angular motion at high frequencies to approximately zero. This means that with heavy damping the phasing question of the energy transfer is not particularly relevant. Suppression of the torsional mode will eliminate classical flutter since the transfer of energy between the torsional and bending modes is eliminated.

1.4 Specific Flutter Suppression Approach

1.4.1 General

The following material is a brief analysis of the use of a hydromechanical pressure feedback circuit in a power actuator in order to damp surface flutter. The particular actuator used by way of an example is the F-4F stabilator actuator. Values of the drive area, stiffness and surface resonance have been taken from hardware drawings and test data. For calculation purposes, a resonant frequency (torsional) of 23 Hz for the surface inertia on the actuator and mounting compliance was used.

The following material generates the mathematical equations showing the effect of pressure feedback on damping the surface motion at its torsional resonance frequency. The numerical calculations show the sizing values for the pressure feedback circuit. These calculations demonstrate the general feasibility of the use of hydromechanical pressure feedback to damp surface flutter.

In the analysis, the effect of the control valve is not included. This omission is valid since the actuator frequency response is well below the surface flutter frequency (2 Hz vs. 23 Hz). By assuming that no structural feedback motion is introduced into the control valve and using a "washout" in the load pressure feedback loop, the operation of the control valve and the pressure feedback spool can be considered non-interacting.

The analysis is divided into the following sections:

1. Undamped Actuator and Surface Mass
2. Actuator and Surface Mass with Load Pressure Feedback

3. Actuator and Surface Mass with Load Pressure Feedback

4. Derivation of Washout Transfer Function

5. Sample Sizing Calculations on F-4 Actuator

1.4.2 Undamped Actuator and Surface Mass

Consider a control actuator with no damping. For simplicity, the control valve is assumed to remain centered and can be ignored. The actuator is assumed operating around its mid-stroke position. The equations of motion for the actuator and surface in response to an applied driving force are:

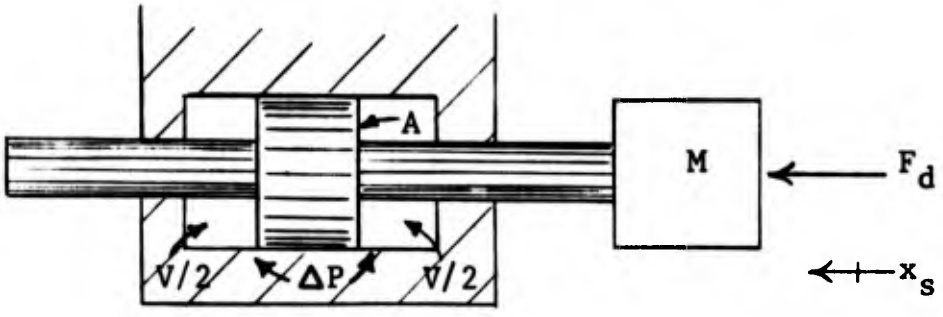

$$F_d = M\ddot{x}_s + \Delta P\, A$$

$$Q_p = A\dot{x}_s$$

$$Q_b = \frac{V}{4\beta}\left(\frac{d\Delta P}{dt}\right)$$

$$Q_p = Q_b$$

Where:

F_d = the driving force

M = surface mass

x_s = surface motion

V = total volume of oil in actuator

Q_p = flow generated by moving piston

Q_b = flow absorbed by fluid compliance

β = bulk Modulus of fluid

A = actuator drive area

ΔP = load pressure

Taking Laplace Transforms and assuming zero inital conditions:

$$F_d = MS^2x_s + \Delta PA$$

$$Q_p = ASx_s$$

$$Q_b = \frac{V}{4\beta}\, S\Delta P$$

$$Q_b = Q_p$$

Where: S is Laplace Operator

Solving the above equations simultaneously:

$$F_d = MS^2 x_s + \Delta PA$$

$$\Delta PS = \frac{4\beta A}{V} x_s S$$

Combining the above:

$$\frac{x_s}{F_d} = \frac{\left(\frac{4\beta A^2}{V}\right)^{-1}}{\left(\frac{V M}{4\beta A^2}\right)S^2 + 1}$$

Comparing the above to the standard second order expression of:

$$\frac{x_s}{F_d} = \frac{K}{\frac{S^2}{\omega_n^2} + \frac{2\zeta S}{\omega_n} + 1}$$

Implies: $K = \frac{V}{4\beta A^2}$, $\omega_n^2 = \frac{4\beta A^2}{VM}$, $\zeta = 0$

This transfer function implies a response to the driving force which resembles the following:

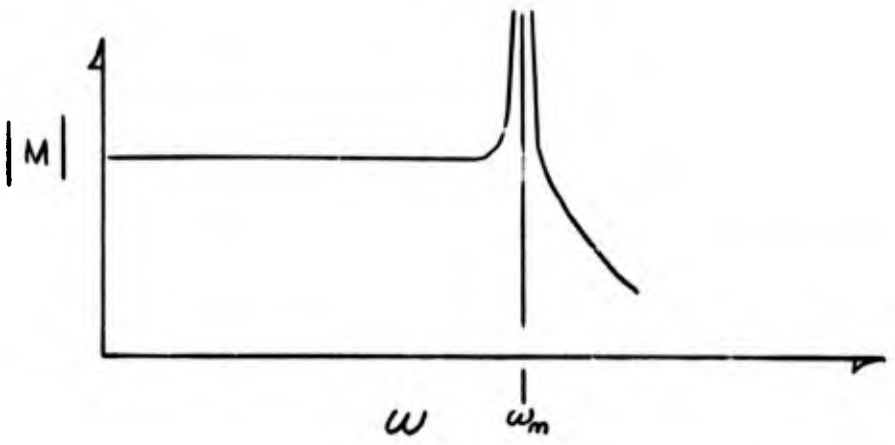

1.4.3 Actuator and Surface Mass With Load Pressure Feedback

For ΔP Feedback, the equations of motion are:

$$
\begin{cases}
F_d = M \ddot{x}_s + \Delta P A \\
Q_p = A \dot{x}_s \\
Q_b = \dfrac{V}{4\beta} \dfrac{d\Delta P}{dt} \\
Q_{\Delta p} = K_f \Delta P \\
Q_p = Q_b + Q_{\Delta p}
\end{cases}
$$

Where: K_f = pressure feedback gain

$Q_{\Delta P}$ = the flow due to the load pressure feedback

all other terms the same as in Section 1.4.2

Taking Laplace Transforms and letting inital conditions = 0:

$$\begin{aligned} F_d &= MS^2 x_s + \Delta PA \\ Q_p &= A\,S\,x_s \\ Q_b &= \frac{V}{4\beta}\,S\Delta P \\ Q_{\Delta P} &= K_f \Delta P \\ Q_p &= Q_b + Q_{\Delta P} \end{aligned}$$

Solving the above equations of motion simultaneously:

$$F_d = M\,S^2 x_s + \Delta PA$$

$$Ax_s S = \left(\frac{V\,S}{4\beta} + K_f\right)\Delta P$$

Letting $C_1 = \frac{V}{4\beta}$

$$\Delta P = \frac{ASx_s}{C_1\,S + K_f}$$

Combining and rearranging:

$$F_d = MS^2 x_s + \frac{A^2 x_s \quad S}{C_1 S + K_f}$$

$$\frac{F_d}{x_s} = \frac{MS^2 \left(C_1 S + K_f\right) + A^2 S}{C_1 S + K_f}$$

$$\frac{x_s}{F_d} = \frac{C_1 S + K_f}{S \left(MC_1 S^2 + MK_f S + A^2\right)}$$

$$\frac{x_s}{F_d} = \frac{\left[\frac{C_1}{K_f} S + 1\right]}{S} \left[\frac{\frac{K_f}{A^2}}{\frac{MC_1}{A^2} S^2 + \frac{MK_f}{A^2} S + 1}\right]$$

Note: that the right hand term above is the normal second order transfer function with:

$$\omega_n = \sqrt{\frac{A^2}{MC_1}} \qquad , \zeta = \frac{K_f \sqrt{M}}{2A \sqrt{C_1}}$$

which implies damping is varied by varying K_f

Sketching the response indicated by the transfer function for $\frac{x_s}{F_d}$ with load pressure feedback (with no washout):

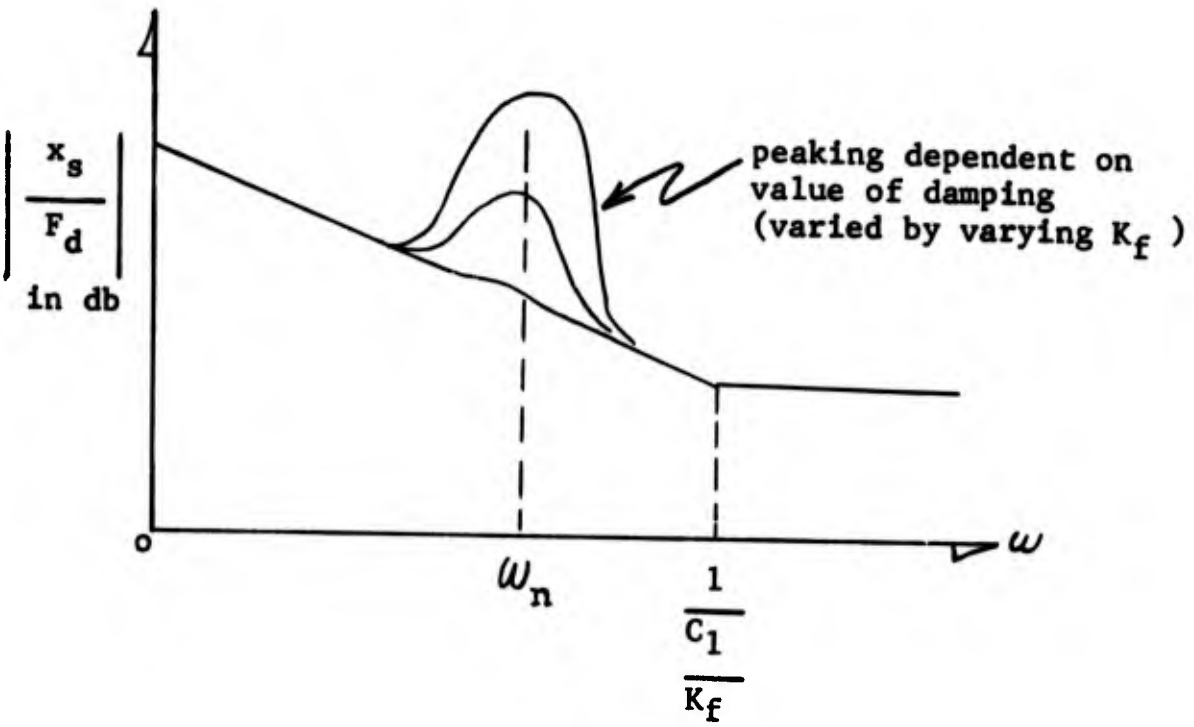

Note: The rising amplitude below $\omega = 1/C_1/K_f$ occurs because no washout circuit was included in the derivation. The Section following shows that the washout circuit eliminates the low frequency rising characteristic.

1.4.4 Actuator and Surface Mass with Load Pressure Feedback Plus Washout Circuit

Consider a low frequency washout circuit in ΔP feedback:

The equations of motion (in Laplace Transform notation) are:

$$F_d = Ms^2 x_s + \Delta PA$$

$$Q_p = ASx_s$$

$$Q_b = \frac{V}{4\beta} S \Delta P$$

$$Q_{\Delta P} = K_f \left(\frac{K_w S}{\gamma S + 1} \right) \Delta P$$

$$Q_p = Q_b + Q_{\Delta P}$$

Where: $\left(\frac{K_w S}{\gamma S + 1} \right)$ = the washout circuit

γ = washout rolloff time constant

K_w = washout circuit gain

Solving simultaneously (letting $C_1 = \frac{V}{4\beta}$)

$$F_d = MS^2 x_s + \Delta PA$$

$$ASx_s = C_1 S \Delta P + \frac{K_f^* S \Delta P}{\gamma S + 1} \quad \text{Where: } K_f^* = K_f K_w$$

or

$$F_d = MS^2 x_s + \Delta PA$$

$$\Delta P = \frac{A\ (\gamma S + 1)}{C_1 \gamma S + C_1 + K_f^*}\ x_s$$

Combining the preceding two equations:

$$\frac{F_d}{x_s} = \frac{MC_1 \gamma S^3 + M\ (C_1 + K_f^*)\ S^2 + A^2 \gamma S + A^2}{C_1\ \gamma S + C_1 + K_f^*}$$

Rearranging:

$$\frac{x_s}{F_d} = \frac{\left(C_1 + K_f^*\right)\left[\frac{C_1 \gamma}{C_1 + K_f^*}\ S + 1\right]}{MC_1\ \gamma S^3 + M(C_1 + K_f^*)\ S^2 + A^2 \gamma S + A^2}$$

Note: this transfer function is of the form:

$$\frac{x_s}{F_d} = \frac{K\ (T_1 S + 1)}{(T_2 S + 1)\ \left(\frac{S^2}{\omega n^2} + \frac{2\zeta S}{\omega n} + 1\right)}$$

which for $T_1 = T_2$ reduces to a simple second order function.
This indicates that the washout circuit can be used to eliminate the rise in amplitude of x_s / F_d at low

frequencies that occurs without the washout circuit (Reference Section 1.4.3).

1.4.5 Derivation of Washout Transfer Function

In the analysis of the load pressure feedback transfer functions, the washout transfer function was not derived. The operation of the washout circuit is apparent from the Flutter Damper Schematic FIGURE 68 . The isolation piston eliminates feeding steady differential load pressures to the damping spool. As the load pressure varies sinusoidally with increasing frequency, the isolation piston movement creates a flow. At low frequencies, the flow from the isolation piston goes primarily through the washout orifice R_2 . As the frequency of the load pressure variation continues to increase, the damping spool moves.

Using Laplace Transform notation and referring to FIGURE 68 , the washout circuit equations are:

$$Q_1 = A_1 S \, x_{ip} \qquad \text{Equation 1}$$

$$\Delta P_1 = \frac{K_1 \, x_{ip}}{A_1} \qquad \text{Equation 2}$$

$$Q_1 = Q_2 + Q_3 \qquad \text{Equation 3}$$

$$Q_3 = A_2 \, S x_{sp} \qquad \text{Equation 4}$$

$$\Delta P_2 = Q_2 R_2 = \frac{K_2 \, x_{sp}}{A_2} \qquad \text{Equation 5}$$

$$\Delta P = \Delta P_1 + \Delta P_2 \qquad \text{Equation 6}$$

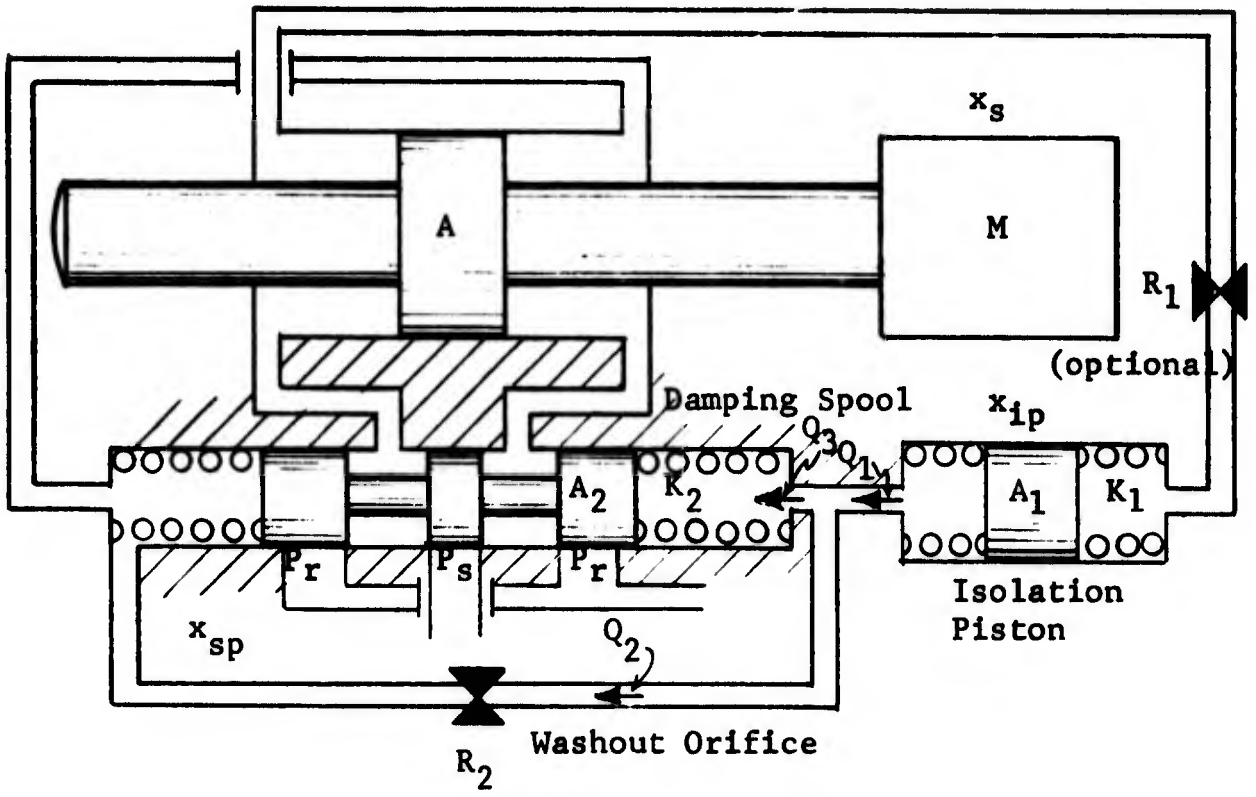

FIGURE 68 - Hydromechanical Damping Circuit Schematic

Where: Q_1 = flow generated by the isolation piston in cis

ΔP_1 = pressure drop across the isolation piston

Q_3 = flow used by damping spool

P_2 = pressure drop across damping spool

ΔP = load pressure drop across actuator piston

x_{sp} = damping spool position

A_1 = isolation piston drive area

A_2 = damping spool drive area

x_{ip} = position of isolation piston

R_2 = washout orifice resistance

K_1 = isolation piston spring rate

K_2 = damping spool spring rate

Solving the washout circuit equations simultaneously:

$$\Delta P_1 = \frac{K_1 \quad Q_1}{A_1^2 \quad S} \qquad \text{(from Eq. 1 and Eq. 2)}$$

$$Q_1 = \left[\frac{K_2}{R_2 A_2} + A_2 \, S \right] x_{sp} \qquad \text{(substituting Eq. 5 and Eq.4 into Eq.3)}$$

Combining the preceding P_1 and Q_1 equations

$$\Delta P_1 = \frac{K_1}{A_1^2 S}\left[\frac{K_2}{R_2 A_2} + A_2 S\right] x_{sp}$$

Since from equation 6, $\Delta P = \Delta P_1 + \Delta P_2$

$$\Delta P = \left(\frac{K_1}{A_1^2 S}\left[\frac{K_2}{R_2 A_2} + A_2 S\right] + \frac{K_2}{A_2}\right) x_{sp}$$

$$\frac{\Delta P}{x_{sp}} = \frac{K_1 K_2 + \left(A_2^2 K_1 + K_2 A_1^2\right) R_2 S}{A_1^2 R_2 A_2 S}$$

$$\left[\frac{X_{sp}}{\Delta P} = \frac{\dfrac{A_1^2 \; R_2 \; A_2}{K_1 K_2} S}{\left(\dfrac{R_2 A_2^2 \; K_1 \; + \; K_2 A_1^2 R_2}{K_1 K_2} \right) S + 1} \right]$$

Washout Circuit Transfer Function

Which is of the form $\frac{K \quad S}{\gamma S + 1}$ as used in the previous sections.

1.4.6 Optional Rolloff Circuit Transfer Function

If desired, the pressure feedback gain at high frequencies can be rolled off by the addition of orifice R_1 on FIGURE 68. The resulting transfer function (derived by the procedure used for the normal washout circuit with equation 2 modified to read

$$\Delta P_1 = \frac{K_1 \quad x_{ip} \quad + \quad Q_1 R_1 \;) \text{ is:}}{A_1}$$

$$\left[\frac{x_{sp}}{\Delta P} = \frac{\frac{R_2 A_2 A_1^2}{K_1 K_2} S}{\left(\frac{R_1 R_2 A_1^2 A_2^2}{K_1 K_2} \right) S^2 + \left(\frac{K_1 R_2 A_2^2 + K_2 R_1 A_1^2 + K_2 R_2 A_1^2}{K_1 K_2} \right) S + 1} \right]$$

Washout Transfer Function with R_1

Which has the general form of:

$$\frac{x_{sp}}{\Delta P} = \frac{K S}{(T_1 S + 1)(T_2 S + 1)}$$

For the above tranfer function, the frequency response will resemble the following:

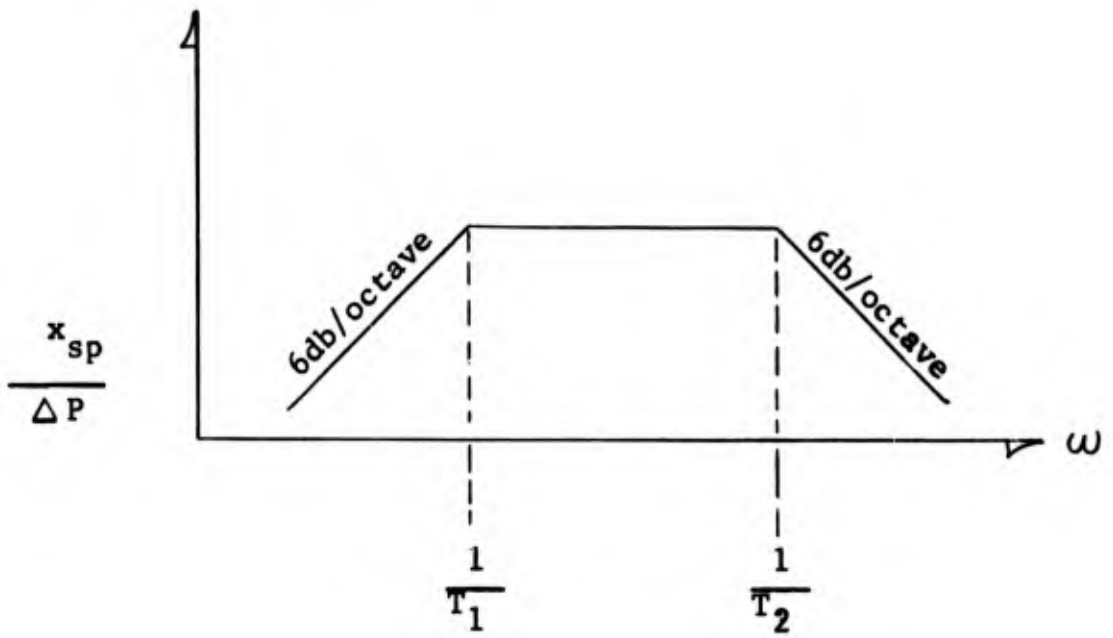

1.5 Example Sizing Calculations - F-4 Stabilator Actuator

1.5.1 General

In applying the flutter damping technique to a slab type surface, there are three general conditions necessary in order to realize an improvement in the weight and size of the actuator or an improvement in the performance of the actuator-surface combination. These requirements are as follows:

1. The stiffness of the actuator and mounting must be predominantly determined by the oil column stiffness.

2. The aircraft is velocity limited by the onset of flutter of the particular slab surface to which the technique is being applied.

3. The stiffness accociated with the lowest torsional resonant frequency of the control surface is primarily the stiffness of the actuator, not the torsional stiffness of control surface itself.

For control actuator situations meeting the above requirements, there are two options in applying the flutter damping technique. The first option applies to an actuator which has not been oversized in area in order to drive the flutter frequency higher. For this situation, the drive area is sized for the hinge moment requirement of the actuator. The damping technique can be applied to the actuator in order to allow higher airspeeds before the onset of flutter. The second option applies to an actuator having a drive area that

is sized larger than that required for hinge moment capability. This is a typical situation for slab control surface actuators such as the horizontal tail surfaces of the F-4, F-111 and YF-16 aircraft.

For the latter situation, the actuator area can be reduced to that required for hinge moment capability. This allows a reduction in the actuator size and hydraulic power requirement. The F-4 stabilator actuator used for the following calculations is of this type.

1.5.2 F-4 Stabilator Characteristics

The following general data for the normal F-4 stabilator actuator and control surface is used in the example calculations:

1. The torsional resonance frequency of the stabilator surface on the stabilator actuator with both sections of the actuator pressurized is nominally 23 Hz. The frequency varies from 21.65 to 23.55 Hz according to Reference 3, AFFDL-TR-71-20, Supplement 2, pages 217 and 218.

2. The actuator drive area for each half of the F-4 actuator is approximately 6.0 $in.^2$.

3. At frequencies above 1.5 Hz the normal F-4 stabilator actuator stiffness is approximately 200,000 #/in. (for one half of the actuator pressurized) according to measured data from Reference 4, AFFDL-TR-72-13, page 190.

---

3. Kisslinger, R.L. and Vetsch, G.J., "Survivable Flight Control System", Interim Report No.1, AFFDL-TR-71-20, Supplement 2, May 1971
4. Goldstein, S.M., et.al., "Test and Development of Flight Control Actuation System Components for Military Aircraft", AFFDL-TR-72-13, February 1972
5. Amies, D.E., et.al., "Survivable Flight Control System", Interim Report No. 1, AFFDL-TR-71-20, Supplement 3, May 1971

4. The normal maximum hinge moment requirement for maneuvering of the F-4 is approximately 8,600 # at the actuator at 6.9 in./sec. rate according to Reference 5, page 179.

5. The actuator stroke is 10.5 inches.

The measured 200,000 #/in. for ½ of the F-4 actuator pressurized compares favorably with the calculated value of oil column stiffness alone, using Mil-H-5606 as having a β of 100,000 #/in.^{2} For example, with one half of the actuator operating, the oil column stiffness at mid stroke of the actuator is:

$$\frac{F}{\Delta x} = \frac{A\ 4\beta}{x_t}$$

Where:

$\frac{F}{\Delta x}$ = oil Column Stiffness

A = actuator area (6 in.^{2})

x_t = total actuator stroke (10.5 in.)

β = bulk Modulus of Mil-H-5606 (100,000 #/in.^{2})

$$\frac{F}{\Delta x} = 228{,}571 \text{ \#/in.}$$

Comparing the measured stiffness value of 200,000 #/in. for the entire actuator to the oil column stiffness of 228,571 #/in. indicates that the stiffness is primarily determined by the oil column in the actuator.

1.5.3 Calculation of the F-4 Stabilator Actuator Inertia Load.

With one half of the actuator pressurized, the stiffness is 200,000 #/in. For both halves pressurized, the F-4 actuator stiffness will be approximately 400,000 #/in. at frequencies above 1.5 Hz. From the resonant frequency equation for a simple spring-mass system, the mass of the surface as seen by the actuator is calculated as follows:

$$f_n = \frac{1}{2\pi}\sqrt{\frac{K}{M}}$$

Where: K' = spring rate (400,000 #/in.)

M = mass in # sec^2/in.

f_n = resonant frequency (23 Hz)

$$23 = \frac{1}{2\pi}\sqrt{\frac{400{,}000}{M}}$$

$$\left[M = 19.15 \text{ \# } sec^2/in.\right]$$

1.5.4 Calculation of the ΔP Feedback Gain For a Specific Damping Ratio

The worst case hinge moment requirement of the stabilator actuator is 8,600 # @ 6.9"/sec. Allowing 2500 PSI across the piston, 500 PSI drop across the control valve, this maneuvering force can be generated with 3.44 in^2 drive area with only one system operating. This is a

considerable reduction from the 6.0 $in.^2$ drive area normally used in the F-4 stabilator actuator.

Reducing the drive area also reduces the stiffness and hence the torsional resonance frequency. For one half of the actuator pressurized, the surface resonance frequency with 3.44 $in.^2$ drive area will be:

$$\frac{F}{\Delta x} = 200{,}000 \left(\frac{3.44}{6.00} \right)$$

$$= 114{,}666 \ \#/in.$$

and

$$f_n = (23) \sqrt{\left(\frac{114{,}666}{400{,}000} \right)}$$

$$f_n = 12.31 \text{ Hz}$$

Consider the transfer function for the surface motion/driving force with ΔP feedback (but without the washout circuit included) (Reference Section 1.4.3):

For $A = 3.44 \ in.^2$

$\zeta = 1.0$ (critically damped)

$M = 19.15 \ \# \ sec.^2/in.$

$f_n = 12.31$ Hz

$$\frac{x_s}{F_d} = \frac{\left(\frac{C_1}{K_f} S + 1\right) \quad \frac{K_f}{A^2}}{S \left(\frac{MC_1}{A^2} S^2 + \frac{MK_f}{A^2} S + 1\right)}$$

The coefficient of the S term in the denominator of the above equation corresponds to the $\frac{2\zeta}{\omega_n}$ of a standard second order transfer function, where ω_n is the resonance frequency, ζ is the damping ratio. Therefore, equating coefficients and substituting in the corresponding values.

$$\frac{2\zeta}{\omega_n} = \frac{MK_f}{A^2}$$

$$\frac{2\,(1.0)}{2\pi\ 12.31} = \frac{19.15\ K_f}{(3.44)^2}$$

$$\left[K_f = .016 \text{ in.}^3 \text{/sec./\#/in.}^2 \right]$$

1.5.5 Calculation of the time Constant C_1/K_f

$$C_1 = \frac{V}{4\beta}$$

Where: V = volume (35.07 $in.^3$)

β = Bulk Modulus Mil-H-5606 (100,000 #/$in.^2$)

C_1 = 8.77×10^{-5} $in.^5/\#$

Therefore:

$$\frac{C_1}{K_f} = \frac{8.77 \times 10^{-5}}{0.016}$$

$$\left[\frac{C_1}{K_f} = 5.48 \times 10^{-3} \text{ sec.} \right]$$

Note that this implies a break frequency of 29 Hz ($f_{3db} = \frac{1}{2\pi \, C_1/K_f} = 29$ Hz).

1.5.6 Calculation of Porting For Load Pressure Feedback

Consider the damping spool configuration shown in FIGURE 68, Section 1.4.5. Note that the damping orifice in a hardware configuration will port the actuator piston alternately to pressure and return. The porting to pressure and return is required to maintain correct polarity of the pressure feedback when operating with a bias load applied to the actuator piston.

For the porting spool shown in FIGURE 68, the flow equations for each damping spool orifice are:

$$Q_{out} = 103\ A_p \sqrt{\frac{P_s}{2} + \frac{\Delta P}{2} - P_r + \frac{P_b}{2}}$$

(Equation a)

$$Q_{in} = 103\ A_p \sqrt{P_s - \left(\frac{P_s}{2} - \frac{\Delta P}{2} - \frac{P_b}{2}\right)}$$

(Equation b)

Where: P_s = supply pressure

P_r = return pressure

ΔP = differential pressure caused by flutter

Q = flow through valve caused by flutter

P_b = static bias pressure

103 = discharge coefficient for Mil-H-5606 fluid of 100° F in $in^2/sec. \sqrt{\#}$

A_p = open area of orifice

For $P_r \cong$ 0 PSI, Equations a and b become:

$$Q_{out} = Q_{in} = 103\ A_p \sqrt{\frac{P_s}{2} + \frac{P}{2} + \frac{P_b}{2}}$$

or

$$Q = 103\ A_p \sqrt{\frac{P_s}{2} + \frac{P}{2} + \frac{P_b}{2}}$$

(Equation c)

For a constant pressure feedback gain, the form of Equation c should be:

$$Q = K \Delta P$$

Where: K = a proportional gain constant

ΔP = differential pressure across the actuator piston

Q = flow through the damping orifice

This relationship can be obtained with Equation c for a spool motion proportional to flutter pressure variation ΔP by using a porting width which varies with spool stroke x_v.

To establish the width of the port at incremental spool positions, Equation c can be written in terms of the flow at each position.

$$\frac{Q_n}{\Delta P_n} = 103 \left[D_n + \sum_{i=o}^{n-1} D_i \right] \frac{X_t}{m} \sqrt{\frac{P_s}{2} + \frac{P_b}{2} + \frac{\Delta P_n}{2}}$$

(Equation d)

Where: D_n = port width at nth position

X_t = total stroke of spool

m = number of increments by which spool stroke is divided

ΔP_n = flutter caused differential pressure across piston which opens damping spool to nth position

P_s = supply pressure

P_b = bias pressure

Since at each position $\frac{Q_n}{\Delta P_n}$ is the pressure feedback gain K_f, the width of the port can at each incremental position be adjusted to maintain K_f constant.

The following table for the values of

P_s = 3000 PSI

X_t = .100 in.

m = 20

used in Equation d shows the porting width for P_b = 0 and a constant K_f = .016. Also tabulated are the values of K_f for two conditions of bias pressure $P_b = \pm$ 2000 PSI.

From TABLE 1, it is apparent that large bias pressures of 2/3 maximum stall force on the actuator affect the damping gain by approximately +28 and -39%. This is an acceptable variation from the standpoint of maintaining adequate damping since the nominal value of ζ can be increased 40% to compensate for bias pressure caused variations of K_f.

TABLE

ΔP	Port Dimensions		K_f		
	X_v	D_p	P_b	P_b	P_b
$\#/in^2$	in.	in.	0 PSI	+2000 PSI	-2000 PSI
150	.005	.0587	.0160	.0205	.0097
300	.010	.0560	.0160	.0303	.0100
450	.015	.0536	.0160	.0201	.0104
600	.020	.0514	.0160	.0200	.0107
750	.025	.0494	.0160	.0198	.0109
900	.030	.0475	.0160	.0197	.0112
1050	.035	.0459	.0160	.0196	.0114
1200	.040	.0443	.0160	.0194	.0116
1350	.045	.0429	.0160	.0193	.0118
1500	.050	.0416	.0160	.0192	.0119
1650	.055	.0403	.0160	.0191	.0121
1800	.060	.0392	.0160	.0190	.0122
1950	.065	.0381	.0160	.0190	.0124
2100	.070	.0371	.0160	.0189	.0125
2250	.075	.0362	.0160	.0188	.0126
2400	.080	.0353	.0160	.0187	.0127
2550	.085	.0345	.0160	.0187	.0128
2700	.090	.0337	.0160	.0186	.0129
2850	.095	.0329	.0160	.0185	.0130
3000	.100	.0322	.0160	.0185	.0131

Pressure Feedback Gain vs. Differential Pressure

TABLE 1

1.5.7 Spool and Isolation Piston Size Calculations

The minimum spool size is determined by the port width dimensions required by the calculations of Section 1.5.6. From TABLE 1, the maximum port width at any valve stroke is .0587 inches. This can be easily accommodated by a spool .188 inches or larger in diameter. For ease of manufacture, a minimum damping spool diameter of .312 inches can be used. To provide parts commonalty, the isolation piston and damping spool can be made with the same diameter. This will allow using the same springs on both the isolation piston and damping spool (since the design point of having equal pressure drops across the damping spool and isolation piston at the flutter frequency can be used.)

For a .312 inch diameter spool, 1500 PSI differential pressure drop for .100 inches of stroke, the following parameters exist:

1. Isolation and damping spool drive areas = $7.645 \times 10^{-2} in.^2$
2. Peak driving force = 115#
3. Centering spring rate = 1150 #/in.
4. Damping spool mass $\cong 1.66 \times 10^{-4} \#sec.^2/in.$

From the preceding parameters, the ratio of force required to drive the mass to force required to deflect the spring can be calculated. For harmonic motion, the peak acceleration = $\omega^2 \hat{x}_v$. Therefore, the ratio of mass driving force to spring driving force (peak) is calculated from the equation:

$$\frac{F_m}{F_{sp}} = \frac{\omega^2 \hat{x}_v m_{sp}}{k_{sp} \hat{x}_v}$$

Where: ω = frequency of interest (76.22 rad./sec.)

m_{sp} = mass of spool (1.66 x 10^{-4}#sec^2/in.)

x_v = peak spool stroke (.100 inches)

k_{sp} = spring rate of centering springs (1150#/in.)

F_m = peak force (in #) to drive mass of spool at the frequency

F_{sp} = peak force (in #) to drive spring to full spool deflection

$$\frac{F_m}{F_{sp}} = .00084$$

This indicates that the response of the damping spool at the flutter frequency will exhibit negligible phase shift.

1.5.8 Washout Circuit Sizing Calculations

In order to minimize interaction between the control valve and the damping spool, the break frequency of the washout circuit is selected to occur just below the surface-actuator resonant frequency. For one half of the stabilator actuator pressurized, the resonant frequency is 12.31 Hz. For both halves of the actuator pressurized, the resonant frequency is increased to 17.41 Hz. For the F-4 configuration, the design break frequency for the washout circuit is selected to be at 10 Hz (slightly below the lowest resonant frequency).

For the general form of the washout transfer function $K\,S/\tau S + 1$, the break frequency requires $\tau = .0159$ secs. The value of the washout orifice is calculated from the following washout circuit transfer function (Reference Section 1.4.5):

$$\frac{X_{sp}}{\Delta P} = \frac{\dfrac{A_1^2\ R_2\ A_2}{K_1\ K_2}\ S}{\left(\dfrac{R_2 A_2^2\ K_1 + K_2 A_1^2\ R_2}{K_1\ K_2}\right) S + 1}$$

Where:

- A_1 = isolation piston drive area ($.0767\ in.^2$)
- A_2 = damping spool drive area ($.0767\ in.^2$)
- K_1 = isolation piston centering spring rate (1150 #/in.)
- K_2 = damping spool centering spring rate (1150 #/in.)
- R_2 = washout circuit orifice resistance ($\#/in.^2 / in.^3 / sec.$)

From a comparison of the coefficients of the "S" term in the derived and general washout circuit transfer functions, it is apparent that:

$$\tau = \left(\frac{R_2 A_2^2 K_1 + K_2 A_1^2 R_2}{K_1 K_2} \right)$$

Substituting in the exact values for the parameters and solving for R_2 :

$$.0159 = R_2 \left[\frac{(.0767)^2 (1150) + (1150) (.0767)^2}{(1150)^2} \right]$$

$$R_2 = 1554 \#/in.^2 / in.^3 / sec.$$

1.5.9 Rolloff Circuit Calculations

For the restriction R_1 operating in series with the isolation piston, the response of the damping circuit attenuates above a design frequency. Selection of the

attenuation break point is based on noise exclusion and is somewhat arbitrary, since the circuit will exhibit a natural rolloff at high frequencies (above 200 Hz) due to the spool and fluid mass and the fluid compliance within the configuration mechanization. The high frequency rolloff break point should not be low enough to affect the damping gain and phase angle at the resonance of the surface-actuator combination. Selecting a break frequency at least 5 times as high as the resonant frequency will ensure minimum effect on the operation of the damping circuit at the resonant frequency. For the F-4 stabilator actuator a rolloff break frequency of 100 Hz will be used. The value of R_1 for this break frequency can be calculated from the transfer function for a washout with R_1 (Reference Section 1.4.6)

From the general transfer function for a second order with real roots (Reference Section 1.4.6) :

$$\frac{x_{sp}}{\Delta P} = \frac{KS}{(T_1 S + 1)(T_2 S + 1)}$$

$$\frac{x_{sp}}{\Delta P} = \frac{KS}{T_1 T_2 S^2 + (T_2 + T_2) S + 1}$$

The transfer function for the washout circuit with R_1 included (Reference Section 1.4.6) is:

$$\frac{X_{sp}}{\Delta P} = \frac{\frac{R_2 A_2 A_1^2}{K_1 K_2} S}{\left(\frac{R_1 R_2 A_1^2 A_2^2}{K_1 K_2}\right) S^2 + \left(\frac{K_1 R_2 A_2^2 + R_1 K_2 A_1^2 + K_2 R_2 A_1^2}{K_1 K_2}\right) S + 1}$$

Comparing the coefficients of the S^2 terms for both transfer functions yields the relationship:

$$T_1 T_2 = \frac{R_1 R_2 A_1^2 A_2^2}{K_1 K_2}$$

This expression is solved for the value of R_1 by using the time constant T_2 corresponding to the 100 Hz break frequency, T_1 corresponding to the low frequency break frequency of 10 Hz and the values of

R_2 = 1554 #/in.^{2}/in.^{3}/sec.

A_1 = .0767 in.^{2}

A_2 = .0767 in.^{2}

$$K_1 = 150 \text{ \#/in.}$$

$$K_2 = 150 \text{ \#/in.}$$

$$T_2 = \frac{1}{2\pi \ 100} = .00159 \text{ sec.}$$

$$T_1 = \frac{1}{2\pi \ 10} = .0159 \text{ sec.}$$

Substituting the values in:

$$R_1 = \frac{T_1 T_2 \ K_1 K_2}{R_2 A_1^2 A_2^2}$$

$$R_1 = \frac{(.00159) \ (.0159) \ (1150)^2}{(1554) \ (.0767)^4}$$

$$\left[R_1 = 621.67 \text{ \#/in.}^2/\text{in.}^3/\text{sec.}\right]$$

1.5.10 F-4 Damping Circuit Summary

FIGURE 69 is a hardware package drawing showing the packaging of the damper circuit into the F-4 stabilator power actuator configuration. The modified actuator with the damper included is illustrated in comparison to the

F-4 STABILATOR ACTUATOR
W/ FLUTTER DAMPER MODULES
CONF. I

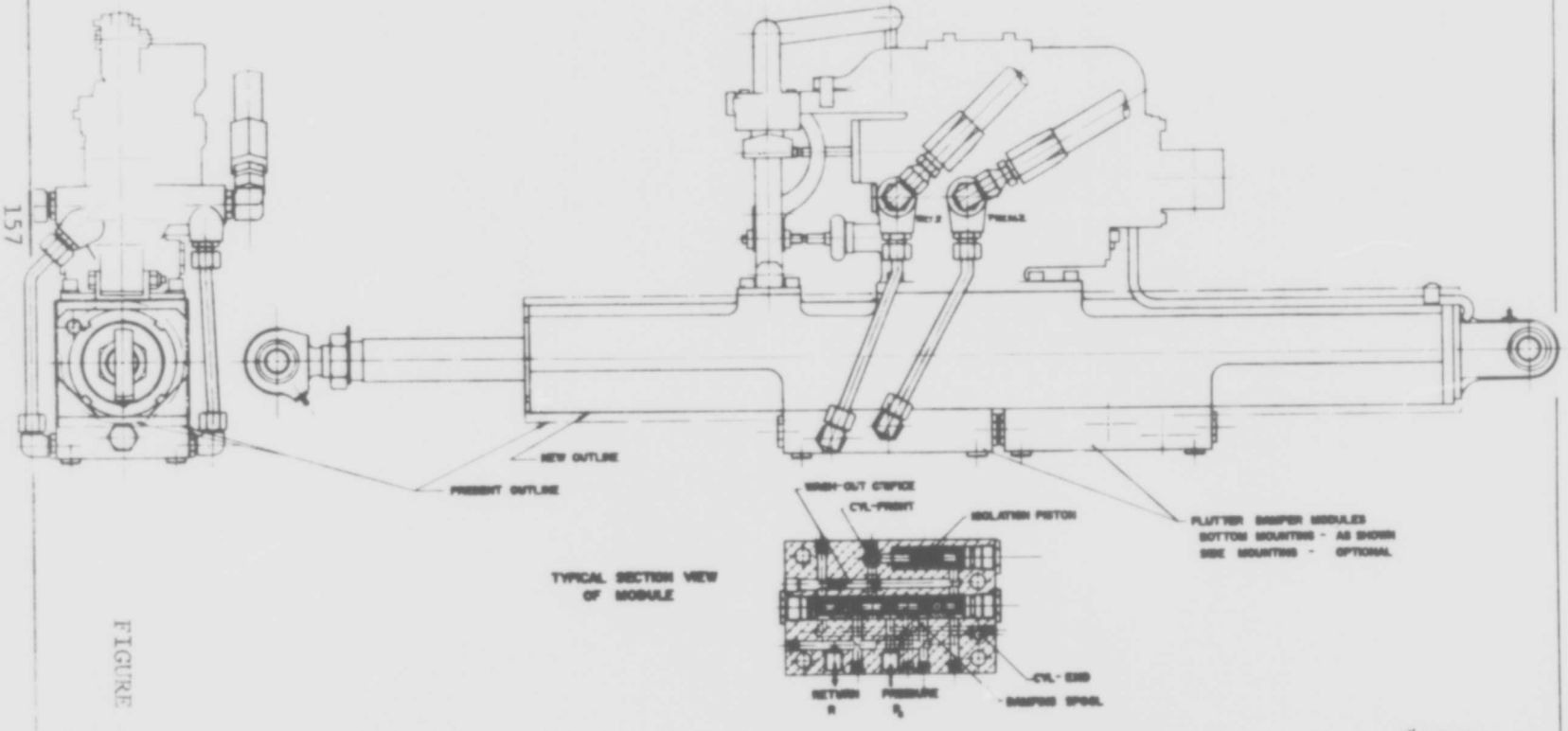

FIGURE 69

standard F-4 actuator outline.

In the configuration 1 shown, the damping modules are mounted below the actuator barrel in two separate packages. Each package is indentical in operation and provides damping redundancy in the event of a supply system failure. External plumbing into the supply and return lines is used in this configuration. Note that the modules can also be mounted on the side of the actuator barrel, shortening the line length for the external plumbing. In FIGURE 69, (configuration 2) the damping module is incorporated in a package immediately under the F-4 control valve package. This would require minor modification to the valve package. This configuration does result in the elimination of the external supply and return plumbing shown in configuration 1.

The damping circuit and actuator values (as calculated in the preceding sections) for the hardware drawing are the following:

Actuator drive area	A	=	3.44 $in.^2$
Damping spool diameter		=	.312 in.
Isolation spool diameter		=	.312 in.
Damping spol centering spring rate	K_2	=	1050 #/in.
Isolation spool centering spring rate	K_1	=	1050 #/in.
Washout orifice resistance	R_1	=	1419 $\#/in.^2/in.^3/sec.$
Rolloff orifice resistance	R_2	=	567.6 $\#/in.^2/in.^3/sec.$
Normal damping ratio	ζ	=	1

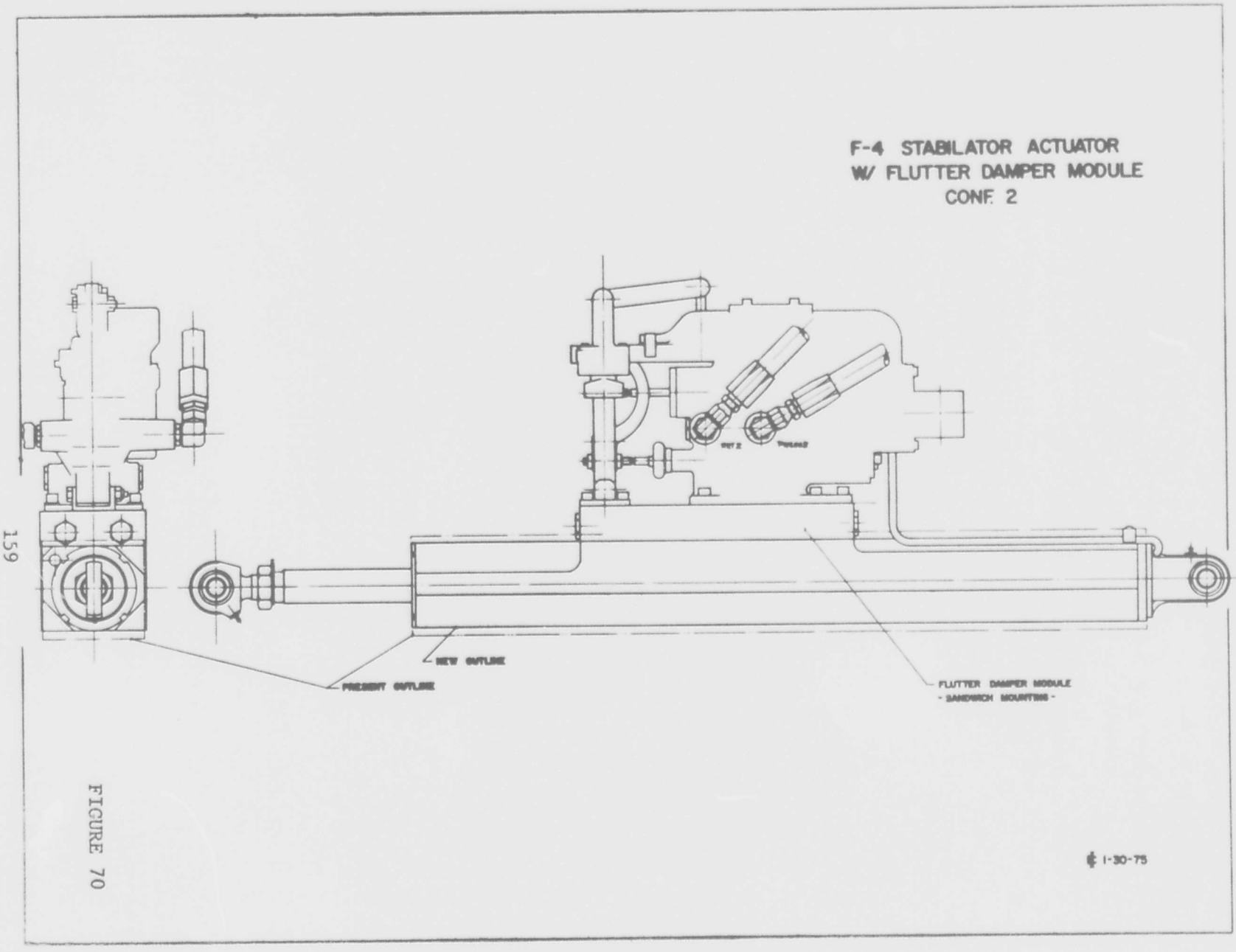
F-4 STABILATOR ACTUATOR
W/ FLUTTER DAMPER MODULE
CONF. 2
NEW OUTLINE
FLUTTER DAMPER MODULE
- SANDWICH MOUNTED -
1-30-75

FIGURE 70

Washout break frequency	T_1	=	10 Hz
Rolloff break frequency	T_2	=	100 Hz
Pressure feedback gain at resonance	K_f	=	.016 $in.^3/sec./\#/in.^2$

2.0 CONCLUSIONS AND RECOMMENDATIONS

The results of the general analysis of the flutter damping technique investigated indicates that the mechanization is feasible and will allow reducing the size of slab type surface actuators. The application of the technique to the F-4 stabilator actuator is feasible and allows a reduction of the actuator drive area to 57% of the standard actuator.

The advantage of a hydromechanical mechanization for flutter damping is one of simplicity, reliability and cost. The mechanization uses conventional hydraulic spool and orifice techniques. The mechanization can be applied both to Fly-By-Wire and conventional power actuators and can be made redundant without difficulty for tandem cylinders.

It is recommended that the mechanization analyzed be applied to an F-4 stabilator actuator in hardware form and be evaluated in the laboratory on effectiveness for load damping. If successful, the actuators should then be evaluated in either a wind tunnel test and/or a flight test program in order to establish flight verification for the technique.

SECTION IV

HIGH TEMPERATURE FLUID TEST

1.0 GENERAL

The objective of the high temperature fluid test investigation was to evaluate Mil-H-83282 hydraulic fluid at elevated operating temperatures in a hydraulic pumping system. The time and temperatures for operation of the fluid were as follows:

100 hours @ 300° F
300 hours @ 400° F
50 hours @ 450° F

To establish the breakdown characteristics of the fluid during the above temperature time cycling, the performance of the pump was monitored and periodically the fluid samples were obtained from the pumping system for analysis.

2.0 TECHNICAL APPROACH

2.1 Test System Description

To evaluate the fluid at elevated temperature conditions, Dynamic Controls, Inc. constructed a test chamber, automatic control system and a test shed. The test shed in which the test chamber was operated was constructed adjacent to Building 195 on Wright-Patterson Air Force Base. (Reference FIGURE 71) Used in constructing and running of the test system were the following Air Force supplied items:

15 gallons of Mil-H-82282 hydraulic fluid
1 hydraulic filter

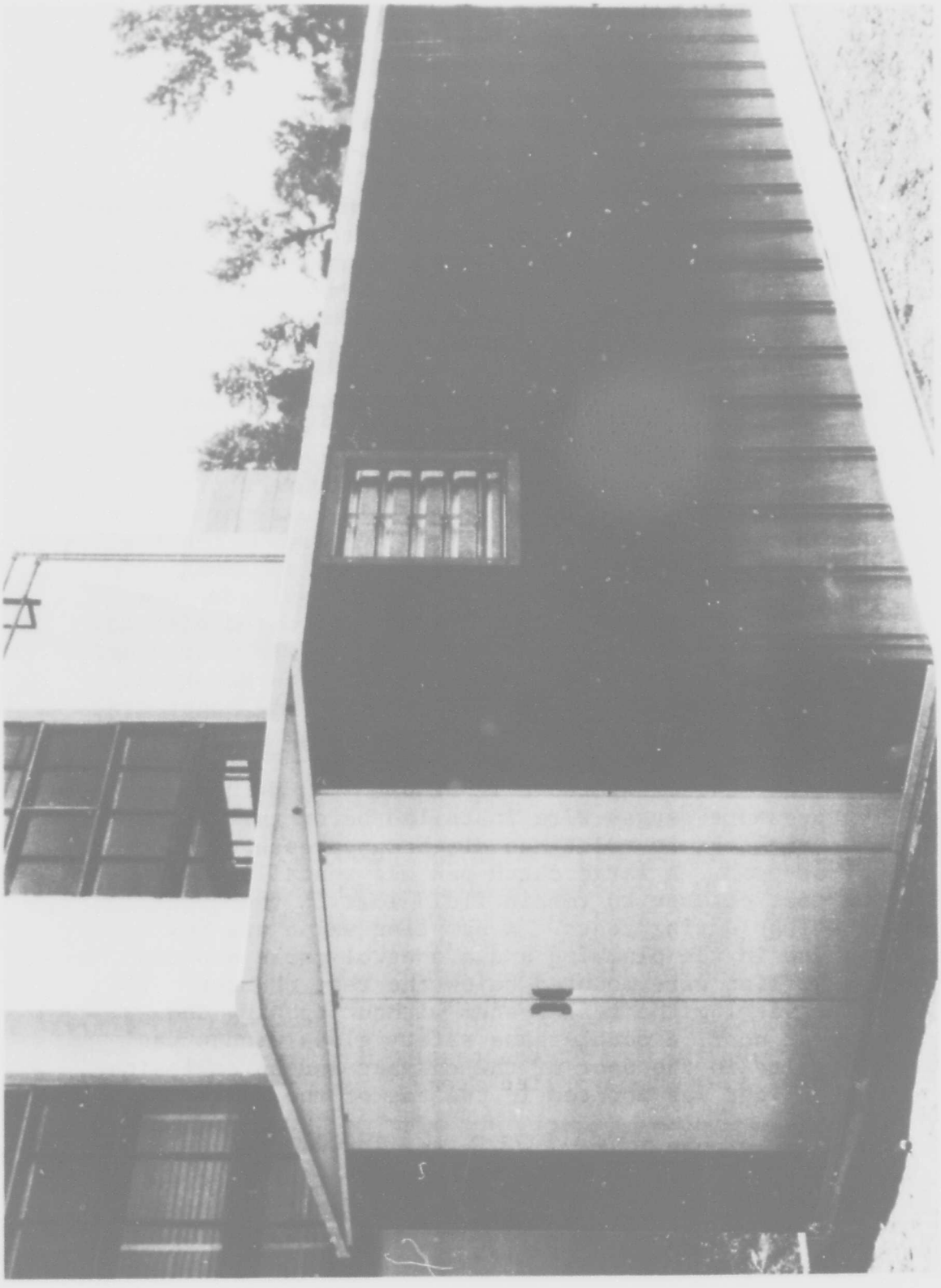

FIGURE 71 Test Shed

1 Vickers variable delivery pump (#MPEV3-044-7)
1 25 HP varidrive unit
1 B-58 bootstrap reservoir

FIGURE 72 is a picture of the test chamber and control unit before installation in the test shed. FIGURE 73 shows the insulated test chamber as installed in the test shed. The test chamber was designed to use only the heat generated in pumping the hydraulic fluid through load restrictions to raise and maintain the desired operating temperature for the test fluid. Cooling of the fluid for temperature control was accomplished by using a fan to blow outside air through two B-52 oil coolers installed in the test chamber. The fan was turned on and off by a temperature controller contained in the control unit and blew air through the chamber and the oil coolers. FIGURE 72 shows the fan before the test chamber was insulated. In front of the fan and in the wall of the chamber opposite the fan were installed shutters. These prevented air flow through the chamber except when the fan was operating. To minimize runup time on the fan, the fan motor was changed from a 1/15th to a 1/4 HP unit. In constucting the hydraulic pumping system for high temperature operation, all seals were replaced with either teflon or Viton seals. As shown in FIGURE 73, direct reading pressure gauges were installed below the chamber and connected to inlet and discharge pressure points on the pump. A large catch pan was installed below the test chamber to retain fluid lost in the event of a leak during tests. A sampling valve was installed in the plumbing and a control cable and discharge line were mounted below the test chamber. To allow viewing the test system without opening the chamber door, a double pane safety glass window was installed in the door of the chamber and an explosion proof light was mounted in the top of the chamber.

FIGURE 74 is a schematic of the test system and shows the plumbing and instrumentation used for the tests. Note that in order to maintain sufficient

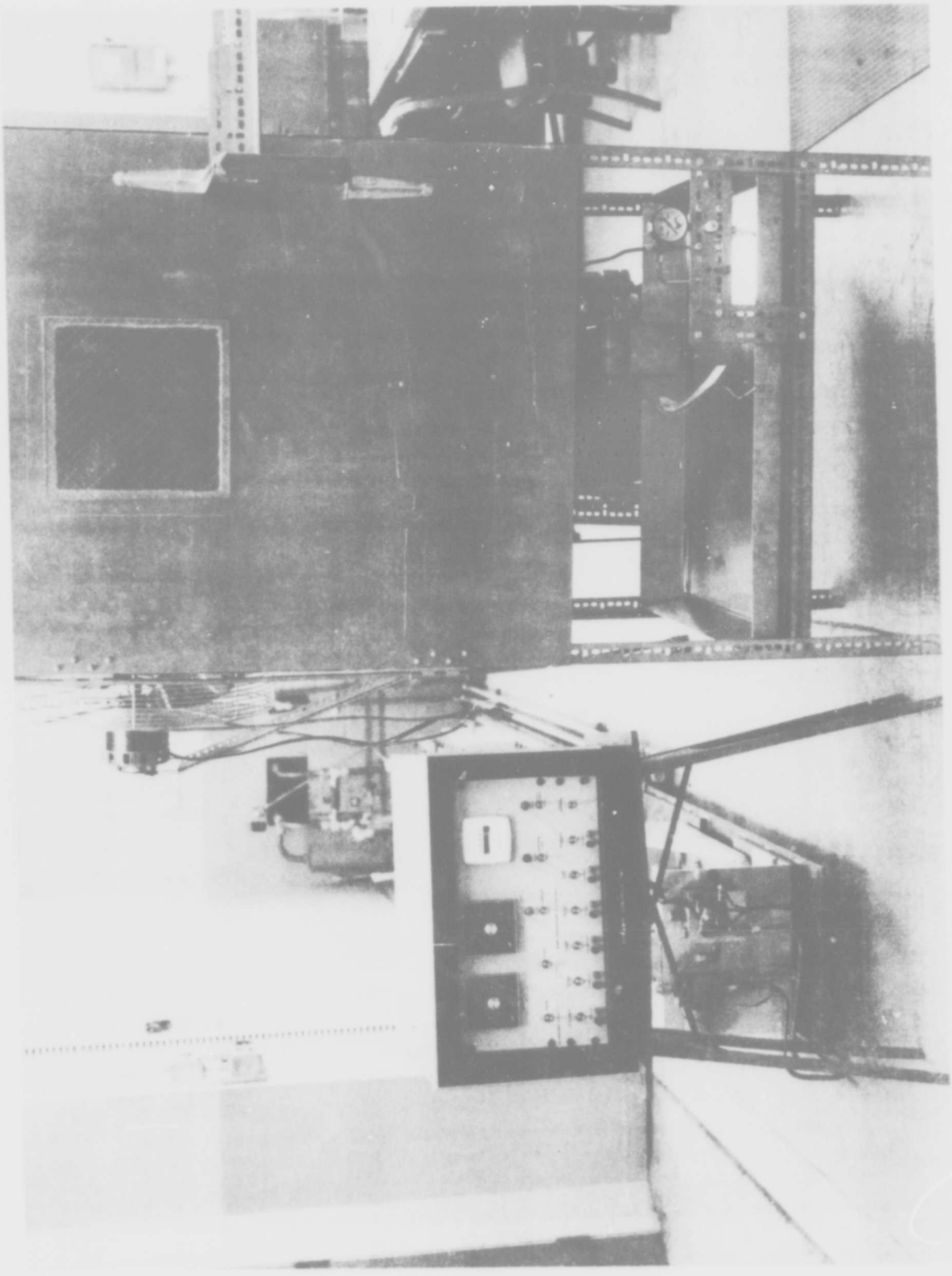

FIGURE 72 Test Chamber and Control Unit

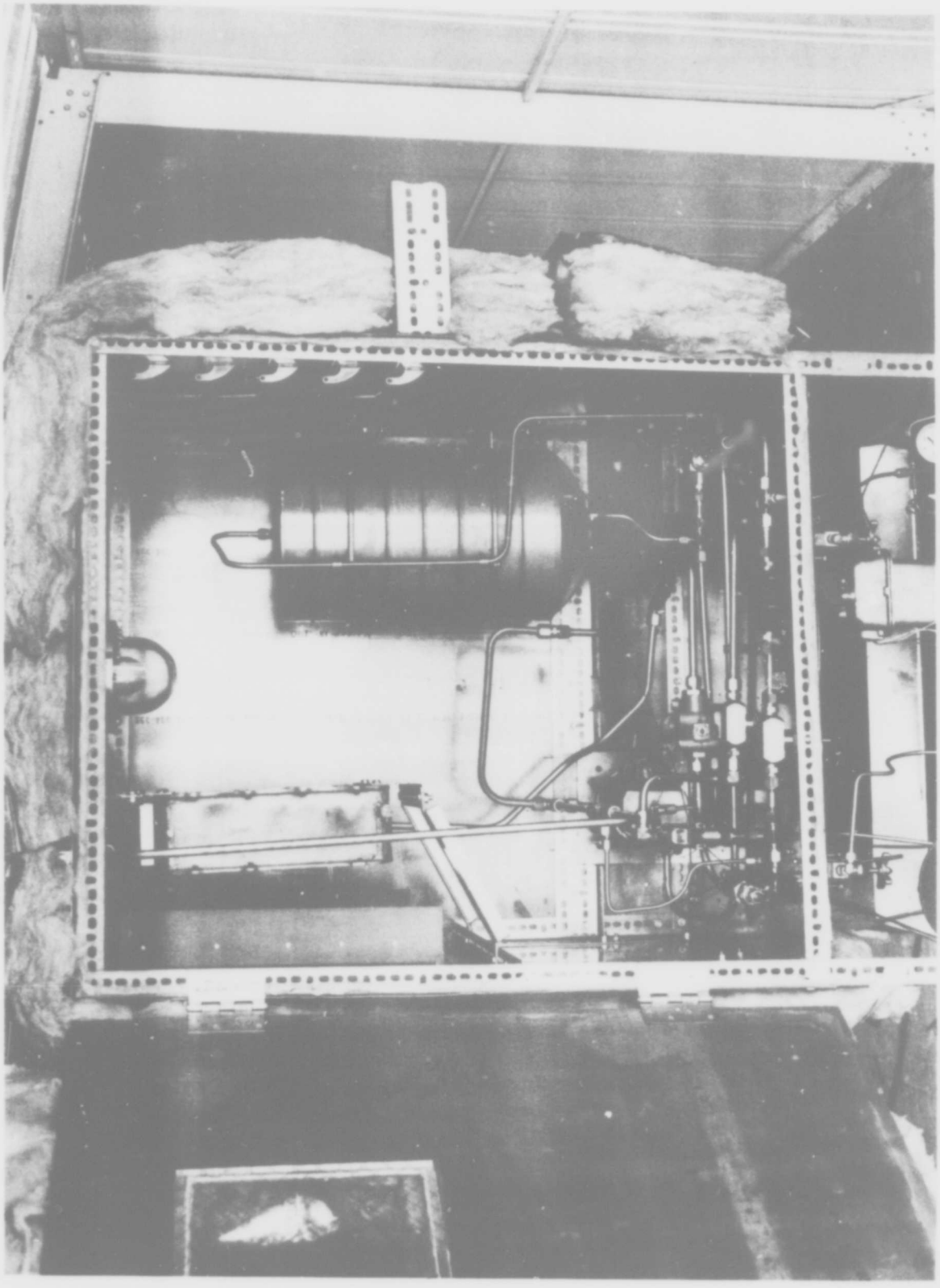

FIGURE 73 Insulated Test Chamber as Installed in Test Shed

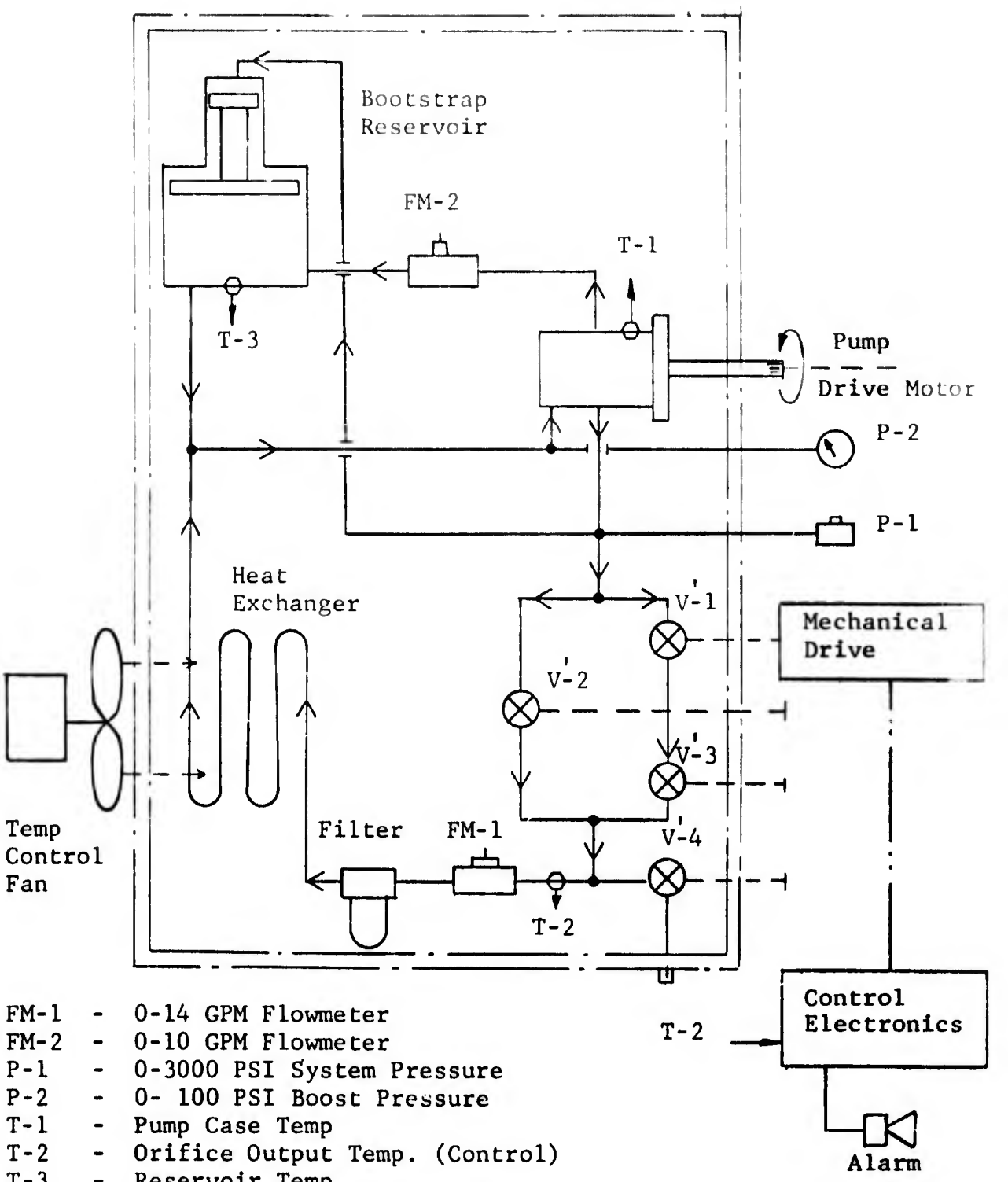

FM-1 - 0-14 GPM Flowmeter
FM-2 - 0-10 GPM Flowmeter
P-1 - 0-3000 PSI System Pressure
P-2 - 0- 100 PSI Boost Pressure
T-1 - Pump Case Temp
T-2 - Orifice Output Temp. (Control)
T-3 - Reservoir Temp.
V'-1 - High Flow Control Valve
V'-2 - Low Flow Regulation Valve
V'-3 - High Flow Regulation Valve
V'-4 - Sampling Valve

FIGURE 74 - FLUID TEST SYSTEM SCHEMATIC

pressure head on the pump inlet (to prevent cavitation), the bootstrap reservoir was plumbed directly into the inlet to the pump. To prevent a time lag in the temperature control system, only case drain flow was connected as a flow through the reservoir. All plumbing components in the test system (with the exception of the oil coolers, filter body and reservoir) were constructed from stainless steel. The oil cooler, filter body and reservoir were made from aluminum.

During the test, 1 1/2, 2 1/2 and 5 micron nominal filtration rate filters were used in the test system to filter the oil from the discharge port on the pump. This was finer filtration than the 10 micron minimum filtration specified by the pump manufacturer.

In order to withstand the high operating belt speeds and loads during the test sequence, the belt drive coupling between the varidrive unit and pump was changed from two 3/8 inch pitch belts to one 1/2 pitch belt. This increased the horsepower rating of the drive belt assembly from approximately 6 horsepower to 25 horsepower. FIGURE 75 shows the original components placed above the single belt drive used between the pump and varidrive units.

The variable load on the pump output was accomplished with two manually set throttling valves. A Jamesbury ball valve, driven by a timer controlled valve operator, was used in series with one of the throttling valves. This provided adjustment of the high and low flow conditions and cycling between them.

FIGURE 76 shows the front panel of the control unit designed and fabricated for the test system operation. Incorporated in the unit were two temperature controllers. The controller on the left was used to drive the cooling fan and control oil temperature. The controller on the right was a safety controller and was connected to monitor oil temperature and shut the pump off in the event of an overtemperature condition. Pump discharge pressure and reservoir level was also instrumented so that loss of pressure head or reservoir level below a design set point would turn the pumping system off. A timing circuit was designed into the control

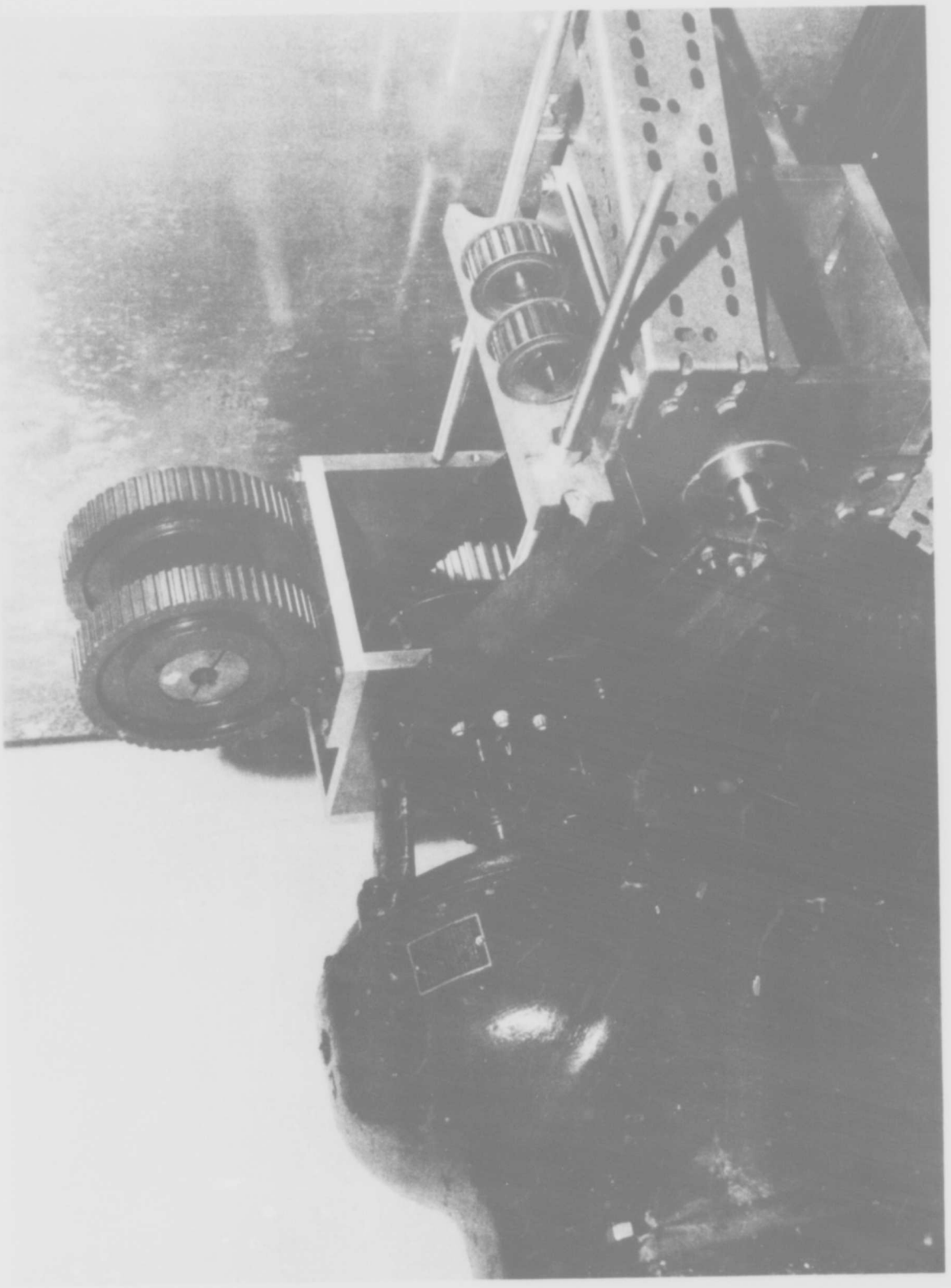

FIGURE 75 Pump Drive Belts

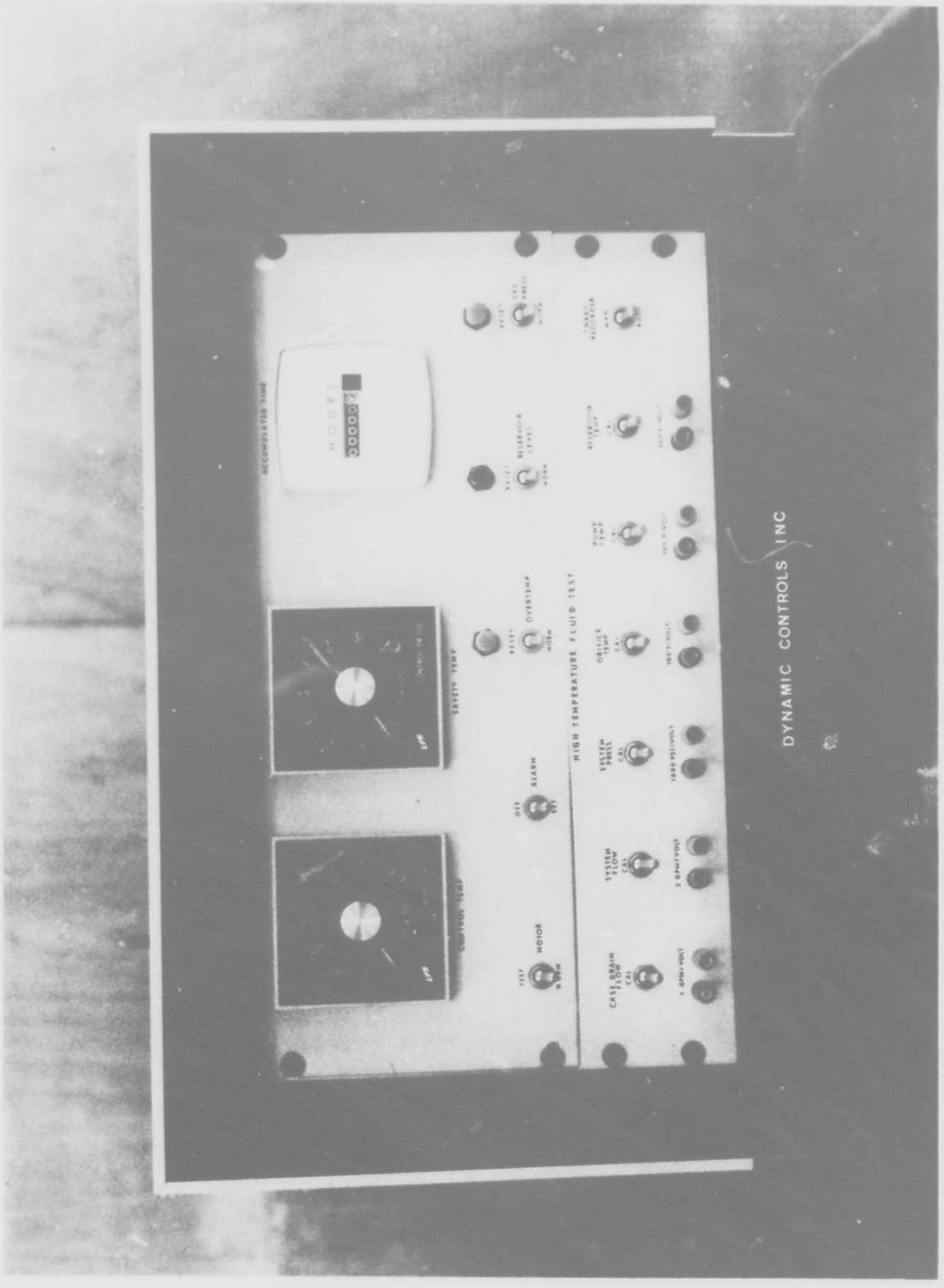

FIGURE 76 Control Unit Front Panel

unit to automatically cycle the hydraulic load on the pump between full flow demand and quarter flow demand. The cycling was set for 5 minute intervals. Each 5 minute interval consisted of 4 minutes of low flow operation and 1 minute of high flow operation. The cycling mechanization also activated the 8 channel Brush recorder once each hour. The timing was designed to operate the Brush recorder for one minute recording 30 seconds of high and 30 seconds of low flow operation.

Also incorporated in the control unit were the frequency to voltage converters for the turbine flowmeters and the signal conditioners for the thermocouples and pressure transducer. The control unit also incorporated an hour meter on the front panel which automatically recorded pump operating hours.

2.2 Test Procedure

Ten hours of running time were accumulated on the pumping system before the extended high temperature testing was started. This time was used to flush the system, clean the filters and check out the instrumentation. Before the start of the continuous testing, 2 gallons of fluid were added to the system. All Mil-H-83282 fluid was pumped into the system through a 2 micron nominal (5 micron absolute) depth type filter.

During the testing, the pump was operated at 7000 RPM. The load flow valve for the high flow mode was adjusted for 20 psig inlet pressure during high flow operation. This was slightly above the 15 psig minimum specified by the pump manufacturer. This inlet pressure (determined by the 50:1 area ratio of the bootstrap reservoir) corresponded to approximately 11 GPM @ 1000 psig pump head. The low flow condition was adjusted to a nominal 2 GPM which corresponded to 1500 psig discharge pressure from the pump.

As much as possible, the temperature tests were run on a 24 hour a day basis. At startup (both

initially and when the filter elements were changed) the system was bled for air at the high point in the plumbing and the top of the reservoir. The bleeding was done with the oil temperature at 80° to 120° F.

The Brush recorder was connected to record case drain flow, pump discharge flow, pump discharge pressure, restrictor discharge temperature, reservoir temperature and pump case temperature. The restrictor discharge temperature (being the highest temperature in the pumping system) was used for the temperature control circuit.

At 50 hour intervals, fluid samples of approximately 100 milliliters were taken from the system. The samples were all taken with the system running at the operating temperature.

The system filter was changed periodically during the test. The filter was changed (or clenaed) when the filter clogged, causing the discharge flow from the pump to fall below an acceptable level. Part way through the test sequence, the filter housing was replaced with a different unit in order to allow using new filter elements which were available.

3.0 TEST RESULTS

No major operational problems with the fluid pumping system were encountered during the test. The filters used in the system for filtering the fluid did block periodically during the test period and required changing. The filters were changed when system flow in the high flow mode was reduced to approximately 4 GPM with the high flow restriction completely opened up (this meant that the entire pressure head of the pump was being dropped across the filter element). The filters used in the system along with the temperature and time history were as follows:

Pall Filter No.	Nominal Filtration Rating	Temp °F	Time Installed Test Hours	Time Removed Test Hours	Comments
AC-3255E-12 #1	2.5 N. 15 A.	300	0	5.4	Furnished with pump Cleaned before install.
AC-3255E-12 #1	2.5 N. 15 A.	300	5.4	10.3	Cleaned at 5.4 hours
AC-3255E-12 #1	2.5 N. 15 A.	300	10.3	12.7	Cleaned at 10.3 hours
AC-3255E-12 #2	2.5 N. 15 A.	300 & 400	12.7	136	(25 hours at 400°F) new filter
AC-3255E-12 #2	2.5 N. 15 A.	400	136	198	Cleaned at 136 hours
AC-3255E-12 #1	2.5 N. 15 A.	400	198	254	Cleaned at 10.3 hours
AC-3255E-12 #3	2.5 N. 15 A.	400	254	310	New Filter
AC-2320E-122	1.5 N. 15 A.	400	310	410	New Filter element from ss housing
AC-2320E-125	5 N. 18 A.	450	410	460	New filter element (Filter plugged at test end)

Filter History

TABLE 2

At the 312 hour point of the test program on the fluid, a hydraulic leak occured in the test system. Automatic shutdown turned off the system before the reservoir was drained. The lost fluid (approximately 1.5 gallons) was collected from the catch drain tray, filtered with a 2 micron nominal, 5 micron absolute depth type filter and pumped back into the test system. The fluid in the reservoir at the restart after the leak was 4.69 gallons. Other than a small amount of the leak fluid which was not recovered and returned to the system, fluid loss to the system occured during air bleeding, minor fitting leaks and fluid test samples extracted from the system. The fluid in the reservoir at the end of the 450 hours was 4.41 gallons.

FIGURE 77 shows a representative section of the Brush recorder data. Note that the case drain flow decreases in the high flow mode. The section of data presented in FIGURE 77 was recorded at 285 and 286 hours after 185 hours at 400° F. The vertical spikes in the recordings are caused by switching noise from the timing circuits. Not shown on the figure is the reservoir temperature which was also recorded.

Fluid analysis on the test samples was conducted by the Air Force Materials Laboratory at Wright-Patterson Air Force Base.

TABLE 3 is the result of an analysis on the fluid samples. Note that samples 5 and 6 correspond to the middle and end of 100 hours of operation at 300° F, samples 9 through 15 correspond to the 300 hours of 400° F operation and sample 16 is the sample taken at the end of 50 hours of 450° F operation. Samples B through 4 were taken during the initial startup running which lasted approximately 10 hours.

DATA ON FLUID SAMPLES FROM AFFDL PUMP TEST OF

MIL-H-83282 IN IAP PUMP

Sample No.	Hours	Temp °F	Viscosity (cs) 100°F	210°F	Acid No.	Flash Point	Fire Point
B	0	amb.	15.4	3.59	<0.1	450°F	475°F
1	4.5	N/A	15.3	3.55	<0.1	440°F	480°F
2	10.3	300	15.3	3.56	<0.1	450°F	485°F
3	10.3	300	15.5	3.56	<0.1	415°F	465°F
4	10.3	300	15.5	3.61	<0.1	420°F	465°F
5	61.5	300	15.4	3.58	<0.1	415°F	480°F
6	111	300	15.0	3.57	<0.1	410°F	470°F
9	160	400	15.3	3.54	0.47	455°F	N/A
11	210	400	15.6	3.48	0.57	440°F	475°F
12	260	400	15.5	3.57	0.61	445°F	475°F
13	310	400	15.3	3.55	0.73	430°F	480°F
14	361.4	400	15.6	3.59	0.84	430°F	485°F
15	410.6	400	15.4	3.53	0.89	445°F	480°F
16	460.7	450	15.2	3.50	2.20	445°F	485°F

TABLE 3

The performance of the Vicker's pump used to pump the test fluid did not appear to degrade during the test program. The following conditions monitored during the test program indicated only the expected increase with temperature and little change with time at each temperature setting.

Case Drain Flow

Hours	Temp. ^{o}F	High Flow System Pressure PSI	GPM High Flow	Low Flow System Pressure PSI	GPM Low Flow
4.5	300	850	.4	1000	.6
71.9	300	900	.45	1250	1.0
109.6	300	950	.5	1250	1.0
209	400	850	.70	1275	1.50
225	400	1000	.75	1350	1.40
230	400	1050	.75	1350	1.40
285	400	1000	.70	1325	1.30
372	400	1000	.65	1300	1.15
379	400	1050	.70	1300	1.15
420	450	950	.70	1250	1.15
430	450	1000	.75	1300	1.20
440	450	1050	.80	1300	1.32
450	450	1100	.90	1300	1.40
460	450	1120	.90	1300	1.30

TABLE 4

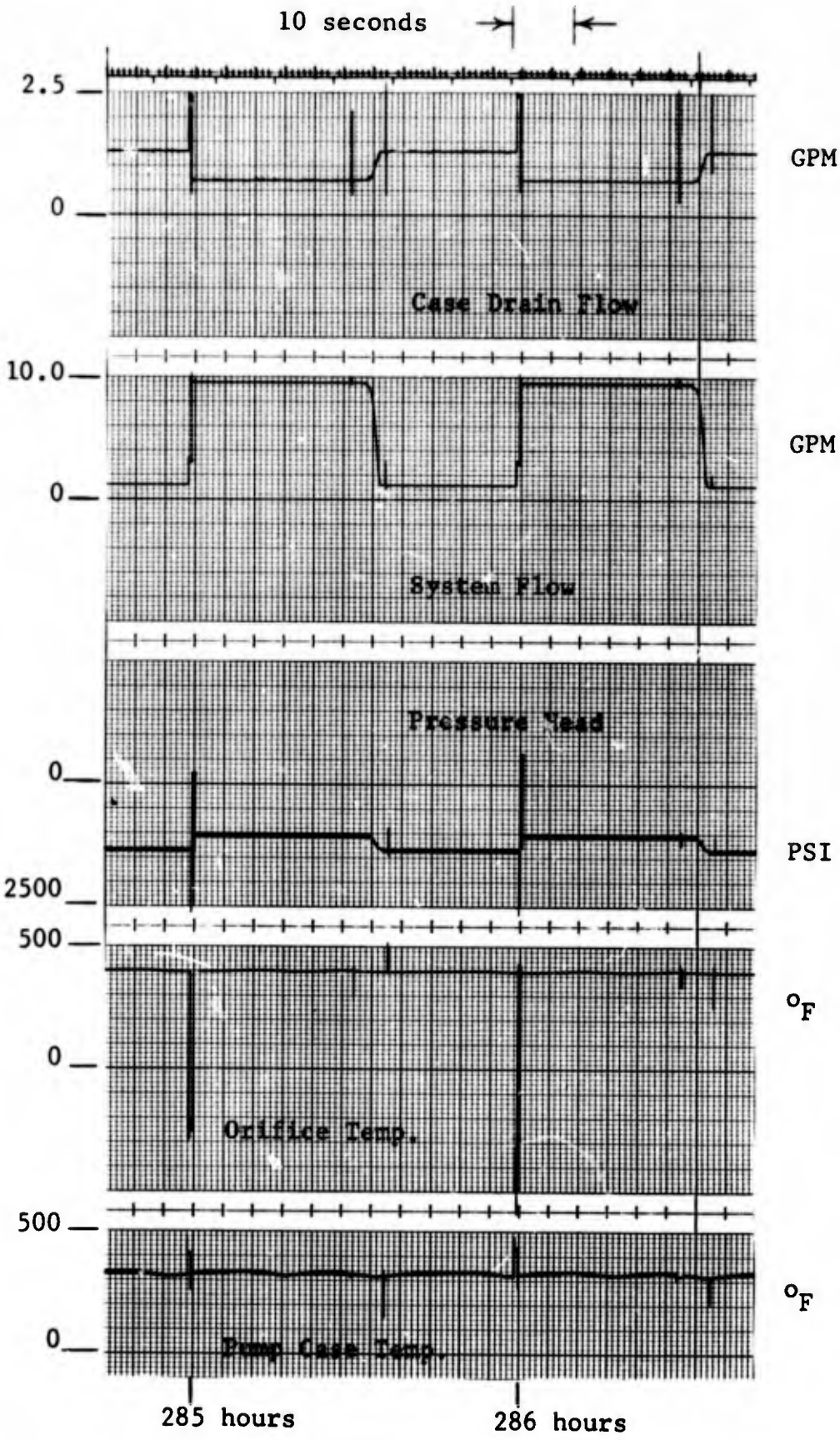
10 seconds
2.5
0
GPM
Case Drain Flow
10.0
0
GPM
System Flow
Pressure Head
0
2500
PSI
500
0
°F
Orifice Temp.
500
0
°F
Pump Case Temp.
285 hours
286 hours

FIGURE 77

4.0 CONCLUSIONS AND RECOMMENDATIONS

The Mil-H-83282 fluid performed satisfactorily with respect to pump lubrication at the temperatures tested. The filter blocking characteristics were less satisfactory. Although the system was operated as a closed system and bled with care when opened, the normal entrained oxygen in the oil may be creating the blockage problem by oxidizing the oil. If so, this would indicate that degassing the system after filling may be required when extended high temperature operation of the fluid is required.

The results of the fluid analysis by the Air Force Materials Laboratory indicate that the fluid properties are not degraded by either mechanical shear encountered in a hydraulic pump or the temperatures at which the fluid was operated. The slight acid buildup at 450° F may be associated with the filter blocking characteristic and the requirement for degassing the fluid when it is to be operated at high temperatures. The cause of the acid buildup and filter blockage should be investigated further.

REFERENCES

1. Fung, Y.C. "The Theory of Aeroelasticity" Dover Publications, Inc., New York 1969

2. Triplett, W. E., et. al. "Active Flutter Suppression Systems for Military Aircraft, a Feasibility Study", AFFDL-TR-72-116, February 1973

3. Kisslinger, R.L. and Vetsch, G.J., "Survivable Flight Control System", Interim Report No. 1, AFFDL-TR-71-20, Supplement 2, May 1971

4. Goldstein, S.M., et.al., "Test and Development of Flight Control Actuation System Components for Military Aircraft", AFFDL-TR-72-13, February 1972

5. Amies, G.E., et.al., "Survivable Flight Control System", Interim Report No. 1, AFFDL-TR-71-20, Supplement 3, May 1971

*U.S.Government Printing Office: 1975 — 657-023/753